IRAPUATO-SALAMANCA CAMPUS

ENGINEERING SCHOOL

"High heat fluxes analysis using microfluidic cooling"

Professional thesis work

To obtain the degree of:

Master in Mechanical Engineering

A Thesis work by:

Ing. Tomás Alberto Moreno Torres

Advisors:

Dr. Abel Hernández Guerrero

Dr. José Luis Luviano Ortiz

Salamanca, Guanajuato, México Noviembre de 2020

Salamanca, Gto., a 12 de Noviembre del 2020.

M. en I. HERIBERTO GUTIÉRREZ MARTIN
JEFE DE LA UNIDAD DE ADMINISTRACIÓN ESCOLAR
P R E S E N T E.-

Por medio de la presente, se otorga autorización para proceder a los trámites de impresión, empastado de tesis y titulación al alumno (a) Tomás Alberto Moreno Torres del ***Programa de Maestría en Ingeniería Mecánica*** y cuyo número de ***NUA*** es: 388509 del cual soy director. El título de la tesis es: **High heat fluxes analysis using microfludic cooling**

Hago constar que he revisado dicho trabajo y he tenido comunicación con los sinodales asignados para la revisión de la tesis, por lo que no hay impedimento alguno para fijar la fecha de examen de titulación.

A T E N T A M E N T E

Dr. Abel Hernández Guerrero
NOMBRE Y FIRMA
DIRECTOR DE TESIS
SECRETARIO

Dr. José Luis Luviano Ortiz
NOMBRE Y FIRMA
DIRECTOR DE TESIS

Dr. Elías Rigoberto Ledesma Orozco
NOMBRE Y FIRMA
PRESIDENTE

Dr. Cesar Eduardo Damián Ascencio
NOMBRE Y FIRMA
VOCAL

Acknowledges

First of all, thanks to God for never being separated from me, for his blessings and love.

I appreciate the education provided for my parents and family. They opened to me the opportunities that they did not have, and there are no words to express my gratitude. The culmination of this word is a shared achievement of all of us.

Thanks to my mates for their help, support, and the good mood. Without them, my academic trajectory during these past two years would have been harder.

Thanks to my advisors. Dr. Abel Hernandez and Dr. Luis Luviano, for helping me to develop my potential, for allowing me to belong to their research group, and for allowing me to be a better professional. Someone who this country deserves.

Thanks to my Georgia Tech advisors Dr. Joshi for accepting me as an associated research in his investigation group and giving me the opportunity to develop the present investigation topic. And mainly thanks to Dr. Lorenzini for his advice, feedback, and support, thanks for showing me the professional and person that I aspire to be.

Finally, thanks to my roommates and Georgia Tech mates, for helping me to have a good experience in ATL.

Index

List of figures I

List of tables VII

Nomenclature VIII

Overview XI

Chapter 1

Introduction

1.1 Background of computational systems
1.1.1 Vacuum tubes 1
1.1.2 Transistors 2
1.1.3 Integrated circuits (IC's) 3

1.2 Evolution of computational systems through time 4
1.2.1 Microprocessor 5
1.2.2 Timeline of computational systems development 6
1.2.3 Computational capabilities and limitations nowadays. 8

1.3 Tri-dimensional integrated circuits (3D IC's) and through-silicon vias 10

11

1.3.1 3D IC´s advantages, disadvantages, and commercial products

1.4 Overheating in computational systems 13
1.4.1 Heat fluxes on computers 14
1.4.2 Predicted heat fluxes on 3D IC´s microprocessors 16

Chapter 2

Background

2.1 Introduction 18

2.2 Traditional cooling technologies for computers
2.2.1 Internal/ External-module cooling 19
2.2.2 Fluidic cooling (heat sinks) 20
2.2.3 Phase change cooling 23
2.2.4 Comparison of heat transfer capabilities 23

2.3 Emerging cooling techniques
2.3.1 Heat pipes 24
2.3.2 Spray cooling 25
2.3.3 Porous media 26

2.4 Microfluidic cooling 26
2.4.1 Embedded micro-pin fins 27
2.4.2 Microchannels 30
2.4.3 Hybrid models 33
2.4.4 Other approaches 35

2.5 Thesis objective
2.5.1 Particular Objectives 35

Chapter 3

Numerical procedure

3.1 Computational domain 36

3.2 Considerations 38
3.2.1 Thermophysical properties 39

3.3 Governing equations and boundary conditions 41

3.4 Mesh analysis 42
3.4.1 Mesh quality 44

3.5 Numerical model validation 45
3.5.1 Extended validation domain 46
3.5.2 Flow rate analysis 48

3.6 Design of experiments (DoE) 50
3.6.1 Parametric analysis 52
3.6.2 Proposed models using DoE 52

Chapter 4

Results

4.1 Predicted thermal performance 57

4.2 Velocity and temperature contours 59

4.3 Statistical interpretation of the obtained results 62

4.4 Optimization of models using statistical tools 64

4.5 Thermal evaluation of optimized models 68

Chapter 5

Conclusion and future works

5.1 Conclusions 73

5.2 Possible future works 74

References 75

Figures

Figure 1.1	Illustration of different versions of vacuum tubes [2].	1
Figure 1.2	Illustration of vacuum tubes modules of ENIAC [6].	2
Figure 1.3	First integrated circuit [8].	4
Figure 1.4	PDP-8 minicomputer [8].	5
Figure 1.5	Illustration of the computer evolution trough the time [11].	6
Figure 1.6	Illustration of a typical embedded system [16].	8
Figure 1.7	Graphical representation of Moore's law and computer clock speed evolution [11].	9
Figure 1.8	Bandwidth trend example.	10
Figure 1.9	Geometrical illustration of typical 2D IC (a) and 3D IC (b) [22].	11
Figure 1.10	Causes of failure in electronic components [23].	14
Figure 1.11	Heat fluxes on high-end computers of the past century [28].	15
Figure 1.12	Heat fluxes on current high-performance chips [29].	15

Figure 2.1	Classification of cooling technologies for computational systems.	18
Figure 2.2	Typical cooling system on computer denoting its internal and external regions [28].	19
Figure 2.3	Illustration of conventional internal-module cooling for an MCM [28].	20
Figure 2.4	Illustration of heat sinks on electronic devices [39].	21
Figure 2.5	Illustration of jet impingement cooling [48].	22
Figure 2.6	Comparisons of heat transfer capabilities of conventional methods [64].	24
Figure 2.7	Illustration of the heat pipe and working principle [37].	25
Figure 2.8	Illustration of porous media heat sinks [77].	26
Figure 2.9	Proposed division of microfluidic cooling systems.	27
Figure 2.10	Illustration of embedded pin-fins for microfluidic cooling [78].	27
Figure 2.11	Embedded pin fin arrangements proposed by Survey et all. [79].	28
Figure 2.12	Validation of Lorenzini numerical model [78].	29

Figure 2.13	Velocity and temperature contours reported by Lorenzini et al. [78].	29
Figure 2.14	Illustration of micro-pin fins gradient array proposed by Feng et al. [81].	30
Figure 2.15	(a) Temperature distribution and (b) axial variation of substrate bottom surface temperature for both simple microchannel (SMC) and recharging microchannel (RMC).	31
Figure 2.16	Thermal behavior comparison of a surface with cooling provided by a uniform microchannel array (a), against optimized channel array (b) and validated by COMSOL (c).	32
Figure 2.17	Illustration of the test vehicle and proposed hierarchical microchannel array by Drummond [85].	32
Figure 2.18	Numerical and experimental thermal results obtained by Wang et al. [86].	33
Figure 2.19	Illustration of hybrid microfluidic cooling system.	34
Figure 2.20	Temperature contour for both NH-RM (a-d) and H-MPF (e-k), using different heat fluxes on the hotspot zone.	34
Figure 3.1	Microfluidic cooling system analyzed by Lorenzini et al. [78].	37

Figure 3.2	Geometric illustration of the portion of a silicon micro-gap with embedded pin fins.	38
Figure 3.3	Graphic of water dynamic viscosity relation with the temperature.	40
Figure 3.4	Graphic of silicon thermal conductivity relation with the temperature.	41
Figure 3.5	Mesh illustration and boundary layer details.	43
Figure 3.6	Vectors used to compute orthogonal quality for a cell [96].	44
Figure 3.7	Predicted surface temperature and comparison with experimental data [78].	46
Figure 3.8	Illustration of the extended validation model.	47
Figure 3.9	Predicted surface temperature and comparison with experimental data [78] in the extended model.	48
Figure 3.10	Illustration of created planes to size the flow rate in different gaps.	49
Figure 3.11	Calculated fluid flow rates in the extended model for different micro-gaps.	50
Figure 3.12	Illustration of in and out information involved in an unknow process.	51
Figure 3.13	Illustration with detail of the Model 7.	55

Figure 3.14	Illustration with detail of the Model 51.	55
Figure 4.1	Surface temperature response of some analyzed configurations	58
Figure 4.2	Illustration of velocity contours in selected microfluidic cooling systems.	60
Figure 4.3	Illustration of temperature contours in selected microfluidic cooling systems.	61
Figure 4.4	Normal effects graphs for pressure drop and the average temperature in proposed microfluidic systems.	62
Figure 4.5	Pareto diagram for the pressure drop.	63
Figure 4.6	Pareto diagram for bottom average temperature.	64
Figure 4.7	Illustration of the predictive graphic model given by JMP.	66
Figure 4.8	Thermal behavior on optimized models against the validation model.	68
Figure 4.9	Schematic illustration of the model Opt1G1.	69
Figure 4.10	Illustration of the boundary conditions in the evaluated model.	70
Figure 4.11	Predicted thermal behavior in model Opt1G1 for different pressure drop (PD).	71

Figure 4.12 Temperature contours for a pressure inlet of 600 kPa in the model Opt1G1. 72

Tables

Table 1.1	3D ICs products and their performance improvements	12
Table 3.1	Thermophysical properties of water and silicon	39
Table 3.2	Key mesh numerical information considering different element sizes.	43
Table 3.3	Selected level values for each parameter and their acronyms.	52
Table 3.4	Normalized parametric dimensions of investigated configurations.	53
Table 4.1	Numerical responses in output parameters of general interest.	56
Table 4.2	Regrouped data for the selection of central models.	65
Table 4.3	Dimensions and results for optimized models and middle points.	67

Nomenclature

c, c_p	Specific heat (J kg^{-1} K^{-1})
h	Height (m)
k	Thermal conductivity (W m^{-1} K^{-1})
P	Pressure (Pa)
Q	Heat flux (W m^{--2})
S	Pitch (m)
t	Thickness (m)
T	Temperature (K)
u	Velocity component in the x-direction (m s^{-1})
v	Velocity component in the y-direction (m s^{-1})
w	Velocity component in the z-direction (m s^{-1})
x, y, z	Cartesian coordinate components
$\vec{A}$, $\vec{c}$, $\vec{f}$	Orthogonal quality vectors

Greek letters

μ	Dynamic viscosity (kg m^{-1} s^{-1})
ρ	Density (kg)
ϕ	Diameter (m)

Subscripts

L, l	Longitudinal
Si	Silicon
T, t	Transversal

Acronyms

AT	Average temperature at the bottom surface
ESD	Extended surface diameter
ESH	Extended surface height
ESS	Extended surface shape
DBC	Distance between extended surface centers
HP	Hotspot position

ID	Increased density of pin fins
PD	Pressure drop
DoE	Design of experiments
2D	Two-dimensional
3D	Tri-dimensional
ICs	Integrated circuits
TSVs	Through-silicon vias
OQ	Orthogonal quality
CFD	Computational fluid-dynamics

Overview

The exponential development in computational systems in the last decades along with new emerging 2.5 and 3D integrated circuits (ICs) geometries allow to overcome some limitations from conventional computers. Due to the small dimensions and the number of micro-circuits contained in new micro-chip geometries, overheating is a significant issue that needs to be solved. Conventional cooling methods are not enough to keep acceptable temperatures on these 3D IC systems. A potential solution is to develop alternatives cooling methods like micro embedded pin fins with pin-fin density variation for hotspot zones. However, experiments to analyze this potential solution have high costs due to manufacturing; hence, numeric simulation is a convenient tool to analyze and to develop different microfluidic cooling models for 3D IC.

The present work shows a numerical methodology for microfluidic cooling, using micro embedded pin-fins on a thin silicon plate. A parametric analysis was performed, using the theory of design of experiments (DoE). The proposed factorial design considers 64 numerical microfluidic cooling models. The pressure drop and the average temperatures were obtained for each model to determine the importance of input parameters utilizing a statistical approach. Through the suggestions made, useful for future experimental and numerical works, some optimized geometries are proposed using statistic tools. Promissory microfluidic cooling systems and conclusions are reported in this thesis work.

Chapter 1 shows the rise of the computational systems and their evolution, giving place to considerable improvements on computers with the implementation of novel technologies. Chapter 1 background allows to understand the capabilities and limitations of current computational systems, and the next computational revolution that represents the implementation of the tridimensional integrated circuits (3D ICs). Each computational revolution generates some problems for their designers, as is the case of the thermal

management due to the increase of the heat fluxes inside the new computational systems.

Chapter 2 makes a review of the cooling methods and systems for heat dissipation on computers. It presents a brief explanation of conventional cooling systems and the new cooling approaches for the heat dissipation on 3D ICs micro-processors. Research works have shown promising experimental and numerical results for the thermal management of 3D ICs, making use of micro embedded cooling systems.

In Chapter 3 a validation methodology is developed using a simplified microfluidic cooling system with embedded pin fins. At the same time, the advantages of statical analysis by the design of experiments theory are discussed. With the combination of both approaches, a factorial design in microfluidic cooling systems is proposed. Besides, taking advantage of the obtained results, some optimized models are generated for their posterior evaluation.

Chapter 4 shows the obtained results from the proposed parametric analysis. It shows the influence of the considered parameters for the thermal management, and the predicted pressure drops generated by these variations. In the same way, Chapter 4 provides an illustration of the predicted thermal behavior in different models. Velocity and temperature contours are presented to illustrate in a better way, the influence of the parametrical variation. Statistical tools are used to post-process the obtained data, giving useful information and conclusions. Thus, some optimized microfluidic cooling models are generated for their evaluation.

Chapter 5 gives the general conclusions of this thesis work, highlighting the contributions in microfluidic cooling systems for computational systems that make use of tri-dimensional integrated circuits (3D IC´s).

Chapter 1

Introduction

1.1 Background of computational systems

1.1.1 Vacuum tubes

The first antecedent who allowed the creation of a computational system is the vacuum tube. A vacuum tube (Figure 1.1) or electrode tube consists of a sealed-glass of metal-ceramic enclosure used to control the electrons flow inside it. The air inside the tube is removed by vacuum to avoid any kind of interference for the electrons flow [1].

Figure 1.1 Illustration of different versions of vacuum tubes [2].

Vacuum tubes were used as switches, making possible the electronic computing for the first time, having some contradictions as the high operation cost and its short lifetime period [3]. By improving the vacuum tubes and operating on specific conditions, they may work with more reliably for long periods, overcoming their limitations. Hence, in 1934 the first experiment using 3 000 vacuum tubes in small independent modules was made [4].

In 1943, the first working programable computer in the world was designed, it was called Colossus. The Colossus was built for military applications in the second world war to execute a variety of routines; it used about 1 800 vacuum tubes. Three years later, the Electronic Numerical Integrator and Computer (ENIAC) was developed. ENIAC was 10 ft high, weighed

30 t, occupied 1 000 ft^2, and used about 70 000 resistors, 10 000 capacitors, 6 000 switches, and 18 000 vacuum tubes [5], an illustration of ENIAC is shown in Figure 1.2.

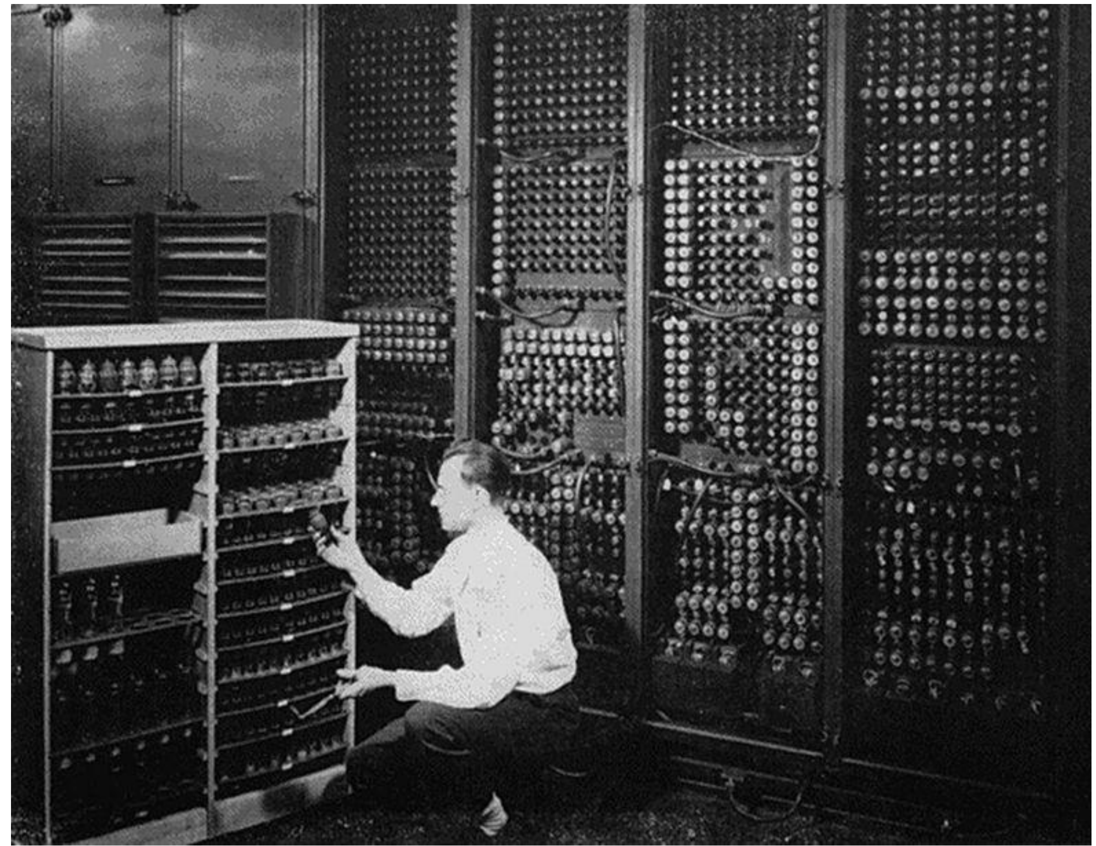

Figure 1.2 Illustration of vacuum tubes modules of ENIAC [6].

1.1.2 Transistors

The early computers like Colossus and ENIAC had big dimensions occupying considerable spaces. They used thousands of vacuum tubes, consuming high amounts of energy, and generating a vast quantity of heat. As a consequence, many vacuum tubes burned out most of the days. The most prolonged period of continuous operation without a failure on ENIAC was five days [6]. In resume, the early computers had troubles with their reliability.

Due to the need of overcoming these reliability issues, Bell Labs created the transistor, an invention that revolutionized the electronics field. The transistor is a semiconductor device used to deliver an output signal in response to an input signal. It is composed of three terminals, and it can control electric current or voltage between two of the terminals by applying other electrical current or voltage on the third terminal. So, the transistor can operate as a switch just like a vacuum tube, and by the stacking many of them (a switch which operates another switch) is possible to create logic circuits. Where the logic circuits are capable of making mathematic and Boolean operations, and even more, depending on the number of the stacked transistors.

The first transistors were smaller, cheaper, reliable, and had less energy consumption than the vacuum tubes. Due to its advantages, functioning, and manufacturing facility, the transistor replaced the vacuum tube [7].

1.1.3 Integrated Circuits (IC's)

The transistor invention allowed to design more complex electronic circuits capable of making complex routines. These electronic devices contained hundreds of components, such as transistors, diodes, and capacitors. However, each component needed to be wired to many other components when the wiring was done manually. This point represented a considerable limitation for the creation of new and more powerful electronic devices.

Summarizing, the new problem on computational devices consisted in interconnecting a considerable quantity of electronic components, avoiding the expensive costs, and reducing the time-consuming. In 1958, Jack Kilby realized that resistors and capacitors might be made from the same transistors material (semiconductors). All the components of an electronic circuit could be made from the same material, allowing an easier interconnection between them. In other words, the solution was to fabricate all the elements of electronic circuits in the same plate to facilitate the electronic connections. Then, they could be used as a complete circuit known as integrated circuit. The first successful integrated circuit contained several quantities of transistors, capacitors, and diodes fabricated on a germanium plate (Figure 1.3).

An integrated circuit (IC) consists of a set of electronic circuits on a small chip of semiconductor material (usually silicon), and it is much smaller than a circuit made from independent components. Nowadays, it is an extremely compact device and may contain millions or billions of transistors and other electronic components in a tiny area [8].

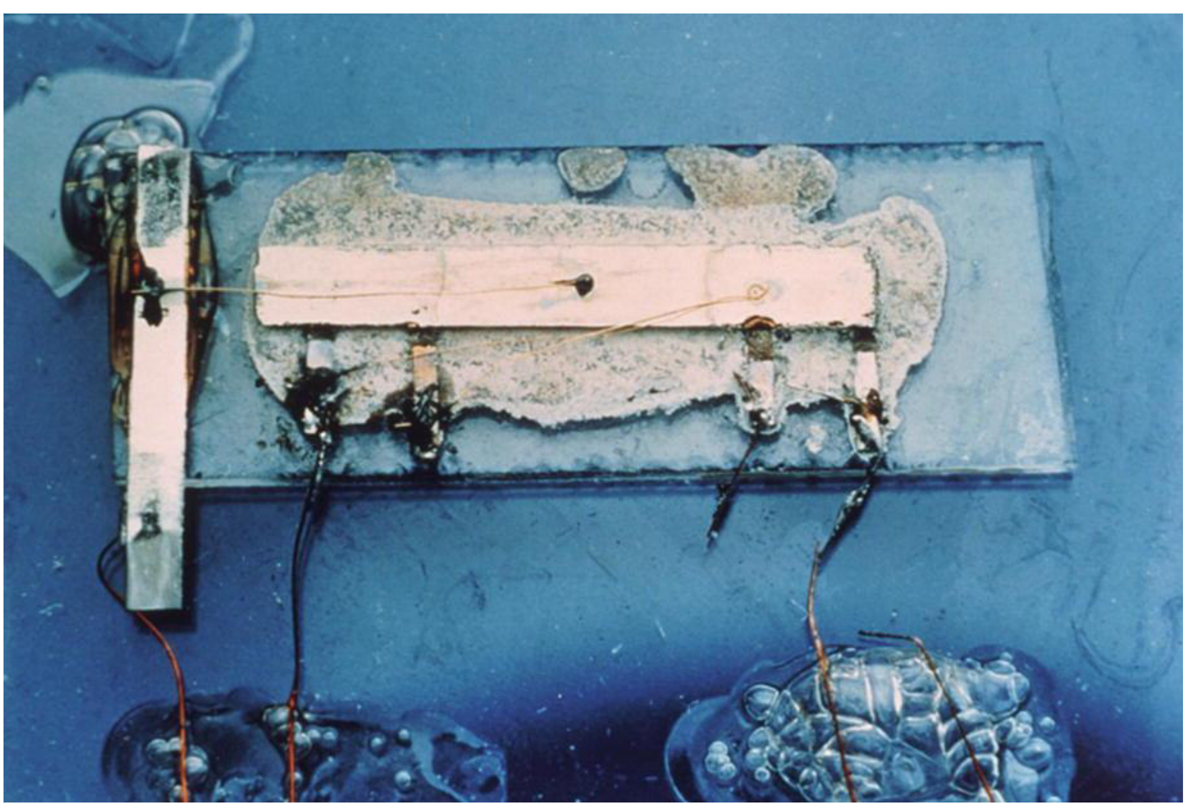

Figure 1.3 First integrated circuit [8].

1.2 Evolution of the computational systems through time.

Along with the invention of Colossus and ENIAC, in 1940 and 1946 respectively, some issues started to arise. One of the most important was the lack of internal memory; all the programs must be executed manually by the computer operators, taking considerable quantities of time to run the asked programs. The solution for this issue gave place to the Electronic Discrete Variable Automatic Computer (EDVAC), considered as the ENIAC successor in 1949. EDVAC implemented the concept of a stored program, following the computer architecture proposed by von Newman [9]. EDVAC was constituted by 6 000 vacuum tubes with a power consumption of 56 000 watts and had 5.5 Kb of memory, remaining in operation until 1961 [6].

The next generation of computers was introduced with the transistor invention. In 1955 International Business Machines (IBM), the IBM 608, was the first product to use transistors circuits instead vacuum tubes and contained 3000 germanium transistors. Few years late, in 1958, the IBM 7090 was introduced. It is considered one of the earliest commercial computers that used a logic transistor. This device was designed to carry out scientific applications 13 times faster than the older vacuum tubes computers, had an address-space of 32 278 words, and could perform 229 000 calculations per second [7].

In the decade of 1960, the creation of the integrated circuits led to new improvements in the computer systems, making them less expensive and more affordable. In 1966, the Apollo flight computer (one of the earliest computers to use integrated circuits) was introduced, developed by MIT/Raytheon. While the first commercial computer to use integrated circuits was the PDP-8 (Figure 1.4). This model is considered like a minicomputer due to the dimensions of its antecessors [8].

Figure 1.4 PDP-8 minicomputer [8].

1.2.1 Microprocessors

Despite the advantages and new capabilities of the 60s computers. The necessities of more powerful computational systems guided to the creation of the microprocessor, between 1971 and 1976. A microprocessor is an integrated circuit with many transistors on a single board in a smaller space than the conventional ICs. The 4004 was the world first microprocessor; it was a four-chip system constituted by a 256-byte Read-Only Memory (ROM), a 32-bit Random Access Memory (RAM), 4-bit data path, and a 10-bit shift register. It used 2 300 transistors to execute 60 000 operations per second [10]. In 1972, Intel presented its microprocessor model, the 8008. It implemented 3 300 transistors and counted with the first compiler called PL/M, used for specific applications. From 1974 forward, many new companies began to explore the microprocessor potential, increasing their speed, density of transistors, and functionality until nowadays [5].

1.2.2 Timeline of computational systems development

Figure 1.5 gives a clear illustration of the evolution of the computational systems through time. These devices have been considerable reductions in their dimensions, according to the new findings on each decade in electronic devices. The 50s gave place to the first computers known as mainframe (Colossus, ENIAC, and ENVAC), used for military and aero-spatial tasks. Due to the mainframes were constituted for hundreds or thousands of vacuum tubes, they were large and robust devices, occupying complete rooms for their operation. As a consequence of their dimensions and number of components, the mainframe had high-energy consumption. Besides, when a single vacuum tube failed a complete module of these computers must be stopped, taking a many time to identify the failure. For previous reasons, the first mainframes were considered non-profitable.

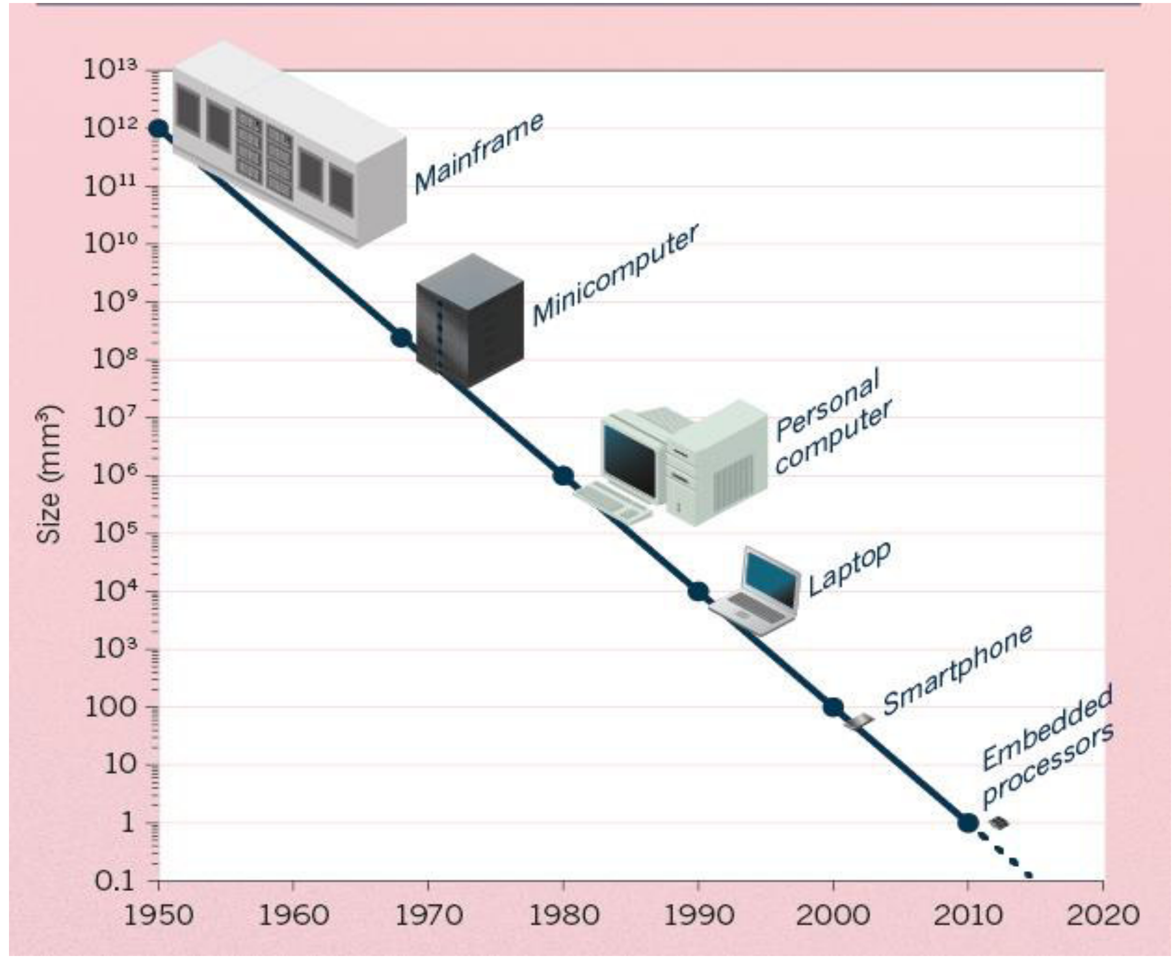

Figure 1.5 Illustration of the computer evolution trough the time [11].

Fifteen years after the creation of the first mainframes, the invention of transistors allowed the implementation of new computational systems known as minicomputers. These computers considerably reduced their dimensions, at least ten times in comparison with

the mainframes. The first computers were installed in complete rooms, in contrast the minicomputers only made use of a locker space, while increasing the computational power.

In 1971, a revolution in computing started with the invention of the microprocessor. The first microprocessor made considerable enhancements on the computer performances (a tiny chip had an equivalent computing power as the ENIAC computer), adding more memory and operation sequences to facilitate their operation. In other words, the microprocessor is essentially a computer on a chip. Its creation made possible the handheld calculators and give place to the personal computer (PCs) [10]. Between 1976 and 1981, when some companies (Apple and IBM) started to create their own software to run their computers, the first commercial PCs were unveiled. These developments started the personal computer industry. A few years later, once incorporated the first reliable batteries in the computational industry, the first portable microcomputers (laptops) were introduced.

The microprocessor improvement continued with the time, until the smartphone arrival. The smartphone is a touch-based computer with its keyboard for making and receiving calls, with internet access and many other integrated features. It has lower dimensions than a microcomputer, capable of fitting in one hand. In 1993, IBM introduced an early precursor of the smartphone, the IBM Simon. It worked as a mobile phone and personal digital assistant (PDA), it included touch screen to dial numbers; it could send faxes and emails as well as making or receiving calls [12].

In the new millennium first decade, with the implementation of the embedded processors, the next computational revolution started. An embedded processor is a microprocessor designed for handling the needs of an embedded system, and the embedded systems are a combination of computer processor, memory, and input/output peripheral devices. An ordinary microprocessor only has its processor on the chip, while the complementary devices into a computer are separated from the main chip, resulting in more power consumption [13, 14]. Today ninety-eight percent of all manufactured microprocessors are embedded processors, and they are widely used in many conventional devices [15, 16]. Figure 1.6 Illustrates an embedded system on a plug-in card with processor, memory, power supply, and external interfaces. This integrated-circuit architecture is the most used of the last decade on computers (PCs, laptops, and others). Embedded processors consist of a thin plate of 0.3 mm thick and millions of transistors in an area 1 cm^2.

Figure 1.6 Illustration of a typical embedded system [16].

1.2.3 Computational capabilities and limitations nowadays.

The microprocessor invention and its new manufacturing technologies motivated to Gordon Moore to propose his empirical law known as Moore's law; this law poses that the number of transistors on a microprocessor will increase twice every two years [18]. Figure 1.7 shows that this empirical law is keeping its trend until nowadays. Thus, the increase in the number of transistors contained in microprocessors provoked the rise of the computational system capabilities. The embedded systems are capable of achieving sophisticated operations, such as:

- Execution of complex algorithms: The operations made by the microprocessor can be very sophisticated, depending on the application.
- User interface: Microprocessors are frequently used to control complex user interfaces and compilers that may include a diversity of menus with many options.
- Process in real-time: Embedded systems have to perform many operations in real-time, due to if the data is not ready at a particular deadline, a specific system could break its operations.
- Multirate and multitask: Microprocessors may simultaneously have control over some operations that run at slow rates and others that run at high rates [14].

In addition, current microprocessors have at least 10^5 more capacities than the first PCs to execute operations. Despite increasing the number of transistors on a microprocessor every year, it not necessarily means to enhance the global performance on computational systems. As it is the particular case of the processors clock speed, which is a variable to evaluate the computer performance, it represents the number of operations that can be made by a computer in a single second.

Figure 1.7 shows that since 2004, the computer clock speed has not had a considerable improvement in the following twelve years, this might be attributed to the high heat fluxes on microprocessors. An increase in clocks speed has a relation with an increment in the operations per second inside of a microprocessor, and such increment implies more energy consumption. When the processors energy consumption is increased, the heat flux rate on these electronic devices rises too. If the cooling system is not enough to dissipate the new high heat fluxes, the allowed temperatures on a microprocessor will be surpassed, having repercussions on the computer performance.

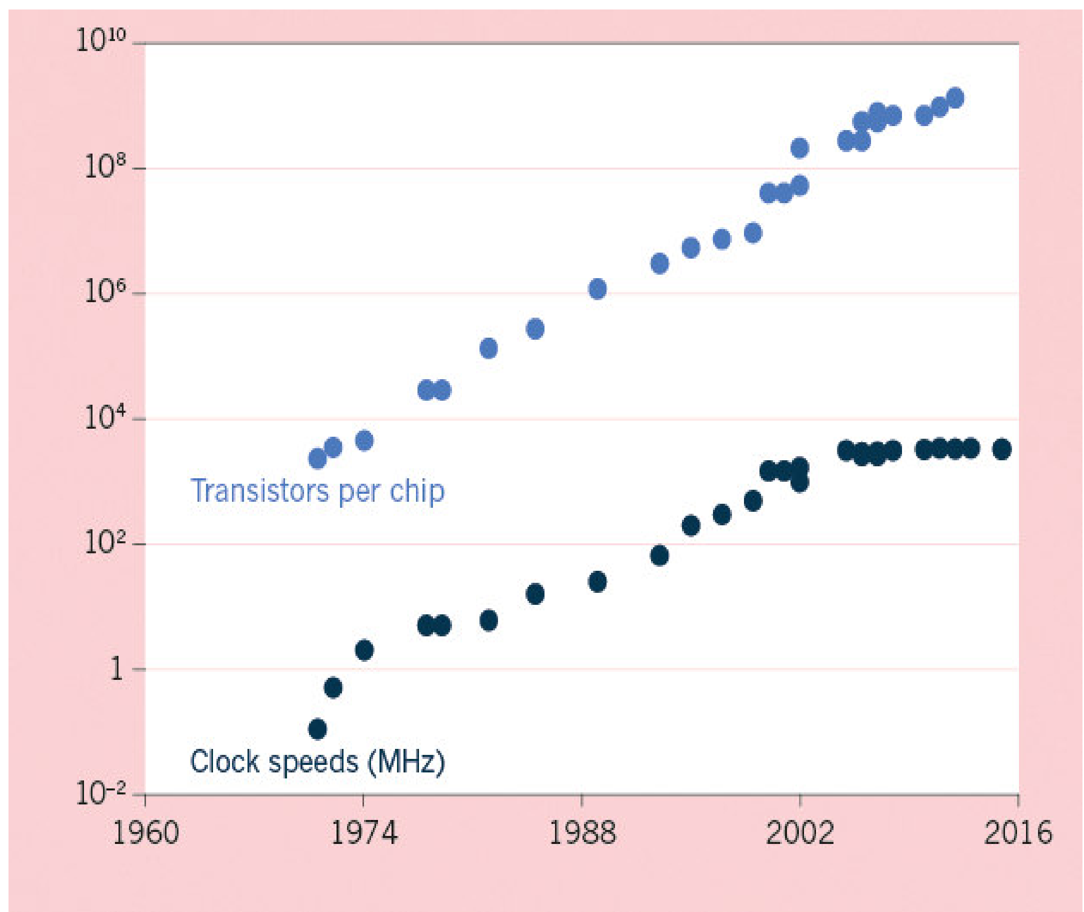

Figure 1.7 Graphical representation of Moore’s law and computer clock speed evolution [11].

Another topic to have into consideration is the data transfer range inside the computer or via internet to be processed. The bandwidth is a useful concept to size this variable, according to Hartley´s law, "the maximum data transfer range in a physical link is proportional to its analog bandwidth"[19]. It means that the maximum transference of analog data inside a computer has a straight relation with its bandwidth. Figure 1.8 exemplifies the bandwidth trend in future years that increases the double every three years in some prestigious companies. Shortly, it will be necessary for the implementation of new processors to accomplish the new requirements of data processed per second.

Source: Peripheral Component Interconnect Special Interest Group (PCI-SIG)

Figure 1.8 Bandwidth trend example.

1.3 Tridimensional integrated circuits (3D ICs) and trough-silicon vias (TSVs)

Tridimensional integrated circuits (3D ICs) are emergent technologies whose use is promissory to overcome interconnect scaling problems and improving the performance of conventional 2D ICs (current microprocessors, shown in Figure 1.6) [20]. 2D ICs consist of a package substrate with multiple transistor wafers and other micro-electronics, known as dies, connected between them by many microwires. While 3D ICs are constituted by vertical stacking of multiple dies without considering all the wire connection for them. The dies are stacked vertically on top of each other, and the bottom die has a straight connection with the package substrate. Figure 1.10 shows both 2D IC (a) and 3D IC (b) geometries, giving a complete illustration of the geometrical differences between the 3D ICs and 2D ICs.

The connection between dies in a 3D IC is possible by the through-silicon vias (TSVs), which is the enabling technology for the 3D integration. As its name refers, TSVs are vertical connections that go across the silicon dies and other silicon surfaces. The typical size of TSV goes from 1 to 5 µm or 5 to 20 µm, depending on the connection case [20]. As a result of the TSVs implementation, the footprint area of each die of a 3D IC becomes smaller than a 2D IC, using less space in the package substrate. Also, the wire connections are reduced [21].

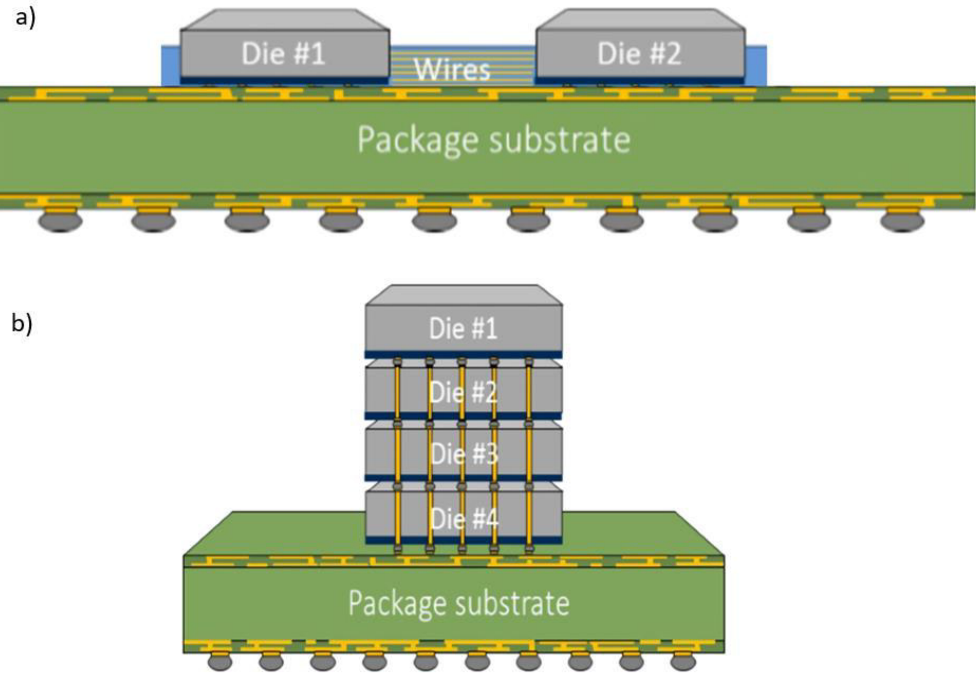

Figure 1.9 Geometrical illustration of typical 2D IC (a) and 3D IC (b) [22].

1.3.1 3D IC's advantages, disadvantages, and commercial products

The implementation of 3D IC geometries carries considerable advantages in comparison with conventional integrated circuits geometries or 2D IC, as is the case of the following:

- Operation as a single processing unit: 3D IC geometries benefit to the operation of transistor wafers in parallel, allowing them to work as a single unit.
- Better performance in less space: vertical stacking reduces the used space, and the spacing between dies, with it, the signals between integrated circuits are gotten in less time.
- Shorter wirelength: vertical integration benefit to reduce the footprint area on each die, decreasing the necessary cabling for connections between dies (illustrated in figure 1.9) [21].
- Less energy consumption: when the wirelength is reduced, the electrical conduction resistance is reduced too. In consequence, the energy requirements decrease due to lower losses by electrical conduction.
- New integrated circuits designs: TSVs allow the implementation of new and unknown geometries on integrated circuits, looking to propose improvements on the performance of conventional ICs.
- Improvements in bandwidth and clock speed: As a part of the operation as a single unit and the space reduction between microelectronics in 3D ICs, the capacities to manage and process more data will increase.

At the end of the last decade, 3D ICs started to be applied in some commercial products, mainly in Dynamic Random-Access Memories (DRAM) and Graphic Processor Unit (GPU). Table 1.1 shows some examples of new technologies that make use of 3D ICs, having considerable improvements in comparison with 2D ICs.

Table 1.1 3D ICs products and their performance improvements [22].

Product/ Year	Description	Performance improvement in comparison with 2D IC
Samsung 3D DRAM/ 2009	Internal memory of dynamic-random access (DRAM) for electronic devices.	50% of increment on in/ out data rate; 50% less energy consumption.
Micron HMC/ 2011	High-performance RAM based on DRAM, designed to compete with the High Bandwidth Memories (HBM).	10X increase in bandwidth; 70% of reduction in energy consumption.
AMD Fiji/ 2015	Graphic Processor Unit (GPU) with High Bandwidth Memory (HBM).	Memory bandwidth increment of 3X per power watt.

Nvidia Tesla P100/ 2016 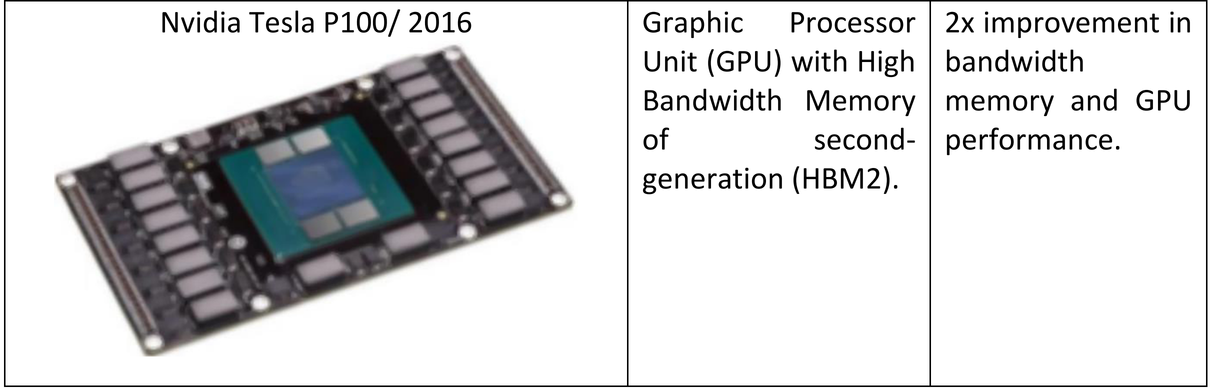	Graphic Processor Unit (GPU) with High Bandwidth Memory of second-generation (HBM2).	2x improvement in bandwidth memory and GPU performance.

Despite the advantages that represent the implementation of 3D ICs, and being used on commercial products, the application of emerging TSV technologies on microprocessors has some limitations. One of them is the fact that only a few specialized companies and universities have the resources and the equipment for their investigation, manufacturing, and production. Also, another critical issue to highlight is the thermal management on this kind of technology, due to the high heat fluxes on 3D IC devices, generated by the high concentration of electronic circuits on tiny spaces.

1.4 Overheating in computational systems

A significant part of the failures in electronic devices during their operation is due to temperature. Figure 1.10 shows that more than 50 % of electronics failures are attributed to high temperatures [23]. As a consequence of high temperatures in electronic devices, thermal failures such as mechanical stresses, thermal debonding, and thermal fracture can occur.

In past decades, it was acceptable to operate a computer with temperatures below 65 °C for an adequate micro-chip performance [24]. In recent years, with the new computational developments, the working limit temperature in electronic devices is ranged from 85 to 100 °C. For reliable performance on a microprocessor, the junction temperature between the processor and its physical connections should not exceed the range from 90-110 °C [25]. The literature has demonstrated that the reliability of a micro-chip is reduced 5%, each time its temperature surpassed 1 °C the established thermal limit. In addition, when the limit temperature of a micro-chip is exceeded, the chip life span is reduced significantly [26]. Thereby, it is essential to avoid overheating in a computational system by adequate thermal management.

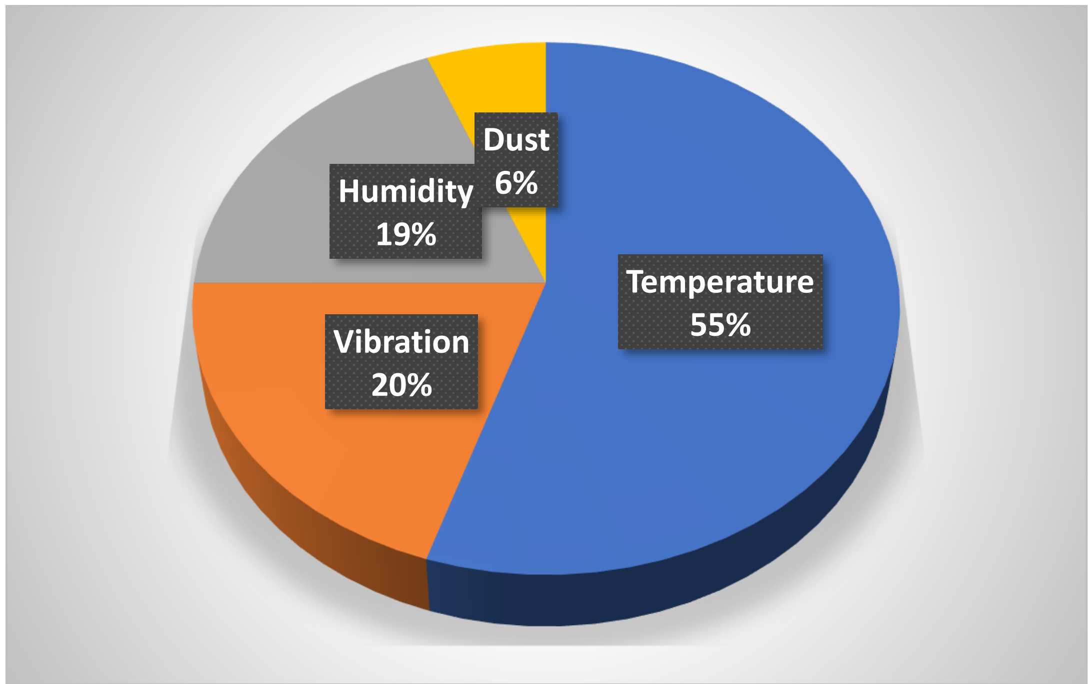

Figure 1.10 Causes of failure in electronic components [23].

1.4.1 Heat fluxes on computational systems.

As was mentioned, remove the heat from a computer has a key role in ensuring the reliable operation on it. One example is the first mainframe, the Electrical Numerical Integrator and Computer (ENIAC) required an array of industrial cooling fans to remove 140 kW from its 18 000 vacuum tubes [27].

Figure 1.11 shows the heat fluxes removed from computational systems, starting from the first mainframes that made use of vacuum tubes until the high-end computers of the new century. The Figure also includes future predictions for heat fluxes on the next computational generation for those days. It is important to highlight that the heat fluxes on computational systems did not exceed 13 W/cm^2. As a complement of the previous information, Figure 1.12 shows the minimum and maximum heat flux on computational systems until 2018, surpassing the predictions made in the Figure 1.11. Nowadays, a desktop computer of high performance may have heat fluxes close to 60 W/cm^2, while a high-end computer is above 180 W/cm^2, or even more. It means that in a period less than 20 years, the heat fluxes on micro-chips have risen twelve times. It suggests that in a short time, conventional cooling systems for computers will reach their limit.

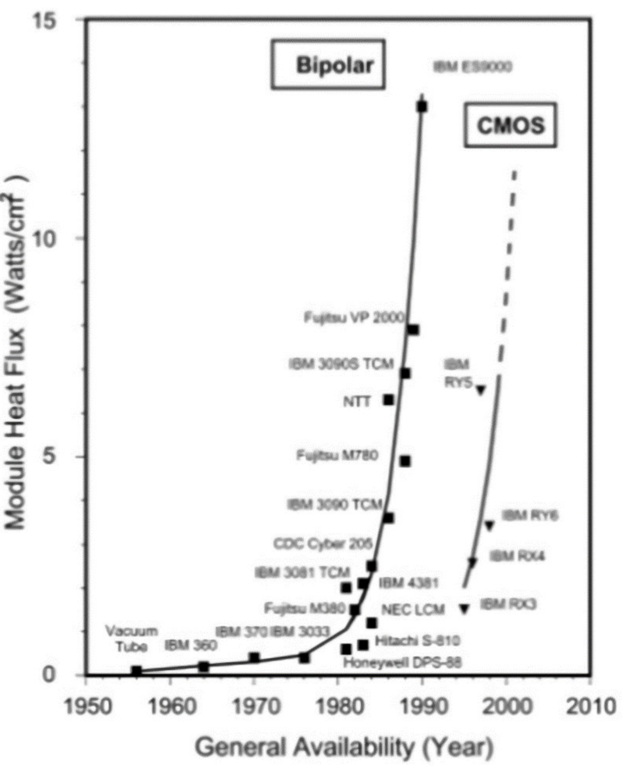

Figure 1.11 Heat fluxes on high-end computers of the past century [28].

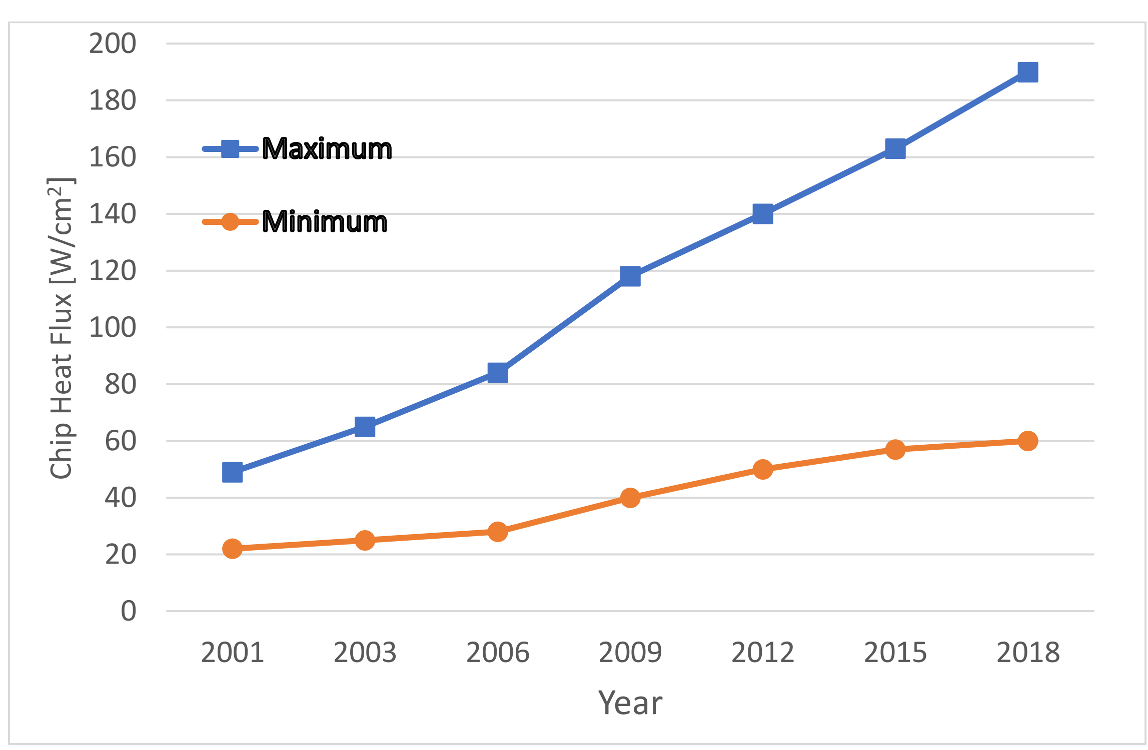

Figure 1.12 Heat fluxes on current high-performance chips [29].

According to Lasance [30], there are three reasons to explain the illustrated trends in Figures 1.11 and 1.12:

1. Designers reduced the package dimensions while increasing density power: This behavior was introduced in previous sections. Due to the new developments in computational technologies, such as the implementation of transistors, the integrated circuits, and the micro-processor invention, allowed to reduce the dimension of computational systems while their power was increased (see Figures 1.5 and 1.7).

2. The electrectronic industries let the thermal design as an afterthought: As a part of the micro-processors design process, many companies did not consider the thermal management. Only if one prototype had any thermal issue, a redesign is considered.

3. The limit of conventional cooling systems is not reached yet: Desktop computers are the most sold computers, and to accomplish its thermal requirements is implemented air cooling, supported by a heat sink and fan. In case of needing a computer with more capabilities, refrigeration by air cooling will not be enough.

1.4.2 Predicted heat fluxes on 3D IC´s microprocessors

Emerging 2.5D and 3D integrated circuits (IC’s) architectures are targeting to overcome some limitations of previous IC designs [31]. However, thermal management continues to be a challenge due to the predicted high heat fluxes in a range of 0.65-5 kW/cm^2 [32], exceeding previous predictions of 1.5 kW/cm^2 in high-performance computers [33]. In other words, predicted heat fluxes on 3D ICs processors would be at least three times higher than the actual microprocessors, this observation is only for zones with global heat fluxes.

Another design challenge is maintaining temperature uniformity in heterogeneously integrated regions, due to local heat fluxes ranging from 1.2 kW/cm^2 to 4.5 kW/cm^2 [32]. It means, it will be specific zones inside the new 3D microprocessors with bigger circuit concentration that will result in higher heat fluxes.

The overheating problem on conventional 2D ICs will become worse on 3D structures due to the dramatic increase of power density, having identical power dissipation in a smaller size [34]. Non-uniform high heat fluxes, and the predicted quantities of heat to be dissipated, make to the thermal management one of the most important points for guaranteeing the performance and reliability of the new 3D ICs processors.

Chapter 2 makes a review of the cooling methods and systems for heat dissipation on computers. It presents a brief explanation of conventional cooling systems and the new cooling approaches for the heat dissipation on 3D ICs micro-processors. Research works have shown promising experimental and numerical results for the thermal management of 3D ICs.

Chapter 2

Background

2.1 Introduction

Chapter 1 talked about the beginning of the computational systems and their evolution, having considerable improvements with the implementation of novel technologies every fifteen years. Chapter 1 background allows to understand the capabilities and limitations of current computational systems, and also gives an overview of the next computational revolution that represents the use of the tridimensional integrated circuits (3D ICs). At the same time, each computational revolution generates some problems for their designers, as is the case of the thermal management due to the increase of the heat fluxes inside the new computational systems.

As was illustrated in Chapter 1, more than fifty percent of the computer failures are due to high temperatures. Besides, there is an exponential increase in computer heat fluxes. Thus, thermal management has played a key role in keeping a satisfactory performance and reliability in the computational systems during previous 70 years. Figure 2.1 illustrates the classification of cooling technologies for computational products, generated by analyzing reviews made by Chu et al. [28 and 35]:

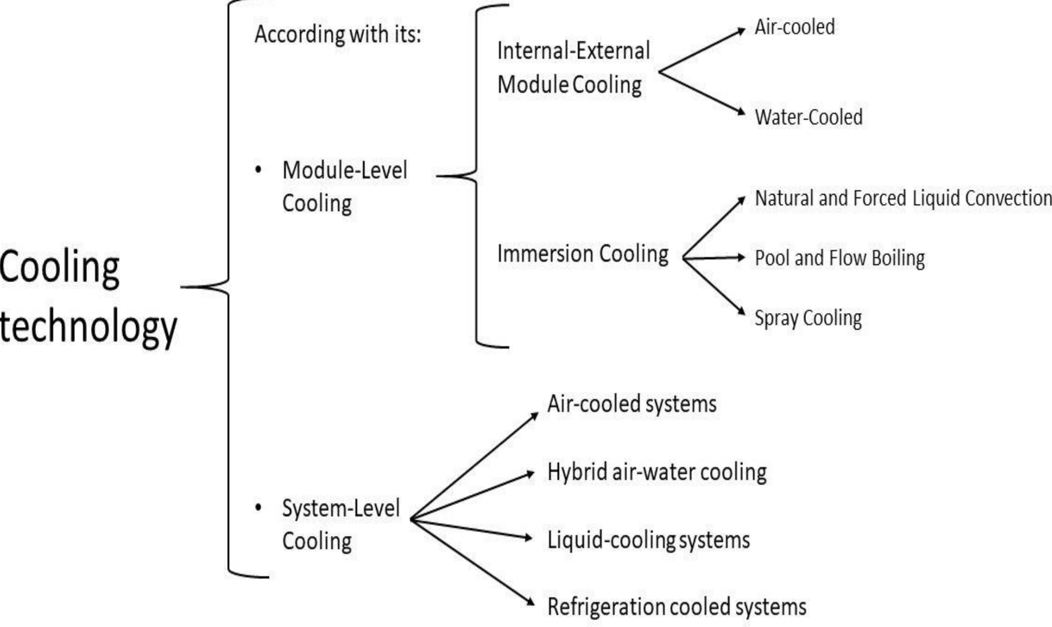

Figure 2.1 Classification of cooling technologies for computational systems.

2.2 Traditional cooling technologies for computers

Typical cooling systems on microprocessors are constituted by two parts: internal and external module cooling. Figure 2.2 gives an illustration of a traditional cooling system. It shows that the internal-module cooling is glued at the top of the chip. On the other hand, the external-module cooling is an external element that provides a considerable increase in the heat exchange area, and it is linked at the top of the internal-module by the use of thermal paste.

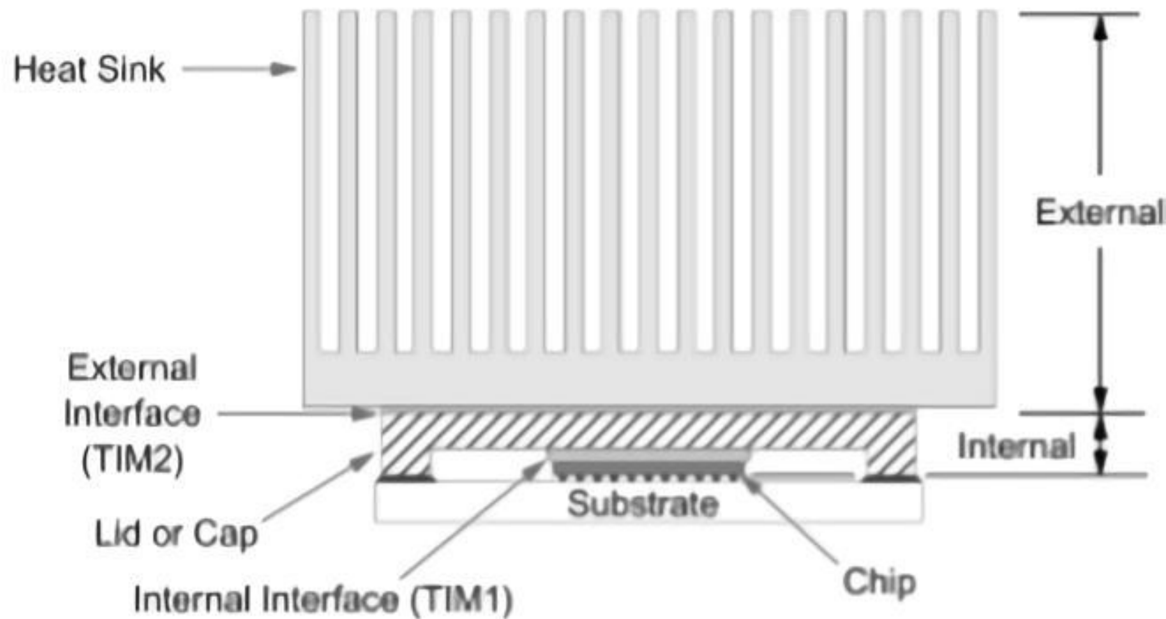

Figure 2.2 Typical cooling system on computer denoting its internal and external regions [28].

2.2.1 Internal/ External-module cooling

The internal module takes advantage of the heat conduction process to dissipate the generated heat by the chip during its operation. Therefore, this physical interaction to transfer energy between the first cooling module and the chip represents a thermal resistance to take into consideration; this is not easy to approximate due to manufacturing issues, like dimensional tolerance.

In the 1990s, when the multichip modules (MCM) were established, IBM made a novel proposal adopting a 'flat plate’ as a substrate for microelectronic integration, reducing the production cost [36]. Figure 2.3 shows the implementation of a multichip module on a flat substrate, taking advantage of a heat spreader to redirect the heat and increase the heat exchange area for a possible connection with an external-cooling module. The 'flat plate' implementation leads to better control of the thermal paste thickness (0.1-0.18 mm) and enhancements on its thermal conductivity, reducing the thermal resistant between the chip and the external-module cooling. This proposed configuration is used until nowadays.

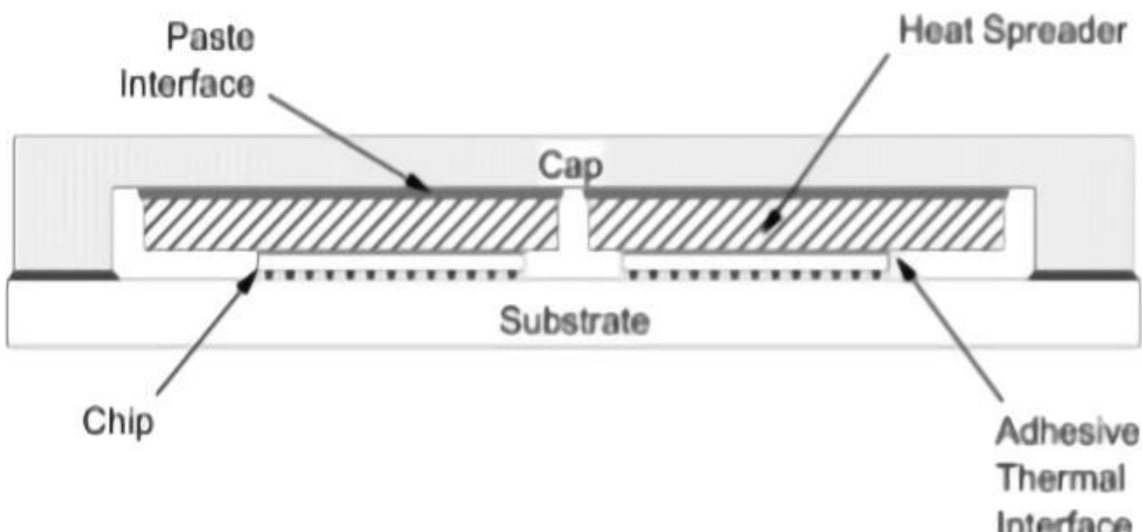

Figure 2.3 Illustration of conventional internal-module cooling for an MCM [28].

External-module cooling serves as a complement to achieve an adequate heat dissipation on a chip and/or microprocessor. Typically, this task is accomplished by attaching a heat sink or another component at the top of the chip or its internal-module cooling, looking for raising the heat exchange with the environments. The most effective method to get it is by increasing the heat exchange area using an external tool. The material selection of the external module will depend on the thermal conditions, and in a lower percentage of the cost. Usually, these external elements are made of all aluminum, all cooper, or a combination of them due to their ranges of thermal conductivity (150-390 W/m K). The implementation of a material with good conductivity will decrease the thermal resistance, improving the thermal performance.

The classification of the external-module cooling can be based on their heat transfer mechanism and type of coolant used, as are radiation and free convection, air cooling, liquid cooling, or liquid evaporation (boiling) [37].

2.2.2 Fluidic cooling (Heat sinks)

Major part of the times, air cooling systems for electronic devices make use of an external-module cooling, known as heat sinks. These devices can be supported by a fan or not (forced or natural convection), depending on the thermal management requirements. A heat sink is composed of a base of a thermal conductor material (aluminum or copper) with a considerable number of fins above the base. The fin addition increases the heat exchange area widely, allowing adequate thermal management on micro-chips. The heat sink is fixed at the micro-chip top; it conduces the heat from its base up to the fins. Consequently, the heat is transferred by convection to the air flowing between the fins. The air can flow either in a horizontal or vertical direction, depending on the fan orientation or the convection

mechanism. Figure 2.4 illustrates different heat sinks with pin-fins and wall-fins, fixed in an electronic device for guarantying the heat dissipation on it. In comparison with the capacitors and chips, the heat sinks fill a bigger space. Typical air-cooling heat sinks have dimensions close to tens of cubic centimeters [38].

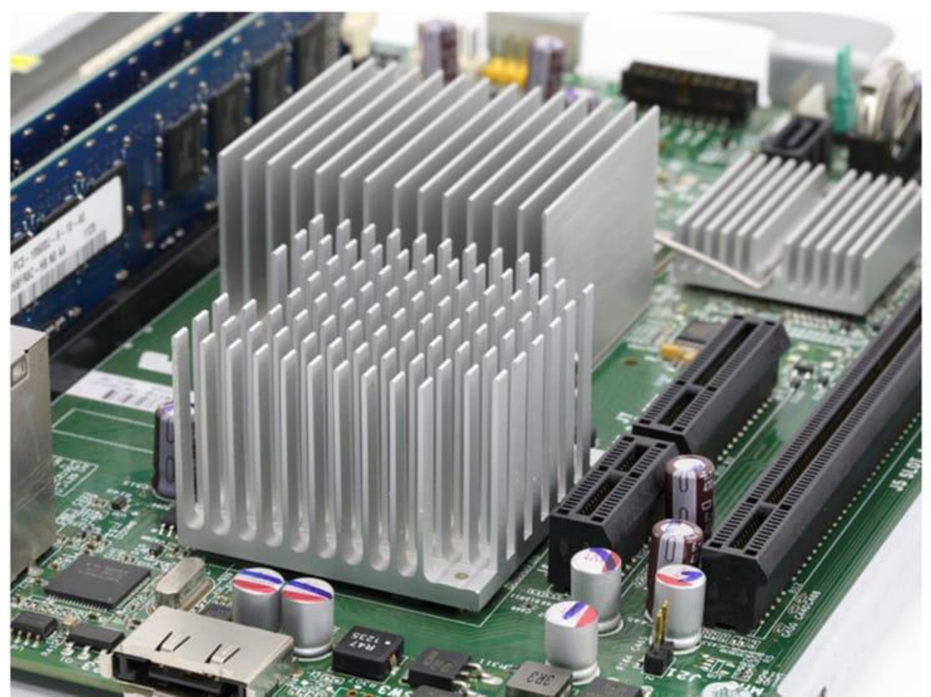

Figure 2.4 Illustration of heat sinks on electronic devices [39].

There is a significant variation on the heat sink models due to its thermal performance depends on many geometric variables such as base thickness and area, pin height, thickness, and spacing. For this reason, recent investigations in the topic focus their efforts on proposing non-uniform pin-fin arrangements varying widths and heights strategically [40-42], analyze the thermal response making perforations on the fin heat sinks [43-44], and give novel proposals considering a heat sink in rotation along with air-jet impingement [45].

When the dissipation requirements surpass the heat dissipation capacity provided by the air, it is necessary to implement another kind of coolant. Liquid coolants offer a high heat transfer coefficient to reduce possible rising temperatures on micro-chips (see Section 2.2.5). Liquid cooling requires a pump to remove the heat fluxes on micro-electronics, meaning a higher power consumption just for the heat dissipation.

One of the first liquid cooling systems were the cold plates. These were introduced in the 80s, and they work like a heat sink due to a significant part of the cold plates are finned structures that make use of fluid for the heat dissipation without having straight contact with the micro-electronics.

An interesting variation of the heat sinks is the implementation of the liquid jet impingement. This coolant technology consists on introduce a vertical flow over the device to be cooled (see Figure 2.5), being one of the most effective cooling methods due to it is capable of removing high heat fluxes with a minimum coolant flow rate [35]. The earliest investigations on this topic report a vast capacity for heat dissipation in tiny areas, using conventional coolants [46-47].

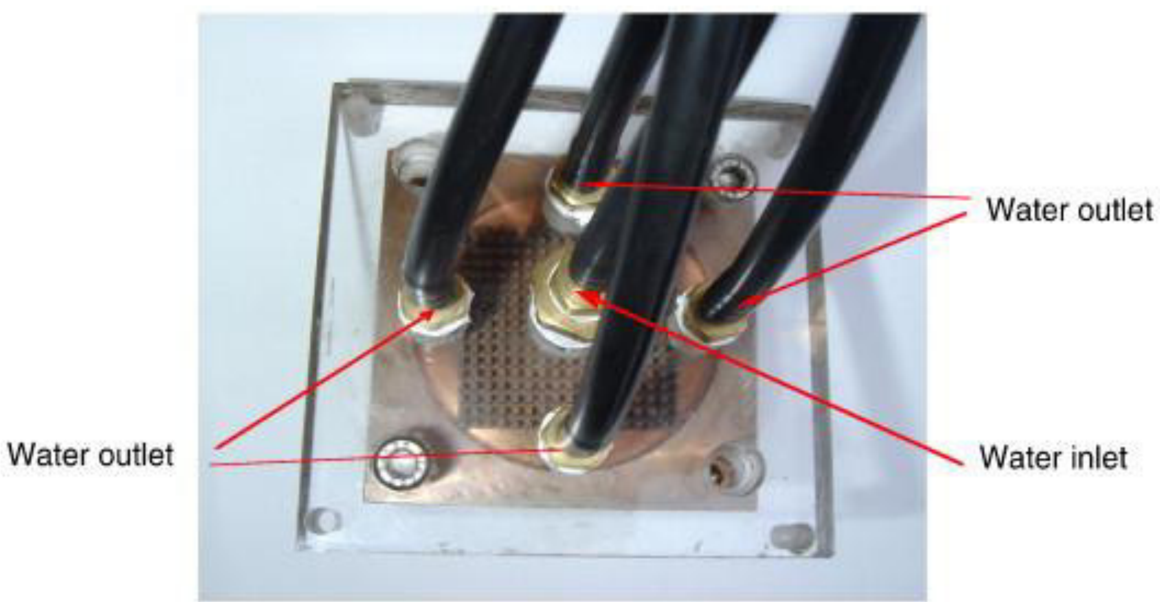

Figure 2.5 Illustration of jet impingement cooling [48].

Another liquid alternative is the immersion cooling. Unlike the cold plates, immersion cooling does not need physical walls for heat exchange. This method proposes to have the coolant in direct contact with the chips, eliminating the thermal resistance that represent the heat sinks. The heat transfer rate associated with immersion cooling depends mainly on the coolant thermophysical properties. Thus, the selection of a liquid for direct immersion cooling is a crucial point to have in consideration. The first experimental studies on this topic were carried out by Incropera [49], who tested the cooling method, using water and some dielectrics liquids (fluorocarbon liquids). The liquid variation with the immersion cooling approach allows to have a broad range of heat fluxes to be removed from the electronic devices [50].

Miscellaneous investigations make use of the liquid cooling approach for heat dissipation on electronics. Proposals such as to make modifications in the heat sink shapes to improve the thermal management are reported [51,52]. In the same way, by making variations on the heat sink inlet and outlet arrangements, it is possible to enhance the heat dissipation process on electronic devices [53-56]. Another useful alternative for the heat sink tool is the substrate material variation; some studies analyze this topic showing considerable differences in the substrate temperature [57-58].

By proposing variations on the cold plates fluid inlets-outlets, the thermal resistance on these devices can be reduced [59]. Like in the previous referred studies, when geometric modifications are analyzed using the jet impingement approach, new alternatives for the thermal management of integrated circuits emerge [48,60,61].

2.2.3 Phase-change cooling

Boiling is a complex phenomenon that involves a heat transfer process, and it will depend on the bubble formation process. Boiling may occur either as pool boiling or flow boiling. The first boiling alternative is when basically the liquid refrigerant is static, and contradictory flow boiling involves a flow rate for the energy transfer process. This cooling method may be used to dissipate higher heat fluxes than the previously presented methods. One of the first electronics package utilizing pool boiling to cool integrated circuits was developed by IBM, the Liquid Encapsulated Module (LEM) made in the 70s [62].

Due to the high heat transfer coefficient that may be achieved, the use of change-phase cooling is considered one of the main alternatives to provide heat dissipation on the next generation of high-end computers. Currently, it is possible to found in the literature some reviews that analyze flow boiling on conventional refrigerants [63] or analyze the critical heat fluxes in a saturated pool boiling [64].

2.2.4 Comparison of heat transfer capabilities

One key factor for the selection of cooling systems in electronic devices is the heat flux rate to be dissipated, depending on the heat range to be removed a cooling method could be selected or not. Figure 2.6 shows a comparison of some cooling methods, according to their heat transfer mechanism. In this figure is denoted that the radiation and free convection are not an adequate option for heat dissipation in computers, due to these alternatives count with the lowest dissipation heat flux rates. The option of forced convection using air is widely used in CPU cooling devices, due to it has an acceptable range for the heat dissipation. In addition, this alternative result to be simple, chip and reliable for modern CPUs, but it is not useful for the new high-end computers. Predicted heat fluxes on 3D ICs exceed by much the forced air-convection capabilities. On the other hand, phase-change cooling may be considered the best technique for heat dissipation on micro-electronics, followed by the forced convection of liquids. Due to these alternatives accomplish the thermal management requirements for 3D ICS (see Section 1.4.2).

It is essential to highlight that the heat transfer rate on each method will depend on many factors such as kind of coolant, inlet coolant conditions, geometrical parameters of the internal/external cooling module, and others.

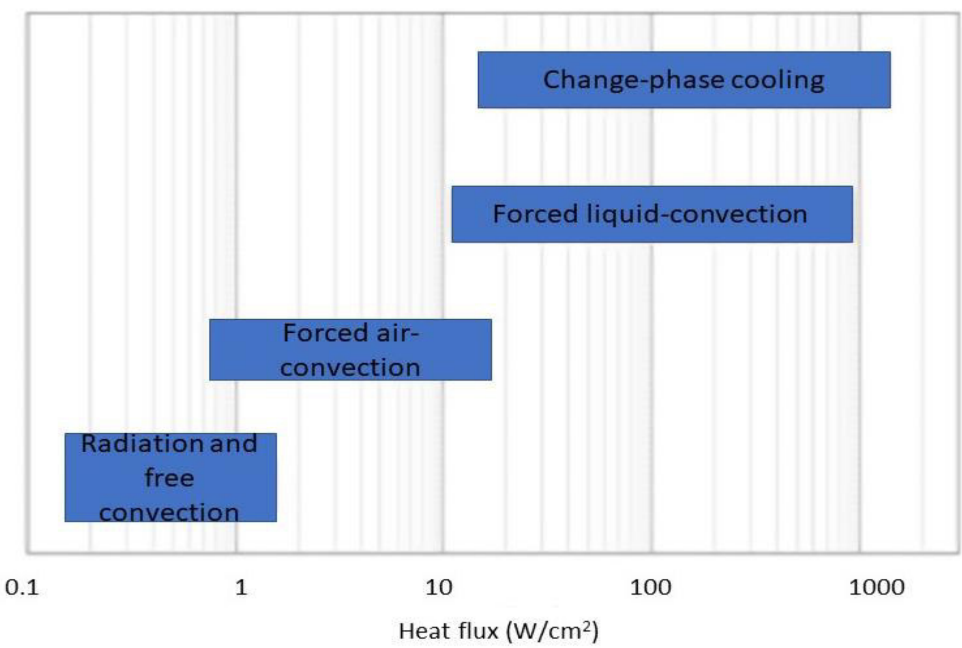

Figure 2.6 Comparisons of heat transfer capabilities of conventional methods [64].

2.3 Emerging cooling techniques

As was mentioned before, traditional external air-cooled heat sinks are not capable of providing adequate cooling to modern electronic devices with high-power densities. Cooling techniques must enhance the heat dissipation to minimize the operation temperature on microchips and maximize their longevity. Thereby, different new cooling techniques such as heat pipes, spray cooling, porous media, microfluidic cooling heat pumps, free cooling, or thermoelectric cooling have gotten attention in recent years for their development. Some of these technologies have already been used in commercial applications. This section will present an overview of the most promissory emerging cooling technologies.

2.3.1 Heat pipes

Heat pipes make use of the working fluid phase change inside them. These devices are capable of providing cooling on many electronic devices, and due to their numerous advantages such as their low thermal resistance [66], heat pipes are considered as a promissory cooling technique.

In comparison with other cooling methods, heat pipes do not have any moving parts making them reliable with minimum maintenance. So, heat pipes do not have energy consumption, hence a low operation cost, and due to their small size and weight, they have a wide application field. There are many types of heat pipes implemented in cooling applications, which are: flat heat pipes, cylindrical heat pipes, loop heat pipes, micro-heat pipes, and oscillating heat pipes.

Figure 2.7 gives an illustration of the heat pipe components and their function. They consist of a metal envelope (pipe), wick, and working fluid. As is illustrated, the working principle is the fluid phase-change inside the pipe. The envelope captures the heat from a hot section (micro-electronic) on its evaporation section and delivers the captured energy in the opposite side (condenser section). The wick is considered the central element of the heat pipe. It acts as a capillary pumping, driving the condensed fluid to the evaporator, even against gravity. More details about their function and applications can be consulted in the literature [67-70].

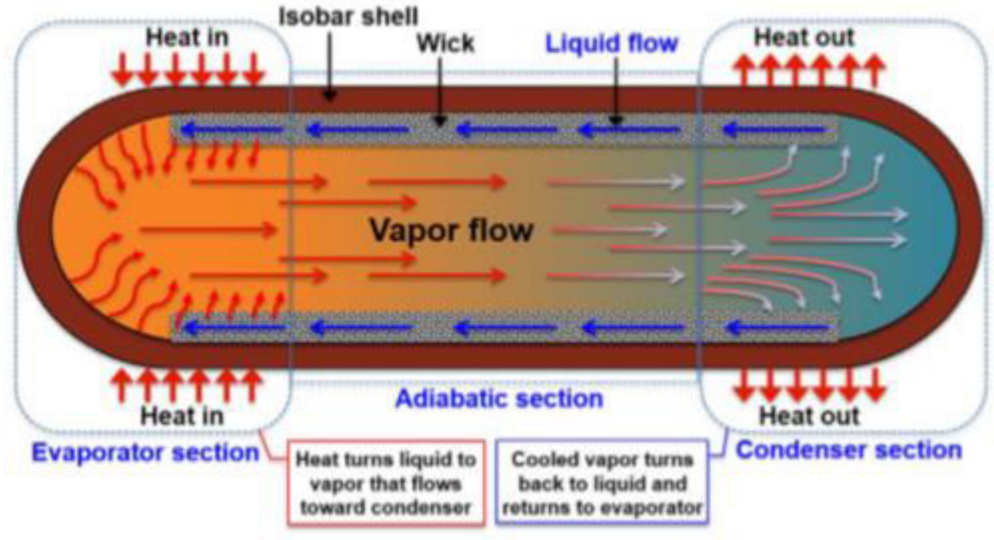

Figure 2.7 Illustration of the heat pipe and working principle [37].

2.3.2 Spray cooling

Spray cooling is a process in which little drops of liquid are sprayed on the microelectronics heated surface to reduce their temperature. This alternative can provide high heat transfer coefficient, due to its heat transfer mechanism (phase-change cooling). The surface is cooled by thermal conduction to the liquid in contact. Then depending on the heat flux, a fast evaporation may occur. By the spray method, the heat exchange area increases dramatically along with the capacity to remove heat, reducing the fluid flow rate considerably. Hence, this cooling method will reduce the operation cost, making the liquid cooling more reliable.

The first investigations on the topic date from the 90s decade [71-72], making use of fluorocarbon liquids and reporting heat fluxes of 32 and 50 W/cm^2. While more recent investigations using the method [73-74] reports higher capabilities to dissipate heat fluxes in a range of 100-500 W/ cm^2, using fluorocarbon liquids or methanol.

2.3.3 Porous media

The application of metal foams to enhance the heat sink thermal performance has received importance in the last decade. The foam, as a porous media being in contact with a liquid, rise exponentially the heat exchange area of the heat sink, improving its capacity for heat dissipation. Typical materials of metal foams are aluminum and copper alloys. The variations on the foams depend on the porosity and pore density. The first parameter represents a fraction of how much space may be occupied by the fluid inside the metal foam, and the second one is a way to measure the metal foam average number of pores.

Two types of heat sinks make use of the porous media, finned metal foam heat sink (FMFHS), and metal foam heat sink (MFHS). The FMFHS is a finned heat sink with a metal foam added by pressure, while the MFHS is only a metal foam fixed at the top of a micro-electronic for the heat dissipation (see Figure 2.8). On its own, an MFHS is capable of dissipating heat fluxes up to 140 W/cm^2, keeping and adequate temperature for electronic devices with low-pressure drop [75]. Whereas the FMFHS removes heat about 1.5-2.8 times more than an MFHS when both have the same dimensions and same flow rate [76].

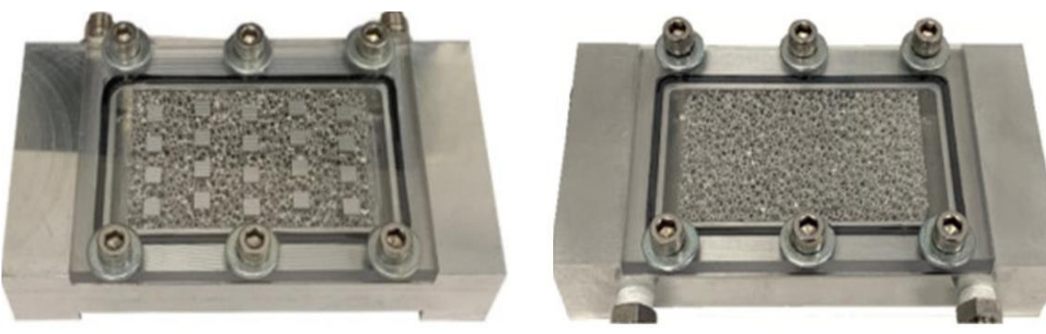

a) Finned metal foam heat sink b) Metal foam heat sink

Figure 2.8 Illustration of porous media heat sinks [77].

2.4 Microfluidic cooling

As a part of the emerging cooling technologies for electronic devices, microfluidic cooling represents one of the most promissory alternatives for the 3D ICs cooling. It consists of the manipulation and control of fluids on a sub-millimeter scale to provide cooling on microelectronic devices. This cooling method has been impulsed in previous years by the U.S. Defense Advanced Research Projects Agency (DARPA), with the launch of Intra/Inter Chip Enhanced Cooling thermal packaging program. The present research project is based in one work in microfluidic cooling, financially supported by DARPA at Georgia Institute of Technology (Georgia Tech).

Figure 2.9 shows a proposed division of microfluidic cooling systems, made by the thesis author. The proposal is based on the bibliographic review carried out, and basically divide microfluidic cooling in two topics: embedded systems and other approaches.

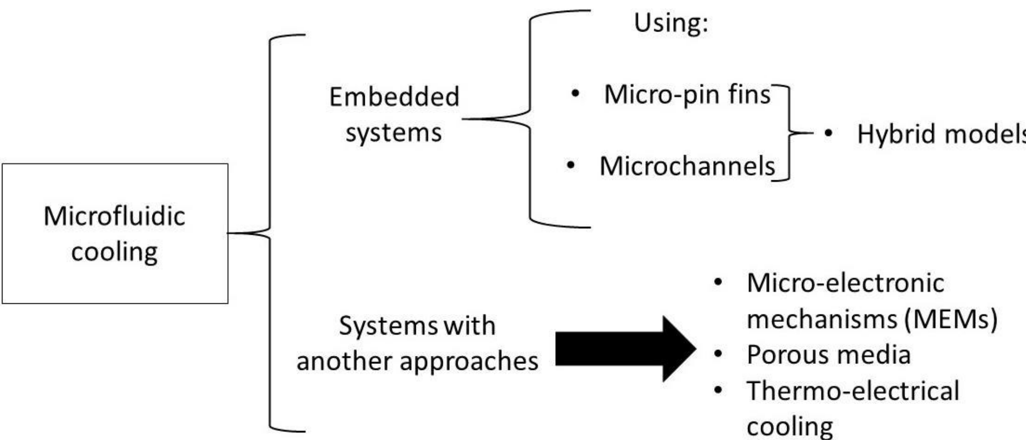

Figure 2.9 Proposed division of microfluidic cooling systems.

2.4.1 Embedded micro-pin fins.

The stacking on tri-dimensional integrated circuits (3D ICs) makes impossible to put an external-module cooling on each die for the heat dissipation. Thus, the solution for this problem is in improving the heat dissipation capacities of the internal-module cooling on micro-electronics, being embedded systems an alternative.

Embedded micro-pin fins consist of micro-structures with a diameter less than 50 µm (lower than the hair diameter), implemented to increase the heat exchange area like a heat sink in fewer scales. These structures are manufactured by lithography on the same silicon die than the micro-electronics. It means that the micro-chips and its micro-heat sink will be printed on opposite sides of the same silicon plate. Figure 2.10 illustrates a silicon die with embedded pin fins; the finned area is about 1 cm x 1cm. Also, it illustrates a pin-fin density change for the thermal management of zones in 3D ICs with higher heat fluxes (hotspots), due to a major circuit concentration. A zoom to denote the finned system is included, due to at first view is hard to identify the pin fins with clarity.

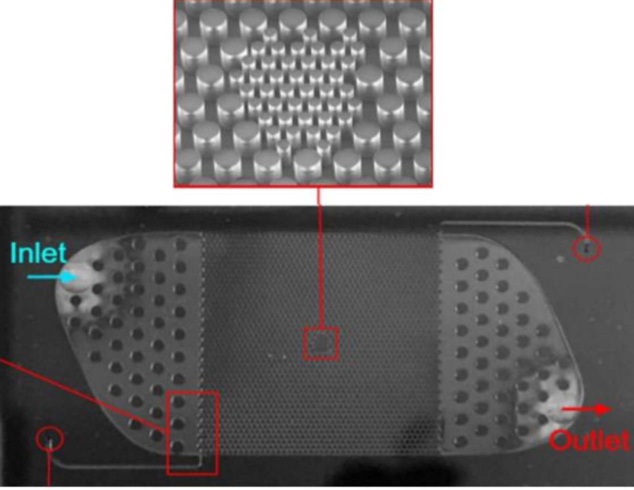

Figure 2.10 Illustration of embedded pin-fins for microfluidic cooling [78].

As recent investigations in the topic; Sarvey et al. [79] reported an experimental investigation employing pin fins with circular and hydrofoil cross-sections in embedded microfluidic configurations. The investigation considers a hotspot and an entire channel with a pin fin density increase (see figure 2.11). For low fluid flow rates (80 mL/min), the hydrofoil profile gives lower thermal resistance, whereas, for flow rates up to 140 ml/min, circular profiles are a better option. Pin fin density increase over a complete gap has a considerable repercussion on the pressure drop, increasing it more than 20 kPa for high flow rates. The influence of different parameters on the pressure drop and thermal behavior also was reported with temperature gradients close to 70°C in hotspot zones for heat fluxes of 625 W/cm^2 and different fluid flow rates.

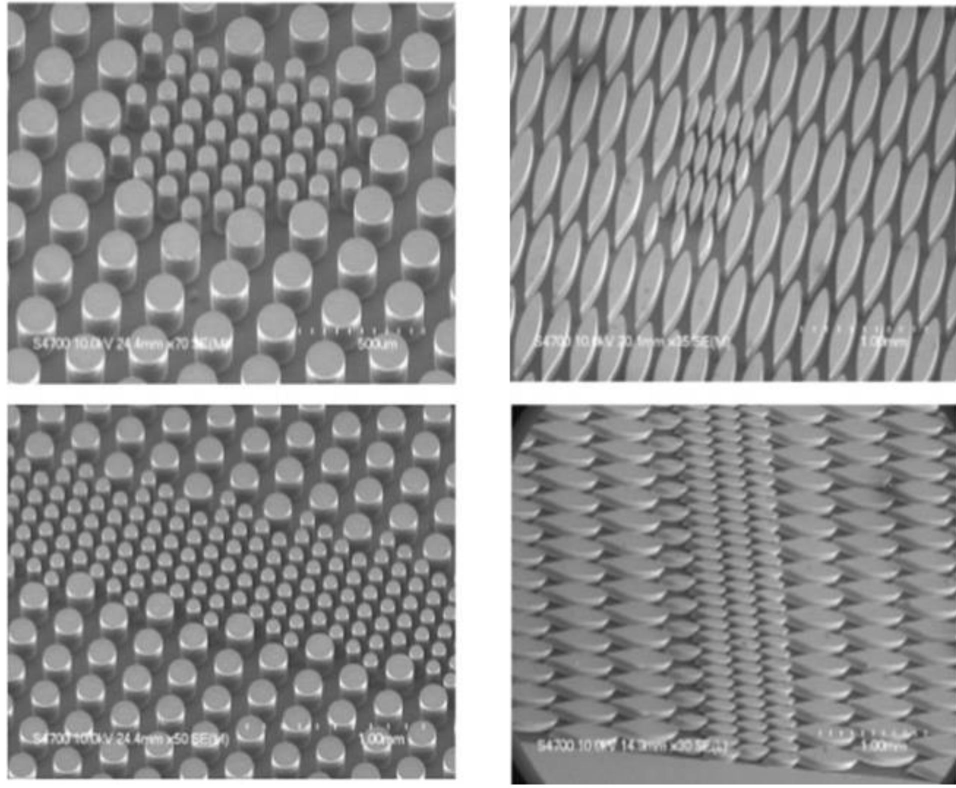

Figure 2.11 Embedded pin fin arrangements proposed by Survey et all. [79].

Lorenzini et al. [78, 80] reported experimental and numerical results for single-phase and two-phase microfluidic cooling with identical embedded pin-fins. Variable pin-fin density for non-uniform heat fluxes (250-750 W/cm^2) were assessed to obtain the thermal and hydrodynamic behaviors on this kind of micro-gaps systems. Maximum temperatures below 60 °C with a pressure drop of 120 kPa were reported, when the fluid inlet temperature is 21.3 °C. Figure 2.12 shows the temperature behavior through the micro-heat sink using different heat fluxes for the model validation. Temperature differences do not surpass 3 °C between experimental and numerical results. Figure 2.13 illustrates the velocity and temperature contours obtained from this study; adequate temperatures are kept for the micro-chips operation with a fluid flow rate close to 200 ml/min.

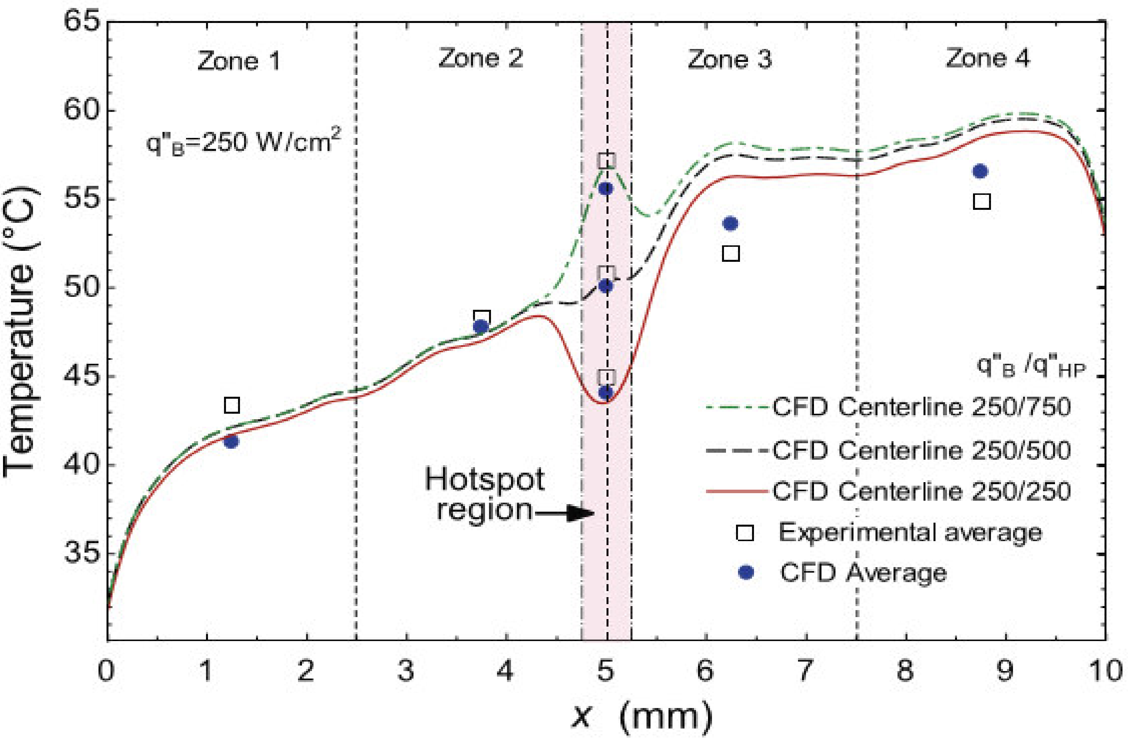

Figure 2.12 Validation of Lorenzini numerical model [78].

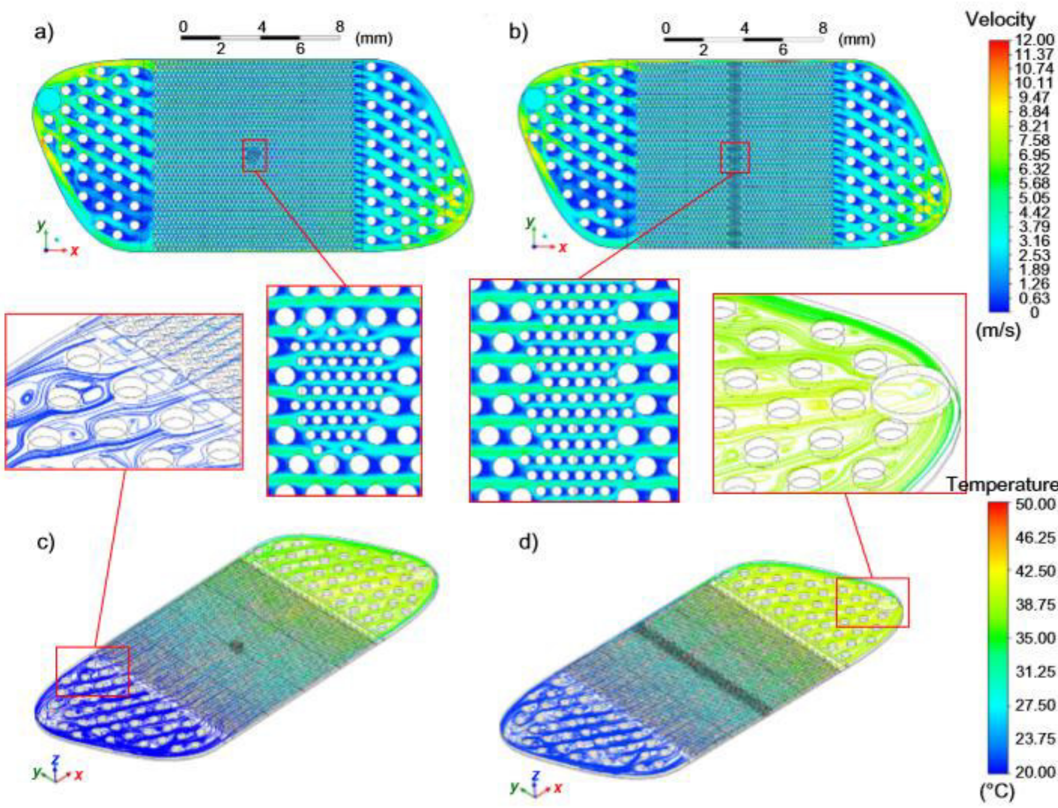

Figure 2.13 Velocity and temperature contours reported by Lorenzini et al. [78].

Feng et al. [81] numerically investigated embedded micro-gaps, with micro pin-fin gradient arrays to achieve better temperature uniformity, Figure 2.14 shows the proposed gradient arrays. At the same time, the pin fin height is reduced, and the pin fin density increased, having as a consequence the variation of the thermal resistance. The numerical model was compared against Lorenzini results [78], getting good approximations not upper to 2.1°C. Peak temperatures of 80 °C with maximum temperature gradients of 60 °C were reported using a constant heat flux of 500 W/cm^2. Also, temperature uniformity is reported in the numerical domain, demonstrating the proposal effectiveness.

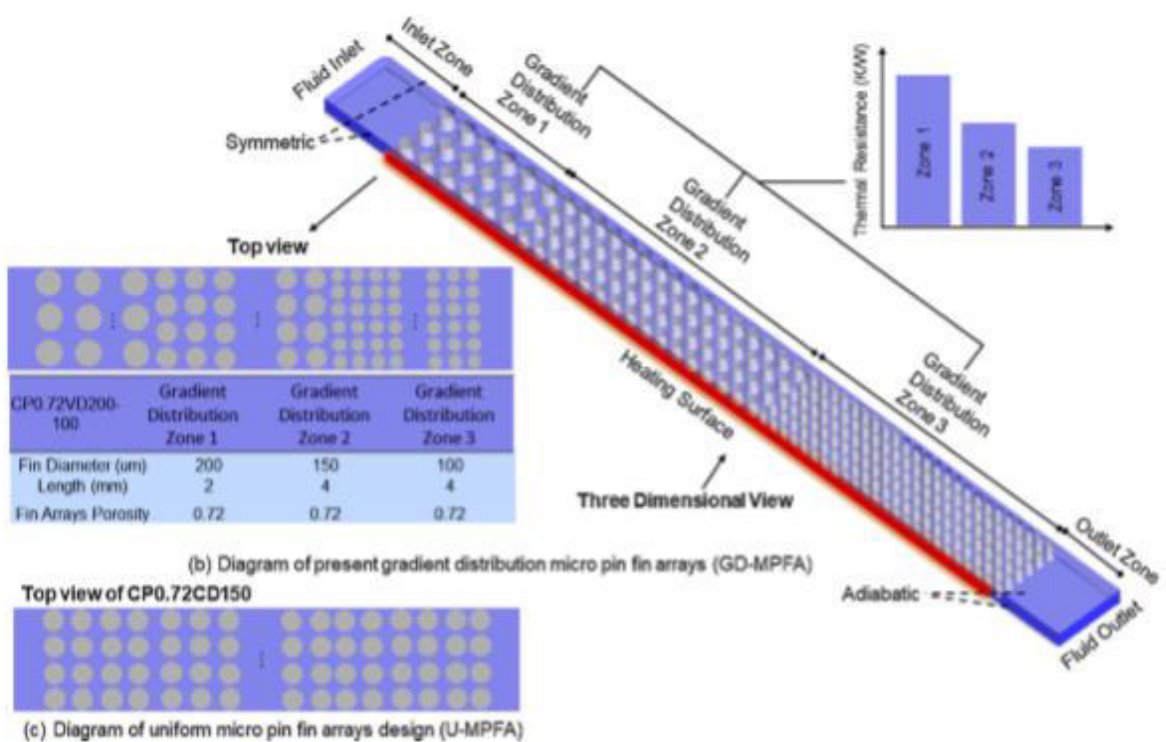

Figure 2.14 Illustration of micro-pin fins gradient array proposed by Feng et al. [81].

2.4.2 Microchannels

In 1981, Tuckerman and Peace [82] proposed the microchannels as an advanced cooling solution, by the use of a water-cooled microchannel they achieved to dissipate a high heat flux of 790 W/cm^2. Ever since, microchannels have been widely investigated, being the most acceptable microfluidic cooling alternative along with the embedded micro-pin fins. They consist of micro-structures used for flow routing, designed to provide cooling on zones of interest in micro-electronics.

Samal and Moharana [83] report current investigations in the topic, the authors numerically analyzed the thermal behavior in a proposed micro-channel with recharges in single-phase flow, through a simplified numerical model. The authors reported better temperature uniformity in comparison with a conventional micro-channel, with peak temperatures

below 50 °C and a pressure drop of 0.5 kPa for a constant heat flux of 10 W/cm^2, considering a coolant inlet temperature of 27 °C. Figure 2.15 shows the temperature contours comparison for both single microchannel (SMC) and the proposed recharging microchannel (RMC). Thermal management is improved by the RMC, keeping practically a constant temperature of 42 °C through the complete channel.

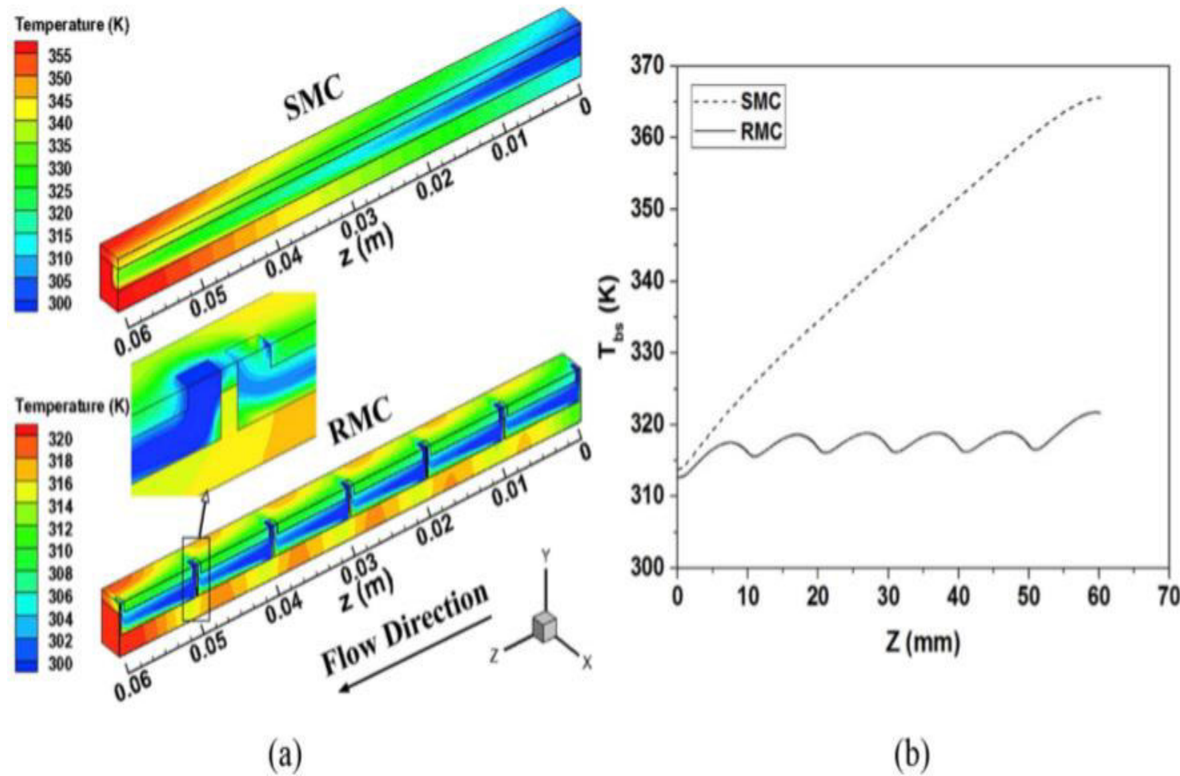

Figure 2.15 (a) Temperature distribution and (b) axial variation of substrate bottom surface temperature for both simple microchannel (SMC) and recharging microchannel (RMC).

Another proposal that makes a different variation on microchannels arrays was developed by Wu et al. [84]. The authors proposed a 3D numerical model, applying a genetic optimization algorithm to decrease surface temperatures for non-uniform heat fluxes. By the variation of local parameters such as channel and wall width, it is possible to calculate the temperature field based on a thermal resistance analysis. Once fixed the boundary conditions, the proposed genetic algorithm makes iterations, looking for reducing temperature fields. Reported results are compared against commercial software (Figure 2.16). The optimized configuration offered temperature uniformity on the chip base with temperatures close to 70 °C for a maximum heat flux of 200 W/cm^2.

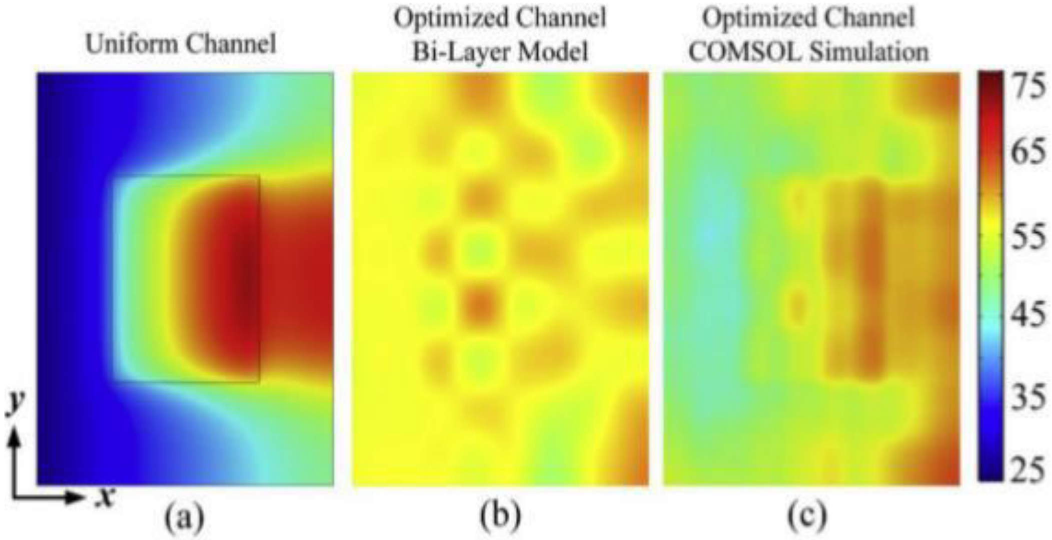

Figure 2.16 Thermal behavior comparison of a surface with cooling provided by a uniform microchannel array (a), against optimized channel array (b) and validated by COMSOL (c).

In comparison with previous numerical models, experimental studies by Drummond et al. [85] examined hierarchical microchannel heat sink arrays (Figure 2.17), using coolant in phase change. They reported temperature gradients less than 69 °C when the coolant inlet temperature was 59 °C and pressure drop below 120 kPa for a maximum heat flux of 1,000 W/cm^2.

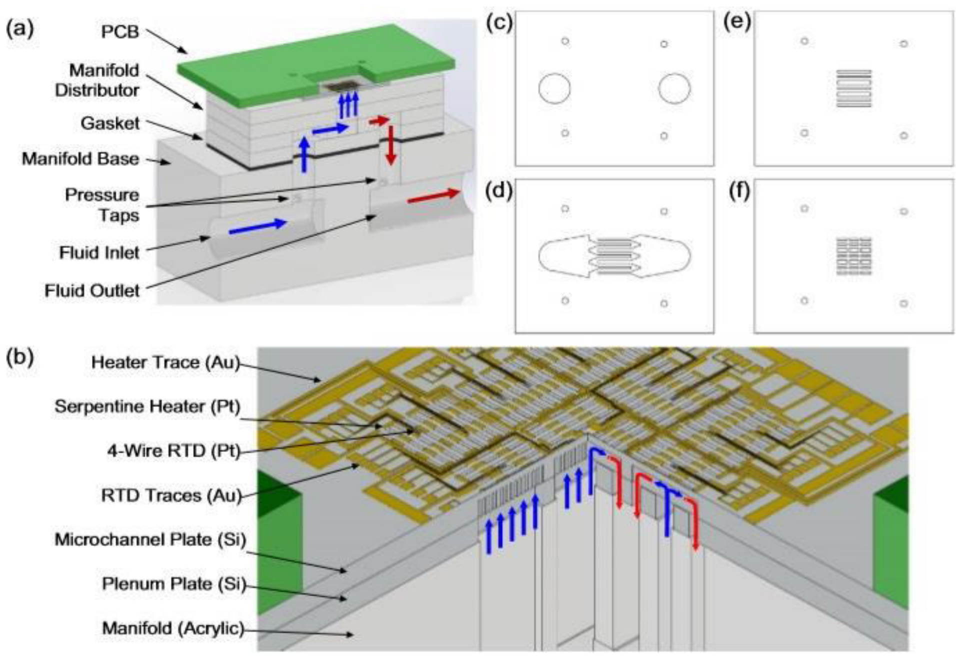

(a) CAD image of the test vehicle with a half-symmetry section removed and fluid inlets (blue) and outlets (red) shown; (b) zoomed-in view of the quarter-symmetry section removed showing the fluid flow paths in the test chip; and (c–f) each plate level of the manifold distributor used to deliver fluid sinks. (For interpretation of the references to color in this figure legend, the reader is referred to the web version of this article.)

Figure 2.17 Illustration of the test vehicle and proposed hierarchical microchannel array by Drummond [85].

2.4.3 Hybrid models

Hybrid models make use of microfluidic cooling systems previously shown; microchannels and micro-pin fins. These take advantage of the flow routing provided by the microchannels and the hydrodynamic boundary layer breaking generated by micro-pin fins. Wang et al. [86] report one of the first experimental works on this topic. They investigated the flow and thermal behavior of a hybrid microfluidic cooling system of one micro-pin fin inside a microchannel for different Reynolds numbers, using a heat flux of 10.7 W/cm^2 with maximum experimental temperatures close to 64 °C, and maximum temperature gradient of 37 °C. Figure 2.18 shows the pin-fin influence in the thermal behavior of the proposed test vehicle for different Reynolds numbers. Experimental results are compared against numerical results, getting a better accuracy for low Reynolds numbers.

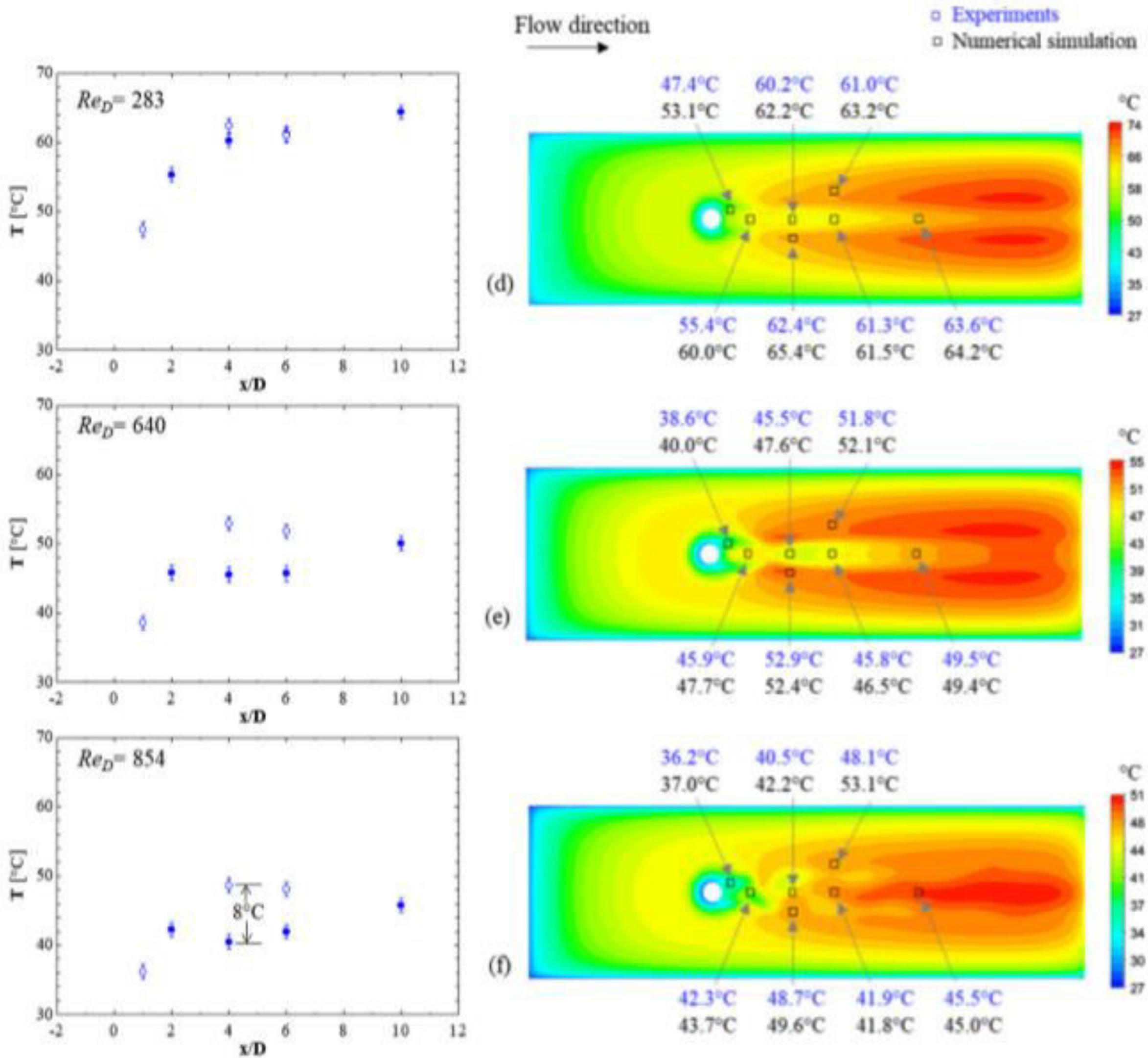

Figure 2.18 Numerical and experimental thermal results obtained by Wang et al. [86].

Ansari and Kim [87] presented a parametric model of microchannel arrays containing micro-pin fin arrays (hybrid model) to dissipate higher heat fluxes on hotspots zones (Figure 2.19), obtaining temperature gradients under 50 °C with a maximum heat flux of 900 W/cm^2. Figure 2.20 shows the temperature contours, comparing results from a non-hybrid rectangular microchannel (NH-RM) against a proposed microchannel-pin fin hybrid (H-MPF), for different heat fluxes on the hotspot and a fixed heat flux of 50 W/cm^2 in the rest of the model. The study demonstrates a better thermal management when the micro-pin array is used on the hotspot zone.

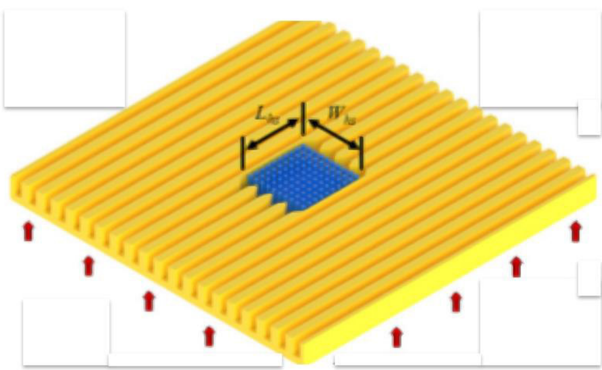

Figure 2.19 Illustration of hybrid microfluidic cooling system.

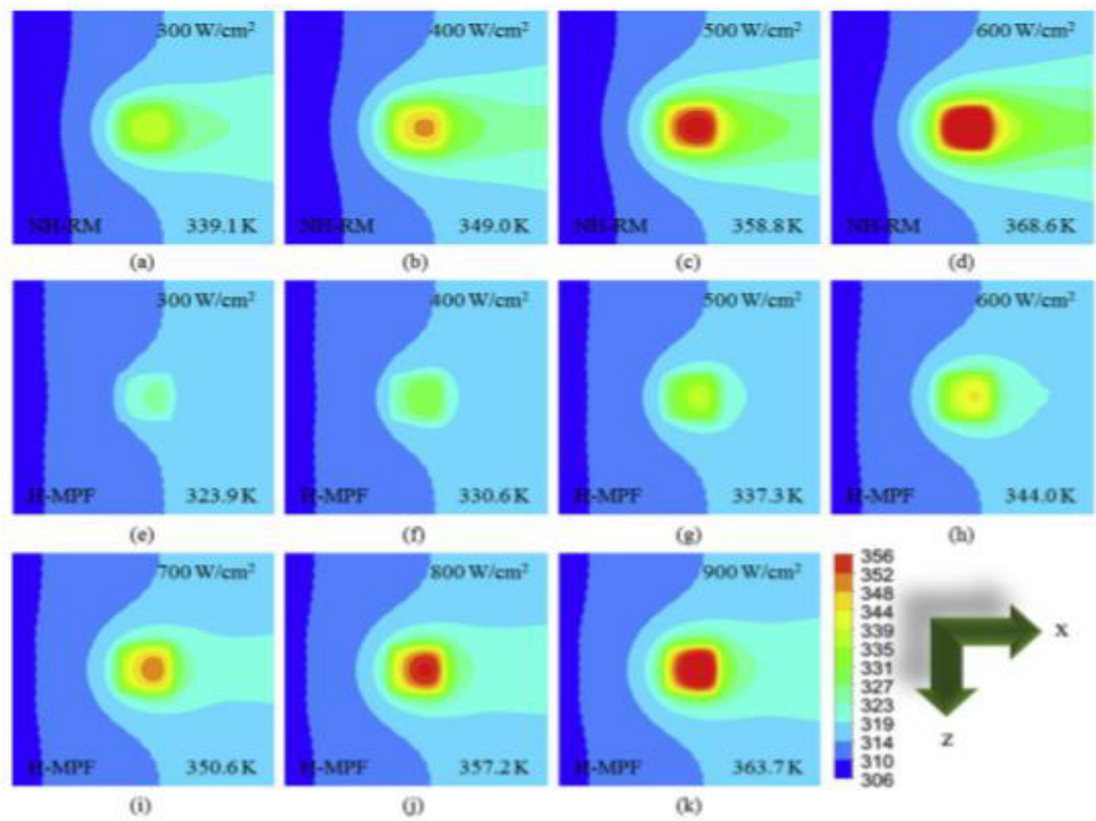

Figure 2.20 Temperature contour for both NH-RM (a-d) and H-MPF (e-k), using different heat fluxes on the hotspot zone.

The reviews by Mohammadi et al. [88] and Wang et al. [89] summarize the extensive development of experimental and numerical models analyzing variations in geometrical parameters, or in the boundary conditions to get a better understanding and to make improvements in microfluidic cooling system configurations previously shown.

2.4.4 Other approaches

At the same time, there are non-common alternatives used to cool microelectronic systems such as the presented by Yuki et al. [90] that developed lotus type foam made of copper, taking advantage of the coolant phase change, having a heat exchange upper to 100 W/cm^2. With their proposal. Kunti et al. [91] show a different concept for heat dissipation on micro-processors, developing a numerical cooling analysis based on thermo-electrical interactions. The main idea of this new concept is to induce movement in a working fluid, taking advantage of the thermal and electrical energy contained on microelectronics to cool nearby areas.

A novel micro cooling dispositive called EWOD is developed and tested by Bindiganavale et al. [92], EWOD provides little drops of electric coolant to hot areas of interest in micro-chips. Drops supplied by the micro-electronic mechanism remove the heat from the chip, until their phase-change, then the follow drop will be introduced to continue the cooling process.

2.5 Thesis objective

The present work analyzes the dissipation process of high heat fluxes on microfluidic cooling systems, searching for an adequate performance on microprocessors, dynamic random-access memories (DRAM), and graphic processor units (GPU) of the last generation. This goal will be accomplished via the use of statistical tools and the finite volume method, determining parameters, and relations of interest for the design of these micro-heat exchangers.

2.5.1 Particular objectives

1.1 Generate a numerical methodology for the replication of experimental results on micro-heat exchangers previously made, through the implementation of specialized software.

1.2 Propose new numerical models through the variation of some parameters of interest for the design of microfluidic cooling systems, using the previously established numerical methodology in the validation model.

1.3 Obtain useful statistical conclusions taking advantage of the Design of Experiments theory (DoE), using the compiled information.

1.4 Analyze the obtained results to propose new designs, looking to get global improvements in the cooling performance by the proposed micro-systems, using different statistical tools.

Chapter 3

Numerical procedure

Chapter 2 talked widely about the cooling systems on computers and how conventional cooling systems are not capable of providing adequate heat dissipation on 3D ICs. Microfluidic cooling results to be an excellent alternative to get a good heat dissipation in the next generation of high-end computers. Currently, many researchers focus their efforts on generating new microfluidic cooling proposals for thermal management on microchips. The new approaches make use of optimization algorithms, experiments to evaluate their performance, proposing new geometries, hybrid models, pin fin arrays, and more.

The present work develops a numerical methodology for the evaluation of different microfluidic cooling systems, making parametrical variations. Compiled information will be useful to propose improvements on the thermal management, by the use of statistical tools such as design of experiments (DoE) theory.

3.1 Computational domain

The analyzed computational domains are a geometrical simplification of a microfluidic cooling system with embedded micro-pin fins on a silicon chip useful for 3D and 2.5D IC architectures, proposed by Lorenzini et al. [78]. The original model consists of a finned system with an active heated area of 1 cm by 1 cm in a silicon stratum. It has a central hotspot of 0.5 mm x 0.5 mm with a pin fin density increase for non-uniform heat fluxes and plenums with thicker pin fins, which serve as structural supports. The described system is shown in Figure 3.1. The model was experimentally tested and validated numerically, getting good approximations (see Figure 2.12).

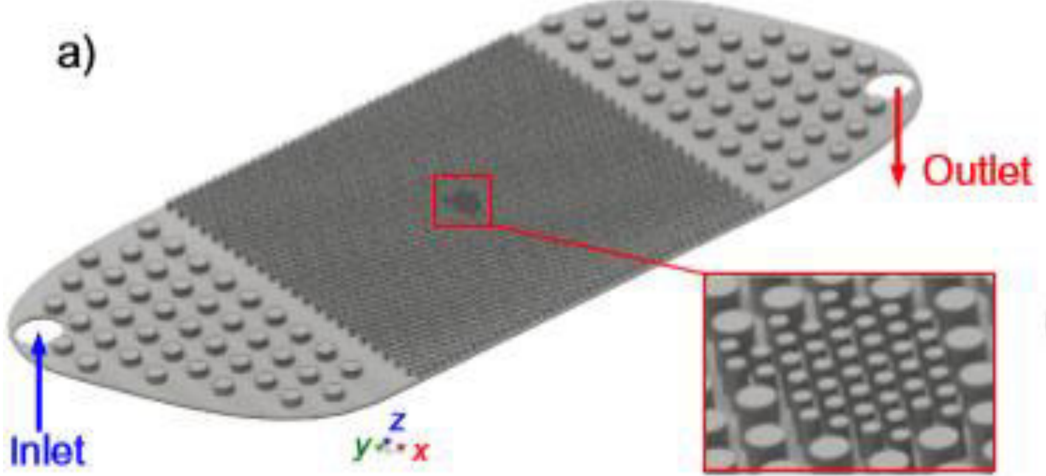

Figure 3.1 Microfluidic cooling system analyzed by Lorenzini et al. [78].

The reduction in the microfluidic cooling system allows proposing parametrical variations and generating similar models, reducing the computational times enormously at the expense of not capturing the entire physics of the thermal issue.

The reduced geometry is composed of a micro-gap strip portion with embedded pin fins, illustrated in detail in Figure 3.2. The total length of the micro-gap is 12 mm, with a heated length of 10 mm and entrance and exit lengths of 1 mm each. Zones 1 to 4 of the silicon chip are subjected to a constant heat flux. Pin fins have a diameter of 150 µm, a height of 200 µm, longitudinal and transversal spacing between pin-fin centers are equal (S_T=S_L=225 µm). The model has non-uniform heat flux inputs, a single hotspot zone is included at the center of the micro-gap with a length of 500 µm. Smaller diameter pin-fins (pin-fin density increase) are considered at the hotspot zone to decrease high-temperature gradients in this area. Smaller pin-fins have a diameter of 75 µm, and a longitudinal and transversal spacing is reduced by half (S_t=S_l=122.5 µm). Thus, the increase in pin-fin density is four times the previous pin-fin density per mm of longitudinal section. Finally, the pin fins have a uniform height of 200 µm, with a silicon layer base thickness of 50 µm, and a micro-gap width of 450 µm.

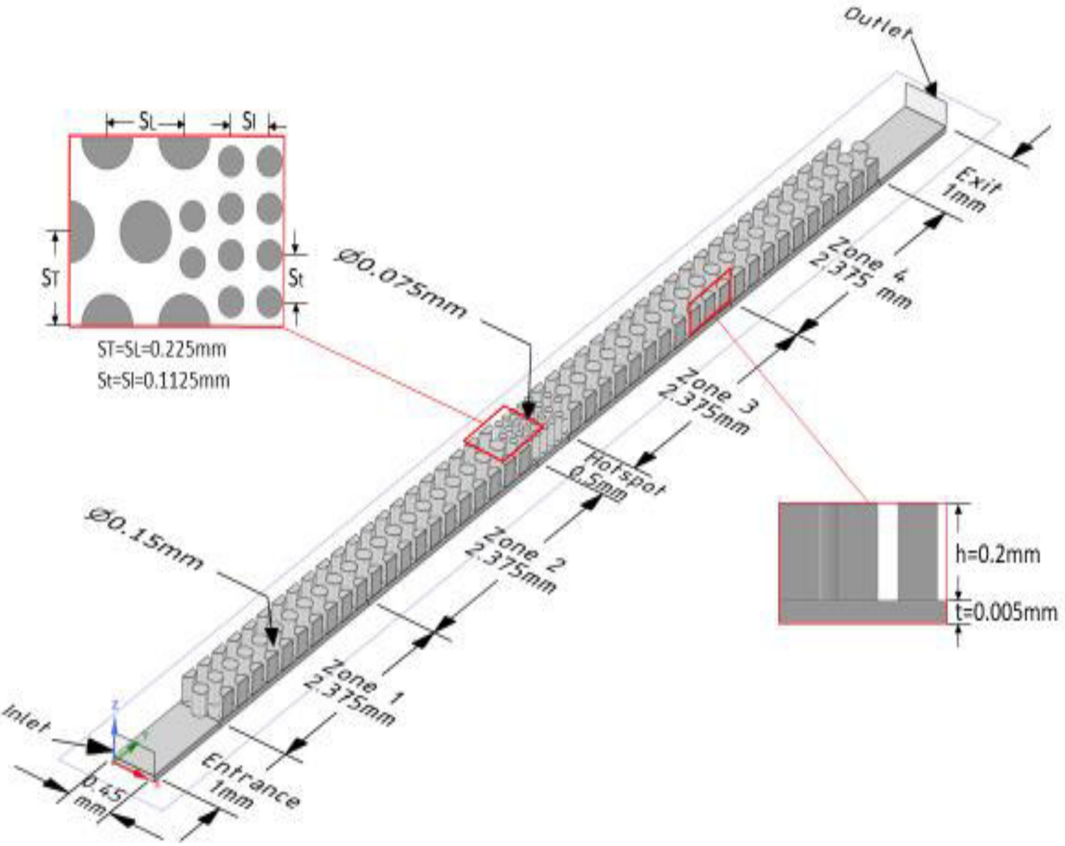

Figure 3.2 Geometric illustration of the portion of a silicon micro-gap with embedded pin fins.

3.2 Considerations

The numerical model is based on the following assumptions:

- Steady state. The proposed microfluidic cooling systems must keep an adequate temperature in all the microchip area during its operation. Thus, the cooling system must be evaluated in stationary state at top operation conditions to guarantee an adequate thermal management.

- Laminar and incompressible flow. The applied working fluid is liquid at not too high velocities and pressures, being right an incompressible flow assumption. Regarding the laminar flow, it is necessary to approximate the Reynolds number (Equation 1), which evaluates the inertial and viscous forces on the fluid to describe its movement.

$$Re = \frac{\rho v D_h}{\mu} \qquad (1)$$

Based on previous studies [77-80], velocity fields for similar models do not exceed values up to 10 m/s (validated in the Section 4.2). In addition, the maximum hydraulic diameter (D_h) of the proposed microfluid system is small, supposing a low Reynolds number, and in consequence, laminar flow in the fluid domain. As a quick approximation in the numerical model, the maximum possible Reynolds number is close to 250.

- Radiation and viscous-dissipative effects are negligible. Due to the numerical model will not present high velocities and temperatures, heat transfer by radiation and viscous-dissipative effects may not considered.

- Uniform fluid flow rate. The complete model presented by Lorenzini [78], counts with a fluid flow rate of 190.66 ml/min distributed in twenty-two channels. So, an equal and uniform flowrate is assumed on each micro-gap.

3.2.1 Thermophysical properties.

The working fluid is des-ionized water (DI-water), looking for avoiding electrical problems in the 3D ICs and obstructions in the micro-heat sinks. Whereas, the stratum material is silicon, due to the embedded systems will be printed in the same plate than the integrated circuits. The thermophysical properties of DI-water and silicon are shown in Table 3.1.

Table 3.1 Thermophysical properties of water and silicon.

Property	*Symbol*	*Water*	*Silicon*
Density (kg/m³)	$\rho,\ \rho_{\mathrm{si}}$	998	712
Specific heat (J/kg K)	C_p, c	4182	2330
Thermal Conductivity (W/m-K)	$k,\ k_{\mathrm{si}}$	0.6	Eq. (3)
Dynamic Viscosity (Pa. s)	μ	Eq. (2)	-

The dynamic viscosity of the water is considered as a polynomial function of the temperature T (K), expressed by the Equation 2 [93]. This consideration is made due to; the dynamic viscosity is a susceptible property to temperature variations, which may lead to overestimate the pressure drops on the order of 30% if a constant value is assumed [94].

$$\mu(T) = 1.6109 - 0.0235T + 1.3830\,x10^{-4}T^{2} - 4.069x10^{-7}T^{3} + 5.9942x10^{-10}T^{4} - 3.535x10^{-13}T^{5} \quad (2)$$

The heat conduction via silicon represents the highest thermal resistance in the cooling system. In consequence, for getting a better accuracy in the temperature fields, the thermal conductivity is also modeled as temperature-dependent with a third-order polynomial expression, as represented in Equation 3 [95].

$$k_{si}(T) = 2122.1 - 16.765T + 4.8183\ x10^{-2}T^2 - 4.7442x10^{-5}T^3 \qquad (3)$$

Equations 2-3 are shown in Figures 3.3 and 3.4 to illustrate variations in the water viscosity and silicon thermal conductivity respectively, as a function of the temperature. As was mentioned, both thermophysical properties have a straight repercussion in the pressure drop and the thermal management of the microfluidic cooling system. In a range of interest, the water dynamic-viscosity presents a maximum variation close to 18%. Whereas the silicon thermal conductivity may have a variation of 30% in the same temperature range, highlighting the importance of considering this parameter as a temperature function.

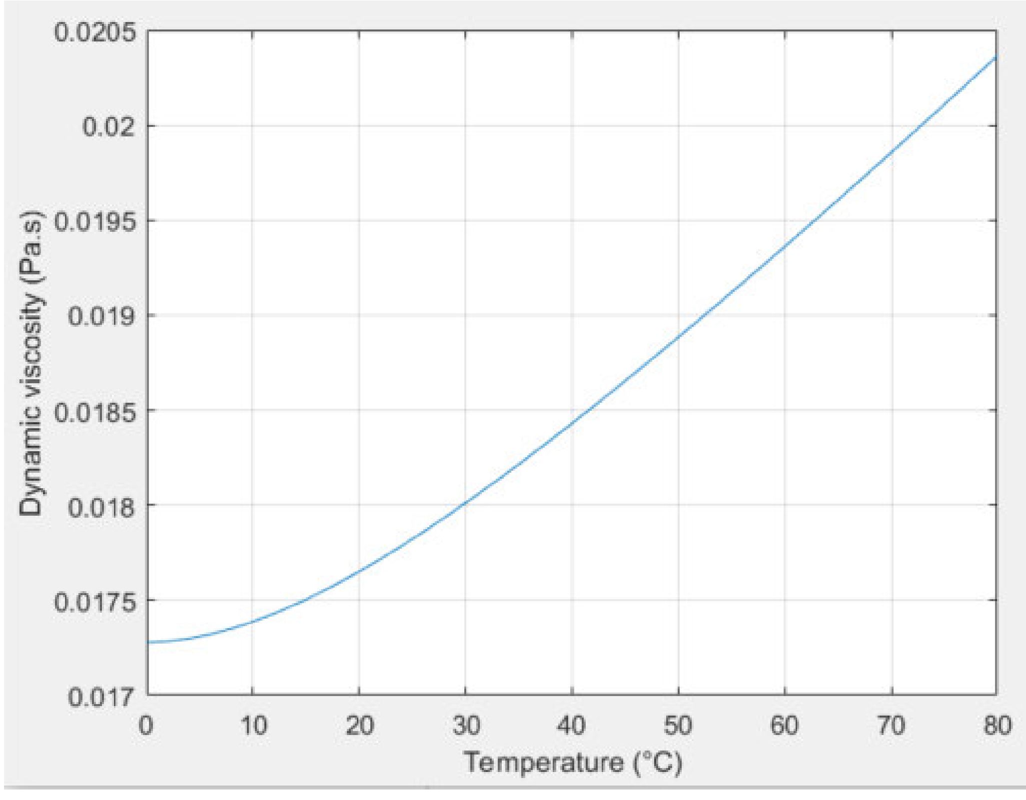

Figure 3.3 Graphic of water dynamic viscosity relation with the temperature.

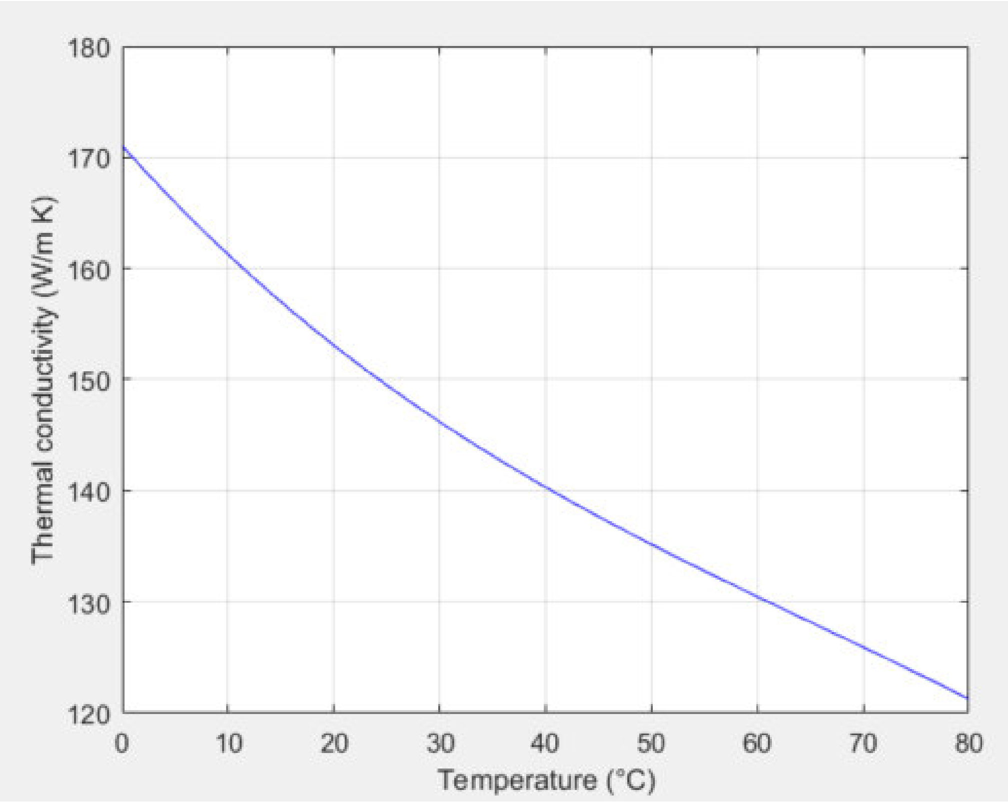

Figure 3.4 Graphic of silicon thermal conductivity relation with the temperature.

3.3 Governing equations and boundary conditions.

The governing equations that describe the fluid-dynamic in the proposed model are the continuity and momentum equations. Their simplified form in Cardinal coordinates are expressed by the Equations 4-7, having in consideration the assumptions previously made:

$$\frac{\partial u}{\partial x}+\frac{\partial v}{\partial y}+\frac{\partial w}{\partial z}=0 \tag{4}$$

$$\rho\left(u\frac{\partial u}{\partial x}+v\frac{\partial u}{\partial y}+w\frac{\partial u}{\partial z}\right)=-\frac{\partial P}{\partial x}+\mu\nabla^2 u \tag{5}$$

$$\rho\left(u\frac{\partial v}{\partial x}+v\frac{\partial v}{\partial y}+w\frac{\partial v}{\partial z}\right)=-\frac{\partial P}{\partial y}+\mu\nabla^2 v \tag{6}$$

$$\rho\left(u\frac{\partial w}{\partial x}+v\frac{\partial w}{\partial y}+w\frac{\partial w}{\partial z}\right)=-\frac{\partial P}{\partial w}+\mu\nabla^2 w \tag{7}$$

The conjugate heat transfer is represented by the energy equation, for the fluid domain by Equation 8 and by Equation 9 for the solid domain:

$$C_p\rho\left(u\frac{\partial T}{\partial x}+v\frac{\partial T}{\partial y}+w\frac{\partial T}{\partial z}\right)=k\nabla^2 T \tag{8}$$

$$\nabla\left(k_{si}\frac{\partial T}{\partial x}+k_{si}\frac{\partial T}{\partial y}+k_{si}\frac{\partial T}{\partial z}\right)=0 \tag{9}$$

Regarding the boundary conditions, considering a uniform and equal flow rate on each micro-gap on the complete model. A flow rate of 8.66 ml/min is assumed in the simplified model, equivalent to a mass flow rate of 1.43 x10^{-4} kg/s. Fluid flow is defined at the inlet face with an entrance temperature of 21.3 °C, while at the outlet a gauge pressure of 0 Pa is defined.

A constant heat flux of 250 W/cm^2 is considered acting on the interior faces of Zones 1, 2, 3, and 4. In contrast, three different heat fluxes of 250, 500 and 750 W/cm^2 are considered for the hotspot zone, allowing a complete data comparison for validation purposes using the experimental results by Lorenzini et al. [78]. No heat flux is considered at the entrance and exit plenums. The side and top walls are considered as adiabatic walls with a no-slip condition. The aforementioned boundaries are indicated in Figure 3.2.

3.4 Mesh analysis

A sample of the meshing scheme used for this study is illustrated in Figure 3.5. Hexahedral elements were used in the fluid zone, looking to reduce numerical errors, and in most of the solid zones. Just a few tetrahedral elements were used for the solid domain to reduce the cell elements and solution time. At the fluid to solid interfaces, a mesh refinement was included to account for the hydrodynamic and thermal boundary layers.

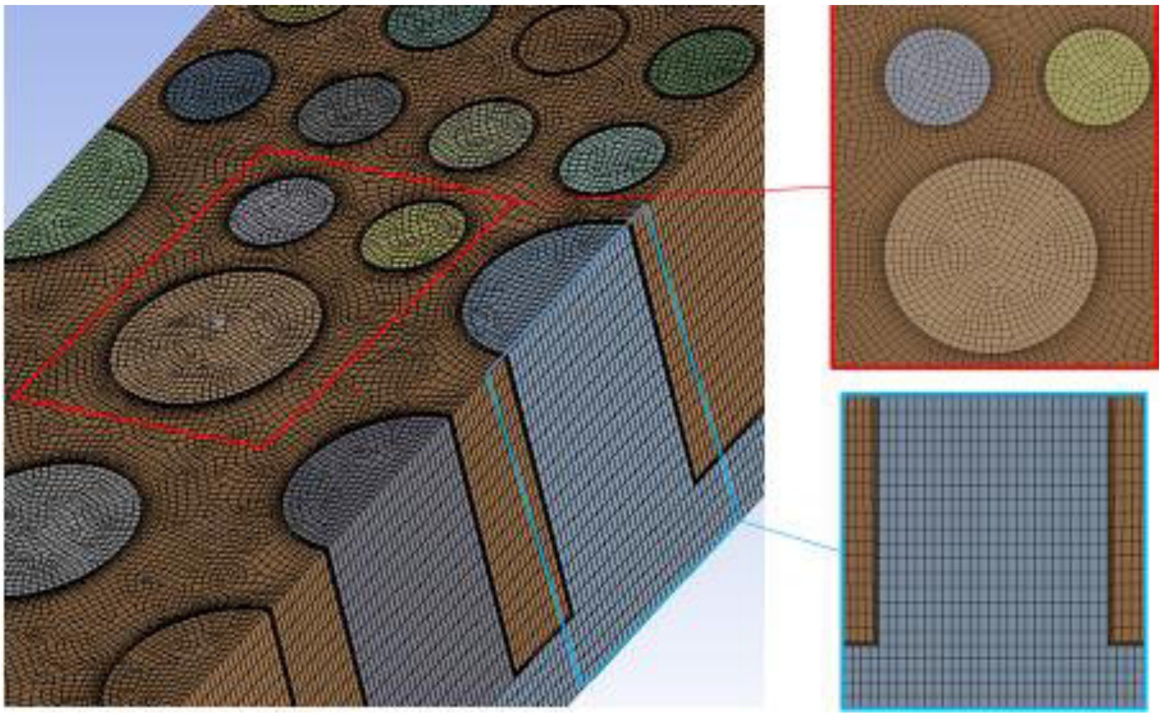

Figure 3.5 Mesh illustration and boundary layer details.

A mesh sensitivity analysis was carried out to select an ideal element size. Table 3.2 lists the different element sizes applied and the approximate computational time to generate each mesh for this analysis, using the specialized software ANSYS Meshing version 18.2, supported by an Intel Core i7 7700 processor. Results for each mesh size are obtained considering a uniform heat flux of 250 W/cm^2 in all the heating areas. Also, output parameters of interest (average temperature on the bottom chip surface, and pressure drops) are compared in Table 3.2 to highlight the effect of mesh size.

Table 3.2 Key mesh numerical information considering different element sizes.

Size element (µm)	*Number of elements (x10^6)*	*Approximate time to build mesh (min)*	*Average Bottom Surface Temperature (°C)*	*Pressure Drop (kPa)*
5	7.665	80	49.89	122.81
6	5.412	32	49.15	126.8
7.5	3.231	16	48.27	130.48
10	1.943	10	46.96	143.2

As a balance among element numbers, quality of results, and computational time invested in building the mesh, an element size of 6 µm was selected for the validation model with a

minimum orthogonal quality close to 0.22, and average orthogonal quality of 0.92. The same element size was applied in the construction of new models for the parametric analysis.

3.4.1 Mesh quality

Mesh quality is an essential factor in the meshing process. A good mesh quality means convergency in the studied process, good physic description, and accuracy in the results. Orthogonal quality (OQ) is one of the used mesh metrics to define the mesh quality, and for the particular CFD case is the method suggested to evaluate the mesh previously made [96]. CFD studies usually make use of hexahedral elements to analyze a fluid dynamic problem. Due to this kind of element has a quasi-fixed orientation, reducing possible errors (false fluid diffusion). In the author words, this method sizes how good is the orientation and shape of a mesh element (cell) to correctly quantify the fluid diffusion inside a cell.

The orthogonal quality for cells is computed using the face normal vector $(\vec{A})$, the vector from the cell centroid to the centroid of each of the adjacent cells $(\vec{c})$, and the vector from the cell centroid to each of the faces $(\vec{f})$. Figure 3.6 illustrates the vectors used to determine the orthogonal quality for a cell.

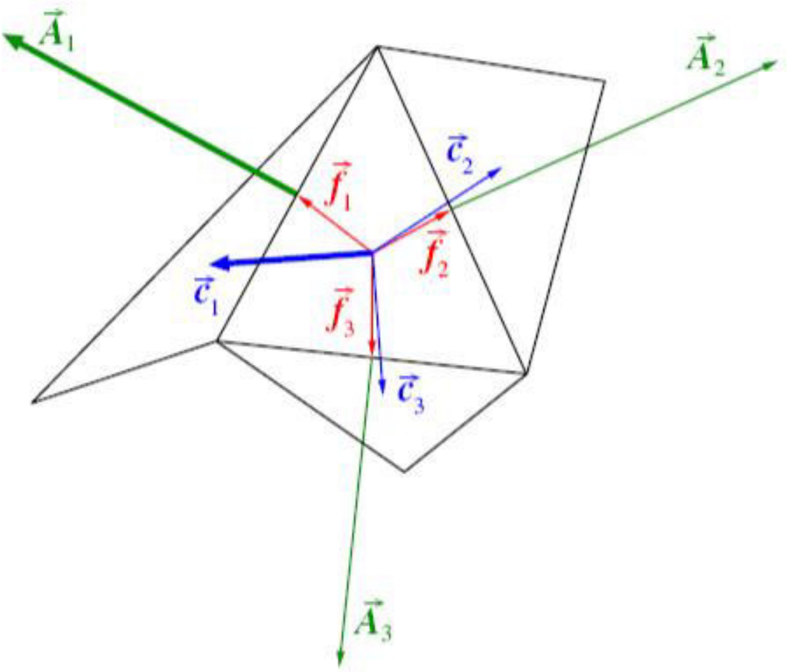

Figure 3.6 Vectors used to compute orthogonal quality for a cell [96].

The orthogonal quality is the minimum value computed in the Equations 10-11, for each face i. In other words, each one of the Equations 10-11 gives a value of orthogonal quality

for each cell face, so a hexahedral cell will have twelve values of orthogonal quality. The minimum value of said calculations is the cell orthogonal quality.

$$OQ = \frac{\vec{A}_i . \vec{f}_i}{|\vec{A}_i||\vec{f}_i|} \quad (10)$$

$$OQ = \frac{\vec{A}_i . \vec{c}_i}{|\vec{A}_i||\vec{c}_i|} \quad (11)$$

The range for orthogonal quality is 0-1. Where a value of 0 is the worst, meaning a poor mesh quality, and a value of 1 is the best. An acceptable value of orthogonal quality is up to 0.16, depending on the analyzed phenomenon. Thus, the obtained mesh quality is adequate to analyze the proposed numerical model [96].

3.5 Numerical model validation

ANSYS FLUENT Version 18.2 is used to solve the discretized partial differential equations, using a second-order upwind discretization. The coupling algorithm used for pressure and velocity fields on each iteration is the SIMPLE algorithm, considering convergence criteria under 10^{-3} for momentum and continuity residuals, and values of less than 10^{-6} for energy residuals. As a part of the model initialization, it was run in transient-state with no heat fluxes until to get steady-state conditions; this action facilitates the model convergence.

Thus, validation simulations were carried out using three different heat fluxes of 250, 500 and 750 W/cm^2 on the hotspot zone, and a constant heat flux of 250 W/cm^2 in the remaining finned areas (background zones). The simulation results were compared against available experimental results from the literature [78]; Figure 3.7 shows the temperature variation along the silicon surface with good agreement compared to the experimental data, except in Zone 4, where the temperature predicted is 9% higher than experimental results. It may be a consequence of the assumption of uniform fluid flow over the single channel in all the proposed zones (see following section). This could be not entirely accurate; the pin fins may work as small flow deflectors due to the additional local flow resistance offered by them. Despite exceeding temperature fields in one zone of the microchip, the numerical results are within reasonable ranges for an adequate microchip performance [24,25], and the thermal behavior in the remaining areas is close to the reported physical model in [78].

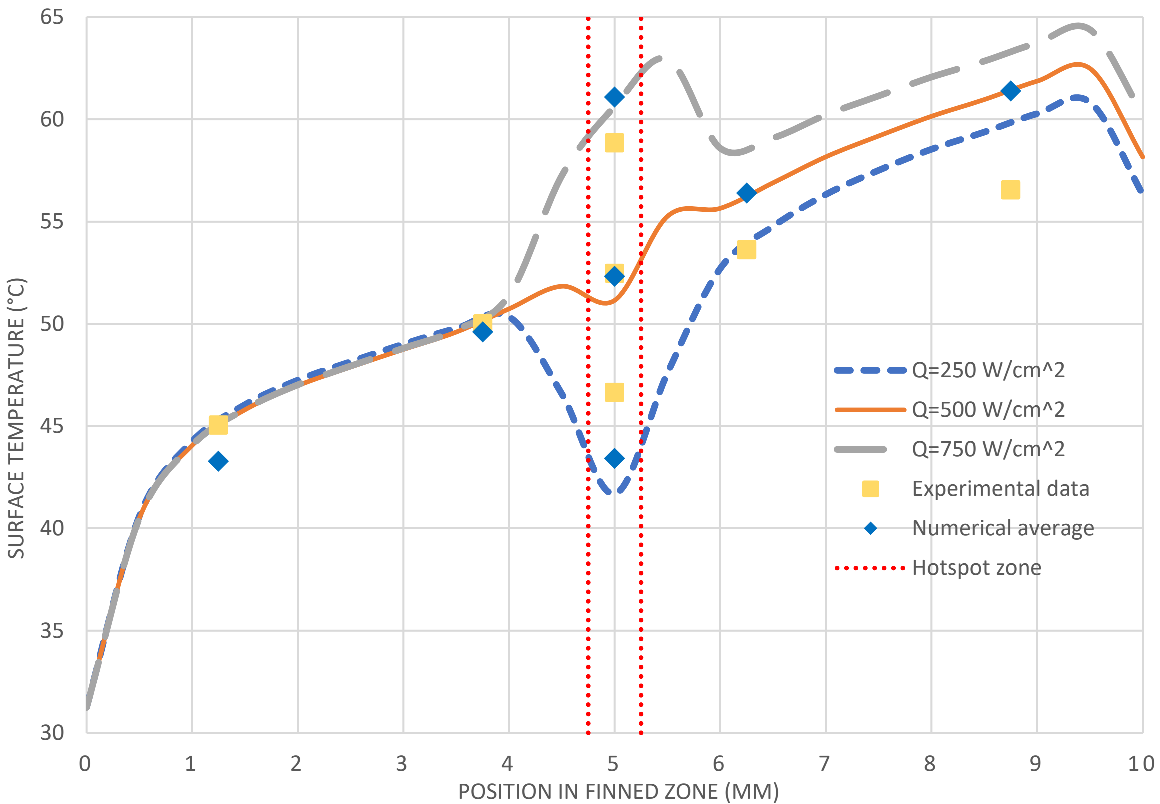

Figure 3.7 Predicted surface temperature and comparison with experimental data [78].

3.5.1 Extended validation domain

As a part of the validation methodology, an extended model was created, looking to get more useful information. New data may provide information to get a better understanding of the discrepancy between numerical and experimental results at the outlet zone in the simplified model. Figure 3.6 shows the new numerical model with its dimensions; it is composed of eight micro-gaps with nine fin files. The extended geometry is three times bigger than the simplified geometry that only has two micro-gaps, and three pin-fin files. The pin-fins in the new model have the same dimensions and spacing shown in Figure 3.2.

The extended model was meshed and run, using the same setup settings than the simplified model: type of mesh element, element size, mesh quality criteria, and boundary conditions. The unique change was in the inlet flow rate, due to the extended model counts with an inlet face three times bigger, involving a proportional increase in the inlet flow rate (going from 1.43 x10^{-4} kg/s to 5.72 x10^{-4} kg/s).

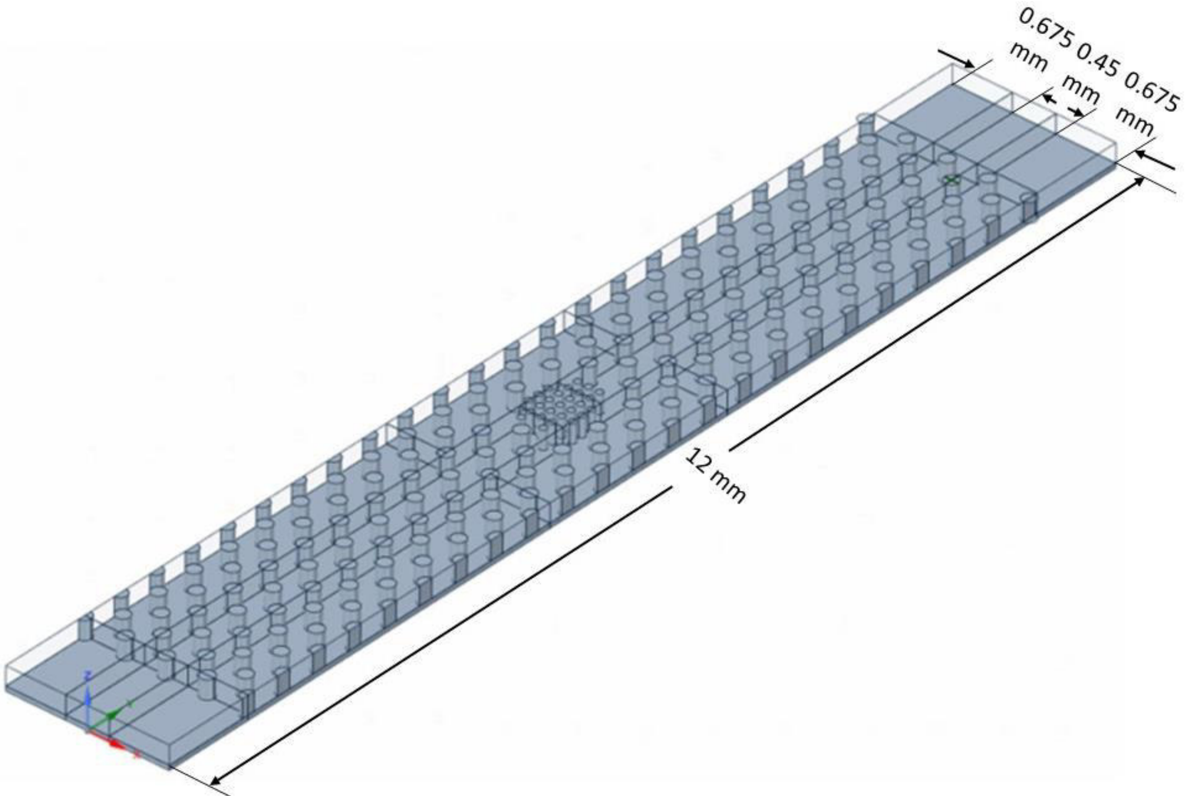

Figure 3.8 Illustration of the extended validation model.

Figure 3.9 shows the thermal behavior in the central gap of the extended model, allowing to make a thermal comparison with the simplified model (Figure 3.7). Once the DI water gets in the silicon plates with embedded micro pin fins, the temperature behavior is the same for both, during the first 4.5 finned millimeters. Extended and simplified models have the same thermal behavior after the hotspot zone, getting excellent approximations with the experimental data in Zones 1-2.

In contrast, when the coolant goes across the hotspot zone with a different pin fin density, there are some differences between Figures 3.7 and 3.9. For the extended model, the numerical results get closer to the experimental data in the hotspot zone, and also in the Zone 3. Further, the numerical error at the Zone 4 was reduced considerably. In the simplified model, numerical temperature exceeds by 4.9 Celsius degrees the experimental data. Whereas the extended model reports a difference of 2.2 degrees Celsius with the experiments, decreasing the numerical error from 9% to 4.3% (more than half). The explanation for previous point resides in the fluid flow rate.

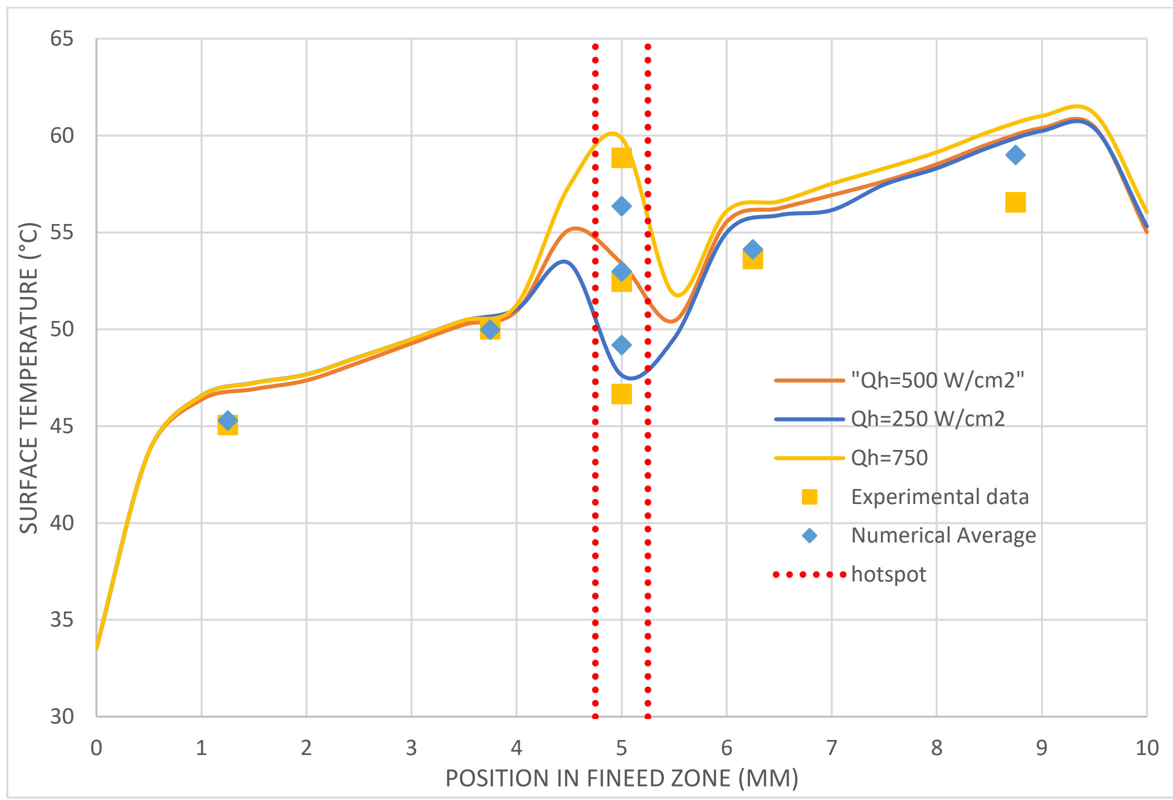

Figure 3.9 Predicted surface temperature and comparison with experimental data [78] in the extended model.

3.5.2 Flow rate analysis

A flow rate analysis was developed in the extended model. It was necessary the creation of different planes in the model center gap, and on its adjacent gaps (right gap and left gap) to size the flow rate across them. Mentioned gaps and planes are illustrated in Figure 3.10.

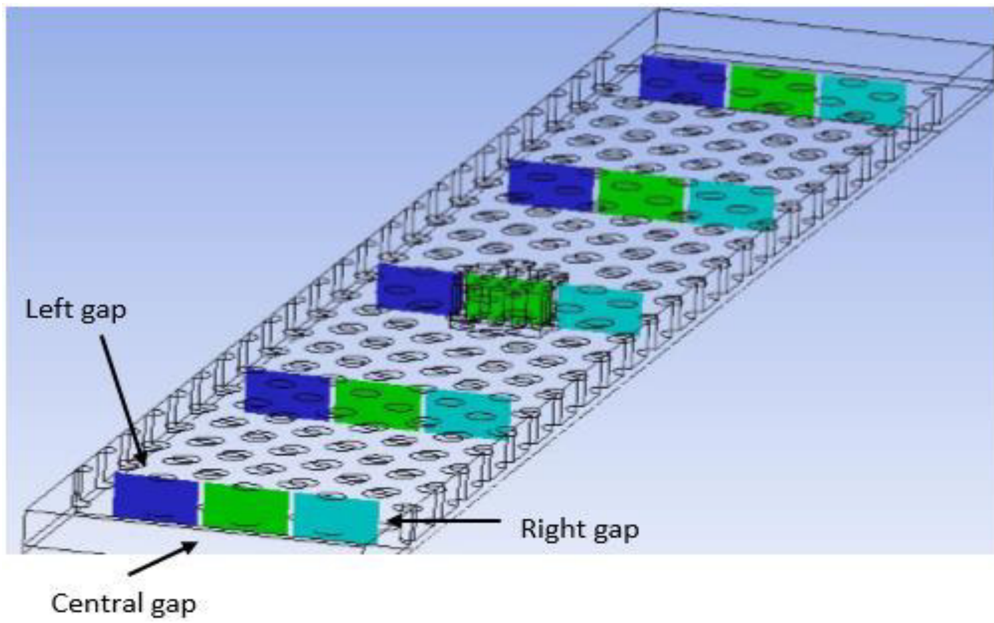

Figure 3.10 Illustration of created planes to size the flow rate in different gaps.

The flow rate fixed in the simple geometry was proposed over the supposition that every single gap in the experimental model has the same flow rate, and it is constant throughout the whole gap. However, according to the extended model such assumption is not totally right. As a consequence, the predicted thermal behavior of the simplified model has no good accuracy at the outlet zone of the model.

The measured fluid flow rate in three different micro gaps is illustrated in Figure 3.11. It shows that the fluid flow in the analyzed gaps is not constant. Also, the graphic shows that the pin-fin density increase on the hotspot zone works like a flow deflector, due to the central gap fluid flow is reduced considerably in such zone. When the fluid gets close to the outlet zone, there is a peak of flow rate in the central gap. It may be the reason why the experimental model and the extended geometry model have a lower temperature than the simplified validation model; in this zone, there is a higher flow rate than in the simple model. In addition, the average flow rate per channel is equal to 1.44 $x10^{4}$ kg/s, being the fluid flow rate assumed in the smaller numeric model, explaining the similarity in the thermal behavior between numerical and experimental models before the Zone 4.

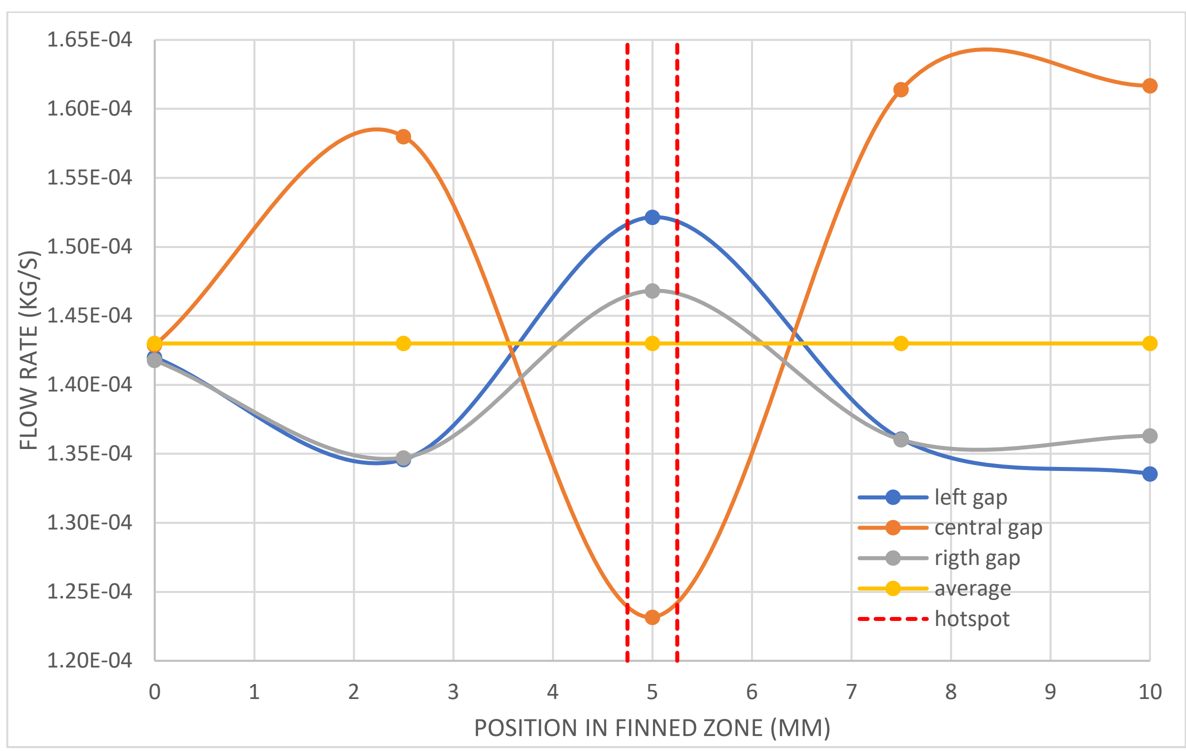

Figure 3.11 Calculated fluid flow rates in the extended model for different micro-gaps.

Summarizing, the temperature difference between experimental data and the simplified model is due to variations in the fluid flow distribution.

So, the predicted temperature in new simplified geometries may have discrepancies with their physical models, due to the flow distribution is not totally represented in the simple models. Besides, the implementation of simplified microfluidic cooling models allows saving computational time in a large degree. Owing to the construction of the CAD geometry, the meshing and simulation process of a simplified microfluidic cooling system takes approximately two hours. On the other hand, the same operations in an extended model take at least two days, without counting some problems involved in the meshing process. Thus, the simplified models are more affordable to propose parametric variations in the microfluidic cooling systems. Thereby, if one simplified model has promising results, it might be extended for a complete simulation.

3.6 Design of experiments (DoE)

The main idea of the design of experiments is: if an analyst does not have an idea how a process works, how to describe its physics, or the resources for the analysis are not enough. The statistics may provide useful information for the analyst to get a better understanding of the process of interest. As shown in Figure 3.12, any process has X_n inlet parameters that can be measure in a qualitative or quantitative way. At the same time, the process possesses Y_m inlet responses of particular interest that could have a dependence relation with the

inlet parameters or not. In consequence, by the comprehension of the relations between inlet and outlet parameters is possible to have better control over the process of interest.

Besides, measurements made in the analyzed process must have errors; hardly the same process will reach precisely the same results because there are some parameters in which it is not possible to have control. Even, said errors could be attributed to the measurement process or others. For this reason, it is necessary to make various tests or experiments, by them is possible to reduce and identify the variations in the studied process. Also, the compiled information during the multiple experiments will be useful for the process interpretation, by the use of adequate concepts such as design of experiments theory. DoE allows identifying key inlet parameters in the analyzed process, find relations between inlet and outlet parameters, identify or reduce errors in the process, and others.

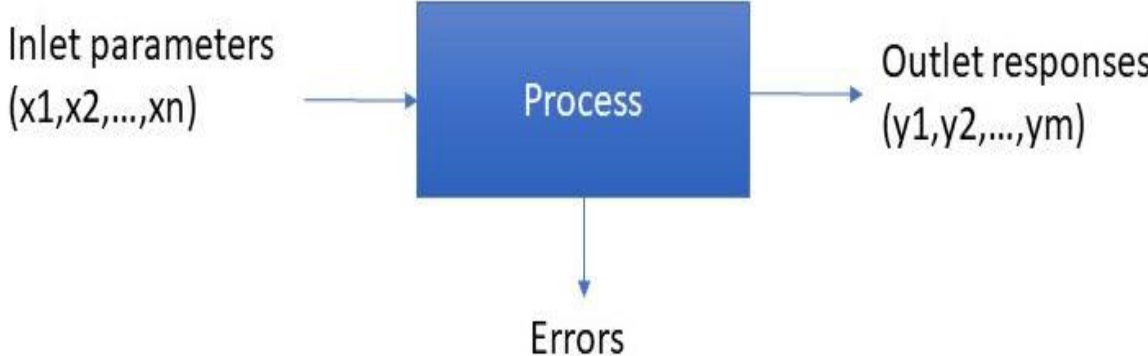

Figure 3.12 Illustration of in and out information involved in an unknow process.

In resume, DoE theory uses inferential statistical concepts, allowing a better understanding of any process. Various tests or experiments evaluate the process of interest. During the tests, numerical or symbolic values are compiled for their interpretation by the statistical hypothesis testing as a part of the DoE theory. Then, through an interpretation of the obtained results, it is possible to have better control of the analyzed process and propose improvements on output responses [97].

In the present microfluidic cooling systems study, the influence of geometrical inlet parameters on the outputs of interest is assessed using the DoE theory. Also, it is necessary to take into consideration the interactions among input parameters because they can influence the output responses. The interactions in DoE are the effects of parameter combinations over the experimental responses [97], whereby several parameter interactions are considered in this analysis.

3.6.1 Proposal of parametric analysis

Once made the validation of the simplified model and compared against the extended model. A factorial design is proposed, based on the DoE theory. By the bibliographic review made in Chapter 2, diverse parameters of interest were selected for their analysis. The variations of six geometrical parameters are listed in Table 3.3; each parameter has two different values or levels. The minimum value in the inlet parameters is considered as the low level, while the maximum value is considered as the high level. The values for the parameters are based on the ranges suggested in [88]. Once defined, low levels take a value of -1 and high levels a value of +1. It is known as parameter standardization to facilitate the statistical interpretation [97].

Further, a comparison between non-conventional parameters is also presented in Table 3.3. The extended surface shape is one of them, using either an embedded wall (microchannel) or an embedded pin fin array (micro gap), where both cases consider an increase in pin-fin density at the hotspot zone. Another parameter that is investigated and not reported in previous publications is the hotspot position and its influence over thermal and fluid-dynamic performance in microfluidic cooling systems.

Table 3.3 Selected level values for each parameter and their acronyms.

Parameter	Acronym	Low level (-1)	High level (+1)
Extended surface shape	ESS	Wall	Pin-fin
Hotspot center position (distance from the beginning of the finned area)	HP	5 mm	9.5 mm
Increased density of pin fins into hotspot zone (per longitudinal mm)	ID	2	4
Distance between extended surface centers (S_T=S_L)	DBC	180 µm	225 µm
Extended surface diameter	ESD	100 µm	150 µm
Extended surface height	ESH	150 µm	200 µm

3.6.2 Proposed models

Geometrical dimensions for all of the 64 generated configurations are presented in Table 3.4, using a normalized notation. The configuration and order of the models were selected randomly from the statistical software Minitab. The creation of the CAD models, their meshing, and simulation were made in the plataform ANSYS Workbench version 18.2.

Table 3.4 Normalized parametric dimensions of investigated configurations.

Model	ESS	HP	ID	DBC	ESD	ESH	Model	ESS	HP	ID	DBC	ESD	ESH
1	1	1	-1	1	1	-1	**33**	1	1	1	-1	1	-1
2	-1	1	1	1	1	1	**34**	-1	-1	1	-1	1	-1
3	1	1	1	1	-1	-1	**35**	1	1	1	1	1	1
4	-1	1	1	-1	1	1	**36**	-1	1	1	1	-1	1
5	1	-1	1	-1	-1	1	**37**	1	1	-1	1	-1	-1
6	1	-1	-1	-1	1	1	**38**	1	-1	1	-1	1	-1
7	-1	1	-1	1	-1	1	**39**	-1	-1	-1	-1	-1	1
8	1	1	1	-1	-1	-1	**40**	1	-1	-1	-1	-1	-1
9	1	-1	1	1	-1	1	**41**	-1	-1	-1	1	-1	-1
10	-1	-1	-1	1	1	-1	**42**	-1	1	-1	-1	-1	1
11	1	-1	1	-1	-1	-1	**43**	1	-1	-1	-1	-1	1
12	1	1	1	1	-1	1	**44**	-1	-1	-1	-1	-1	-1
13	-1	1	-1	-1	1	-1	**45**	1	1	-1	-1	1	1
14	1	-1	1	1	1	1	**46**	1	-1	-1	1	-1	1
15	-1	1	1	-1	-1	1	**47**	-1	1	-1	1	-1	-1
16	-1	1	1	-1	1	-1	**48**	-1	1	1	1	-1	-1
17	-1	-1	1	1	-1	-1	**49**	1	1	-1	1	-1	1
18	1	-1	-1	1	1	-1	**50**	-1	1	-1	1	1	1
19	-1	-1	1	1	1	-1	**51**	1	-1	1	1	-1	-1
20	1	-1	-1	-1	1	-1	**52**	1	1	1	-1	-1	1
21	1	-1	1	1	1	-1	**53**	-1	-1	1	-1	-1	1
22	-1	1	-1	-1	-1	-1	**54**	-1	1	1	-1	-1	-1
23	-1	1	1	1	1	-1	**55**	1	1	-1	1	1	1
24	-1	-1	-1	1	-1	1	**56**	-1	-1	1	-1	-1	-1
25	1	1	-1	-1	-1	-1	**57**	1	1	-1	-1	-1	1
26	-1	-1	-1	1	1	1	**58**	1	-1	-1	1	1	1
27	-1	-1	1	-1	1	1	**59**	1	-1	1	-1	1	1
28	-1	-1	-1	-1	1	1	**60**	1	1	-1	-1	1	-1
29	-1	1	-1	-1	1	1	**61**	1	-1	-1	1	-1	-1
30	-1	-1	-1	-1	1	-1	**62**	-1	-1	1	1	1	1
31	1	1	1	1	1	-1	**63**	1	1	1	-1	1	1
32	-1	1	-1	1	1	-1	**64**	-1	-1	1	1	-1	1

As an example for interpretation of the configurations listed in Table 3.4, Model 59 represents a finned system with a hotspot at the center of the domain, a 4x pin fin density increase, longitudinal and horizontal distances between pin-fins of 180 um, and pin-fin diameter and pin-fin height of 150 and 200 µm, respectively.

One geometric difference in the proposed configurations is that the pin fin density increase begins 0.25 mm before the hotspot zone, continues through the hotspot zone, and extends 0.25 mm beyond, whereas in the validation model, a pin-fin increase is only considered at the hotspot zone. It was done to reduce high-temperature gradients and for achieving better temperature uniformity.

Models 7 and 51 are shown in Figures 3.13 and 3.14, respectively, to illustrate the geometrical differences between distinct microfluidic cooling systems proposed. The first one represents a hybrid cooling system with its hotspot at the edge and a pin fin density increase of two. Whereas, the second is a micro-cooling system with embedded pin fins, a hotspot at the center of the model and a pin fin density increase of four.

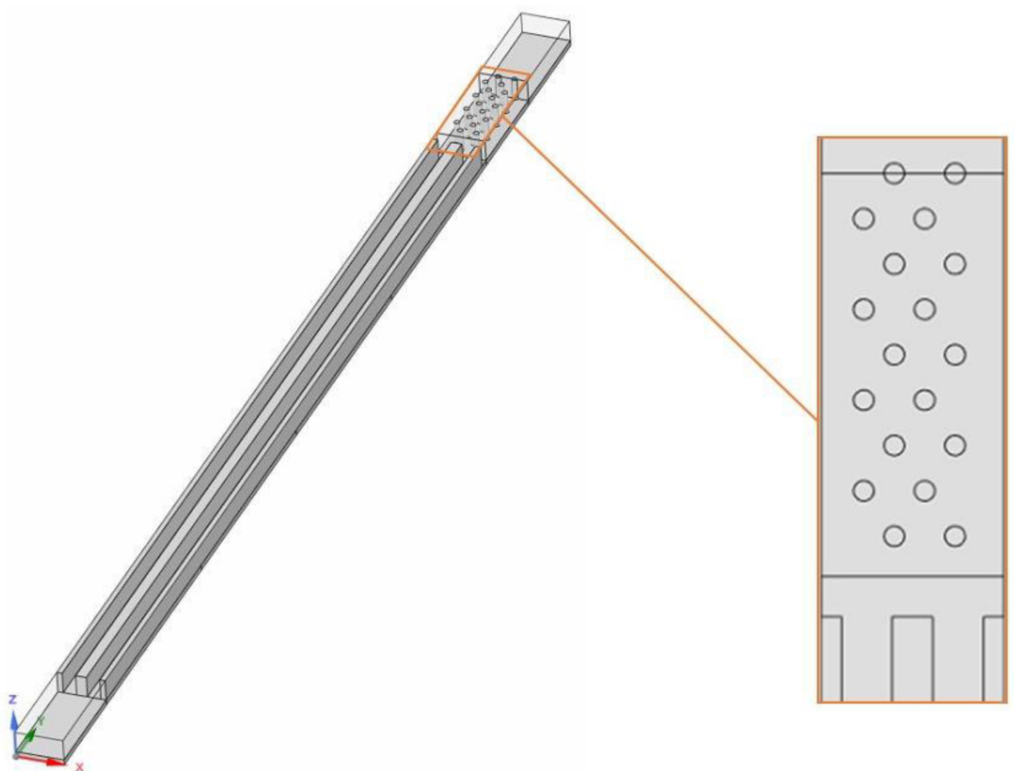

Figure 3.13 Illustration with detail of the Model 7.

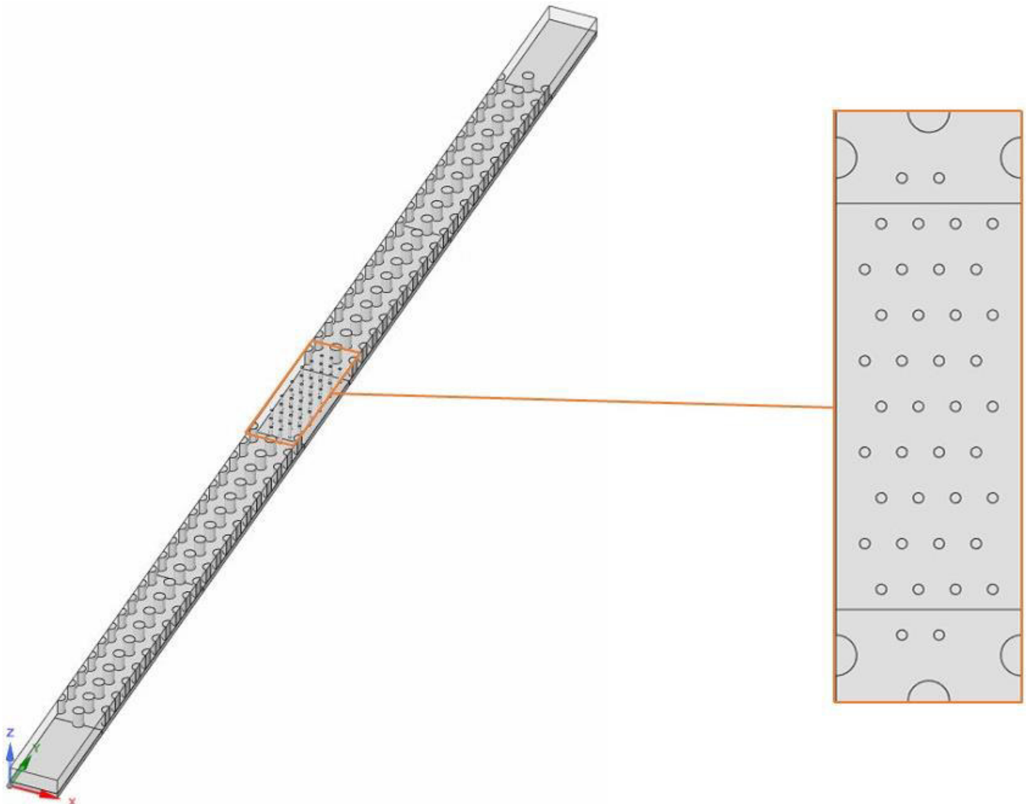

Figure 3.14 Illustration with detail of the Model 51.

Chapter 4 shows the obtained results from the proposed parametric analysis. It shows the influence of the considered parameters for the thermal management, and the predicted pressure drops generated by these variations. In the same way, Chapter 4 provides an illustration of the predicted thermal behavior in different models. Velocity and temperature contours are presented to illustrate in a better way, the influence of the parameter variation and to make a more in-depth analysis for the proposed models. Statistical tools are used to post-process the obtained data, giving useful information and conclusions. Thus, some optimized microfluidic cooling models are generated for their evaluation.

Chapter 4

Results

In Chapter 3, a validation methodology was developed using a simplified microfluidic cooling system. At the same time, the advantages of statics analysis by the design of experiments theory were discussed. By the combination of both approaches, a factorial design in microfluidic cooling systems was proposed. The results and discussion of the parametrical analysis are presented in this Chapter. Also, taking advantage of the obtained results, some optimized models were generated for their posterior evaluation.

As part of the parametrical design, 64 configurations were generated and modeled in ANSYS Workbench, which facilitates parametric numerical studies. Models were run using an Intel Core i7 microprocessor with four cores working at 3.4 GHz, and 32 GB of RAM. The analysis of these 64 configurations follows the methodology previously established for the validation model, following the order of Table 3.4. The numerical tests were carried out once because numerical procedures guarantee repeatability, being not necessary to repeat the experiments more than once, which is an essential concept in the design of experiments theory [97].

For these simplified models, the heat flux is 500 W/cm^2 at hotspots, while the heat flux in background zones 1-4 is 250 W/cm^2. The mass flow rate was adjusted according to the geometry extension in order to guarantee the same mass flux and similarity of conditions. For the low level (-1) a mass inlet flow of 1.044 x10^{-4} kg/s is defined, and for the high level (+1) a mass flow rate of 1.43 x10^{-4} kg/s is employed. The remaining boundary conditions in all configurations were kept the same as in the validation model.

Output parameters in the present study are the average temperature (AT) at the bottom surface, and the pressure drop (PD). Both of these parameters are useful to evaluate the thermal performance and the invested pumping power on the proposed microfluidic cooling models. Table 4.1 quantifies these parameters on each one of the 64 models, and also, includes results from the validation model and experimental data used as a reference frame. As can be denoted, the experimental model and validation model have small differences, 6 kPa in the pressure drop, and 0.9 °C in the average temperature.

As shown, diferent models improve the thermal performance reducing the average temperature, decreasing the pressure drop, or both being this the optimal case when are compared with the experimental results. A brief analysis of the improvements in the thermal performance is presented in the following sections, by the proposed micro-cooling systems.

Table 4.1 Numerical responses in output parameters of general interest.

Model	PD (kPa)	AT (°C)	Model	PD (kPa)	AT (°C)	Model	PD (kPa)	AT (°C)
Experimental	119.8	51.6	**21**	181.0	51.0	**43**	69.2	53.8
Validation	125.7	52.5	**22**	120.9	58.4	**44**	133.6	55.3
1	166.2	50.1	**23**	173.9	61.7	**45**	522.0	41.0
2	110.9	58.1	**24**	39.5	64.1	**46**	34.2	63.0
3	67.7	62.9	**25**	115.5	50.4	**47**	62.0	67.5
4	967.4	44.6	**26**	127.3	54.3	**48**	63.5	68.4
5	73.2	54.7	**27**	998.3	43.9	**49**	34.6	62.6
6	542.2	40.9	**28**	1019.3	43.1	**50**	110.9	57.8
7	36.5	66.1	**29**	955.3	43.9	**51**	62.0	62.7
8	118.5	51.0	**30**	2473.5	67.0	**52**	70.4	54.3
9	36.4	63.6	**31**	169.3	42.7	**53**	85.5	54.8
10	204.9	56.1	**32**	175.6	60.4	**54**	126.8	58.4
11	179.7	45.5	**33**	963.3	39.8	**55**	101.8	51.0
12	36.6	60.8	**34**	1435.9	45.6	**56**	137.8	56.3
13	1338.0	45.3	**35**	101.3	49.3	**57**	64.9	54.4
14	105.7	51.3	**36**	36.9	67.1	**58**	102.2	50.7
15	79.6	55.2	**37**	62.2	61.5	**59**	547.8	41.0
16	1345.6	46.0	**38**	952.2	40.1	**60**	934.0	39.5
17	71.5	64.7	**39**	82.0	54.0	**61**	59.4	62.3
18	176.7	51.0	**40**	118.7	51.0	**62**	127.0	54.9
19	194.9	62.7	**41**	68.5	64.2	**63**	543.2	41.2
20	960.7	39.6	**42**	75.8	56.1	**64**	41.6	64.2

4.1 Predicted thermal performance

Figure 4.1 shows the temperature response for selected models with noteworthy performance results in order to illustrate the parameter variation influence over temperature distribution. Models with a central hotspot describe a different thermal behavior, in the zones near the hotspot, in comparison with the validation model included in Figure 4.1; this is because the new models have the pin-fin density increase before and after the hotspot zone.

The Figure 4.1 presents various models which present three different approaches:

1. Temperature decrease and pressure drop increase. - Models 4, 20, and 60 considerably decrease the average temperature at the expense of a restrictively high-pressure drop (almost 1 MPa). These models can guarantee proper thermal management for the considered heat fluxes, and even, they could provide a higher energy dissipation. In contradiction, the high-pressure drop will generate considerable energy spending but adequate temperatures for the operation of a microprocessor.

2. Temperature increase and pressure drop decrease. - The opposite case is the Model 24, which reduces the pressure drop to one-third in comparison with the available experimental data [78]. However, the thermal performance is not optimal due to high temperatures resulting from the lack of heat transfer area (pin fin density) in this configuration. This configuration results to be a good alternative when it is not necessary to keep the microelectronics temperatures below 80 °C, saving energy consumption during the PC operation. In the other hand, model 43 has almost a 50% lower pressure drop than the validation model, increasing the average temperature only by 1.22 °C.

3. Temperature and pressure drop decrease. - Similarly, Figure 4.1 illustrates models that keep a balance between temperature fields and pumping power. Models 35 and 40 are also noteworthy due to their balanced improvements on output parameters, reducing both drop pressure and average temperature, improving experimental and validation results.

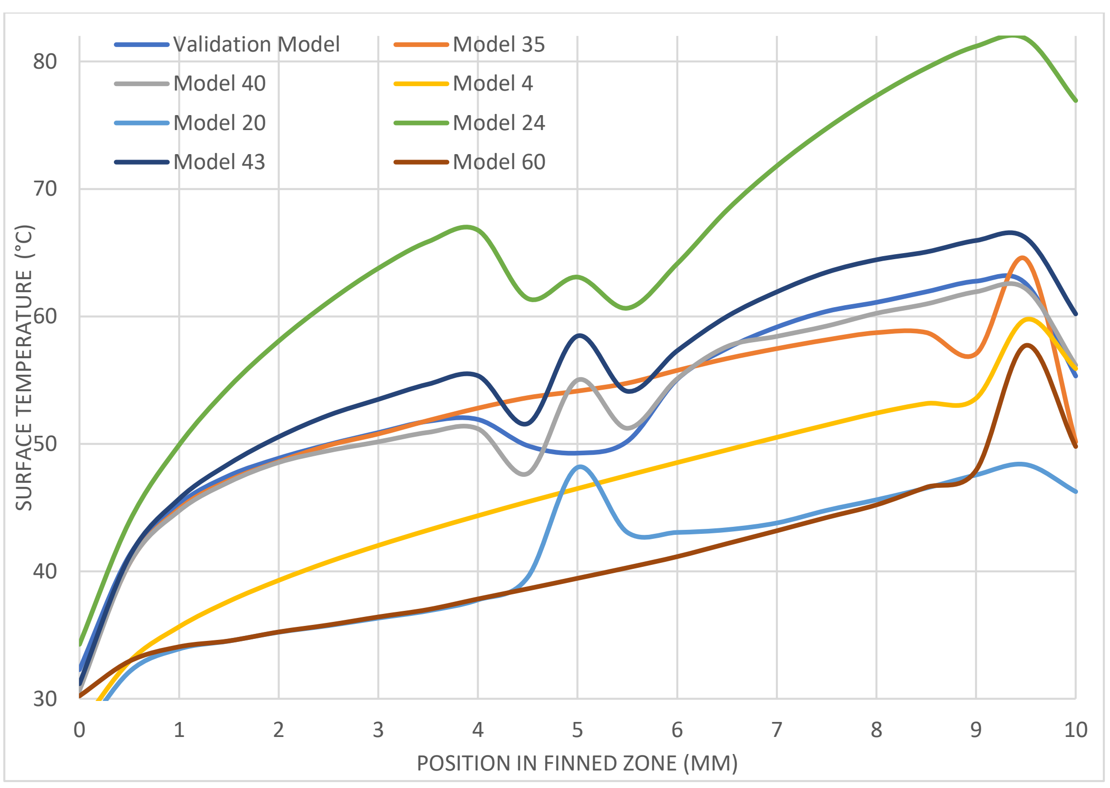

Figure 4.1 Surface temperature response of some analyzed configurations.

4.2 Velocity and temperature contours

The hydraulic/thermal results for the selected configurations 24 (a), 40 (b), 35 (c) and 2 (d) are shown in Figures 4.2 and 4.3. In these figures, the geometrical variations can be observed. Noticeable differences are the change in hotspot position, extended surface shape (microchannel or pin fins), and hotspot pin fin density increase due to the number and dimensions of smaller pin fins in the hotspot zones.

The comparisons of fluid-dynamic behavior are shown in Figure 4.2, using velocity contours in a horizontal cross-section plane created inside the fluid domain (top view). Models with microchannels have a better uniformity in the absolute velocity and higher velocity values in comparison with configurations using micro pin-fins in the background zones 1-4. A significant change in observed velocity magnitudes is due to the spacing between extended surfaces having variations of few micrometers between models, indicating that the velocity fields have a higher sensitivity to this inlet parameter. A point to highlight is the change in flow distributions when the fluid goes across the hotspot zone, whereby, effects of the pin-fin increase at hotspot zone and their geometrical arrangements are essential points to be analyzed in future studies. Also, the maximum velocity in the selected models does not exceed the 8 m/s, validating the approximations made in Section 3.2. So, the consideration of laminar flow in all the models may be considered as right.

Figure 4.3 illustrates the temperature fields at the silicon base through a top view. The configurations with micro-pin fins (b, c) show a better temperature uniformity than models with microchannel (a, d). Even though models with micro-channels have the highest velocities, these also have the highest temperatures (Figures 4.2, 4.3), which is attributed to boundary layer development, having influence in the heat transfer process. Thus, for the comparison of simplified microfluidic cooling systems, the models with only embedded micro-pin fins are capable of providing better thermal management than hybrid models, composed by microchannels and embedded pin-fins in the hotspots zones.

Regarding the overall parameters analyzed, hybrid models (a, d) in Figures 4.2 and 4.3 possess low pressure drops of 39.5 and 110.9 kPa respectively, but relatively high average temperature of 64.1 and 58.1 °C, overpassing by much the experimental data. In contradiction, the models with only pin fins (c, d) have low pressure drops of 118.7 and 101.3 kPa with very acceptable average temperatures of 51 and 49.3 °C, making them a better option for the heat dissipation on 3D ICs. The previous point is confirmed in Section 4.4 when a new data aggrupation is made. At the same time, the different configurations presented provide an illustration of the changes in the fluid-dynamic and thermal behavior when parametric variations are proposed.

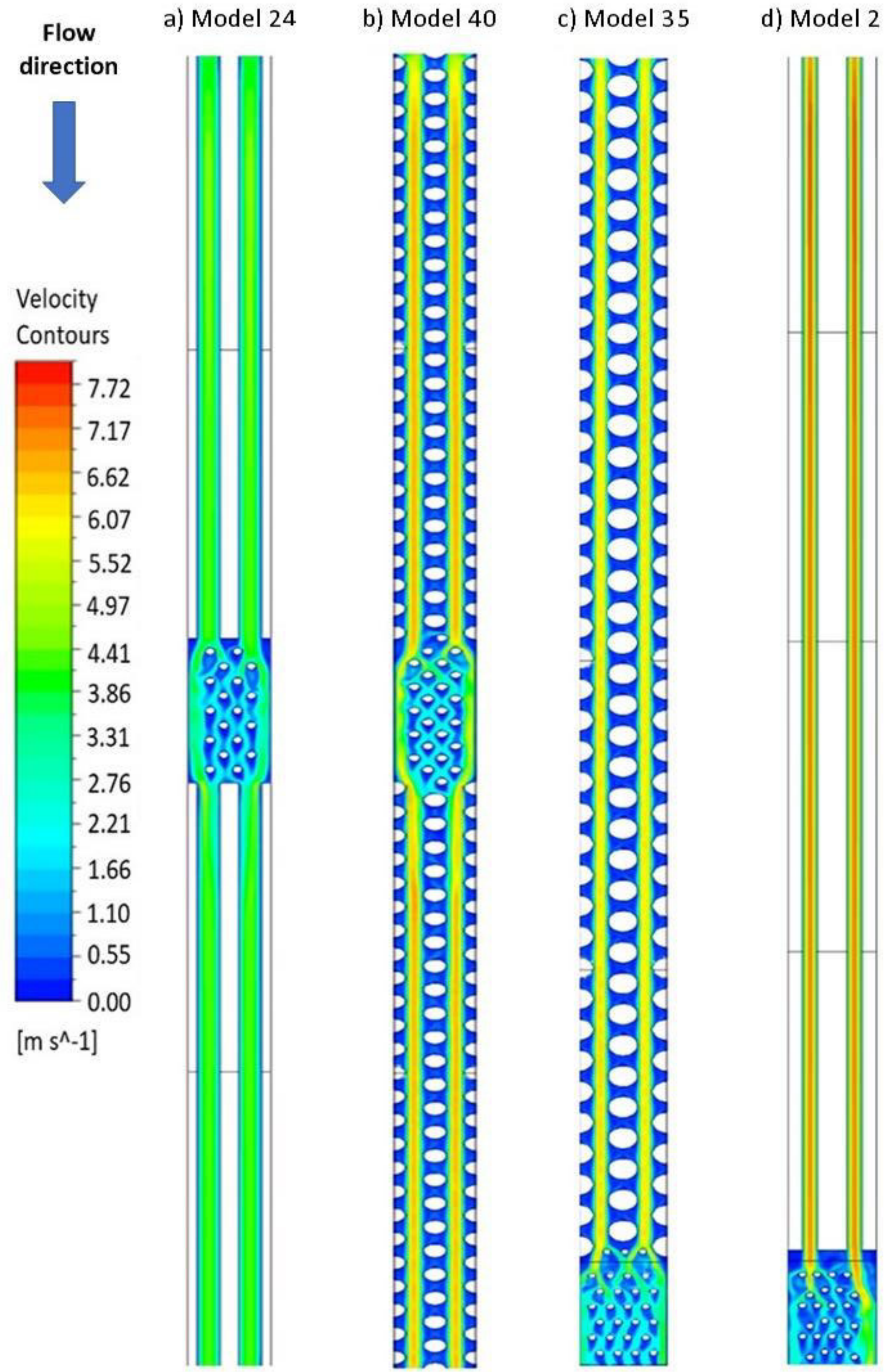

Figure 4.2 Illustration of velocity contours in selected microfluidic cooling systems.

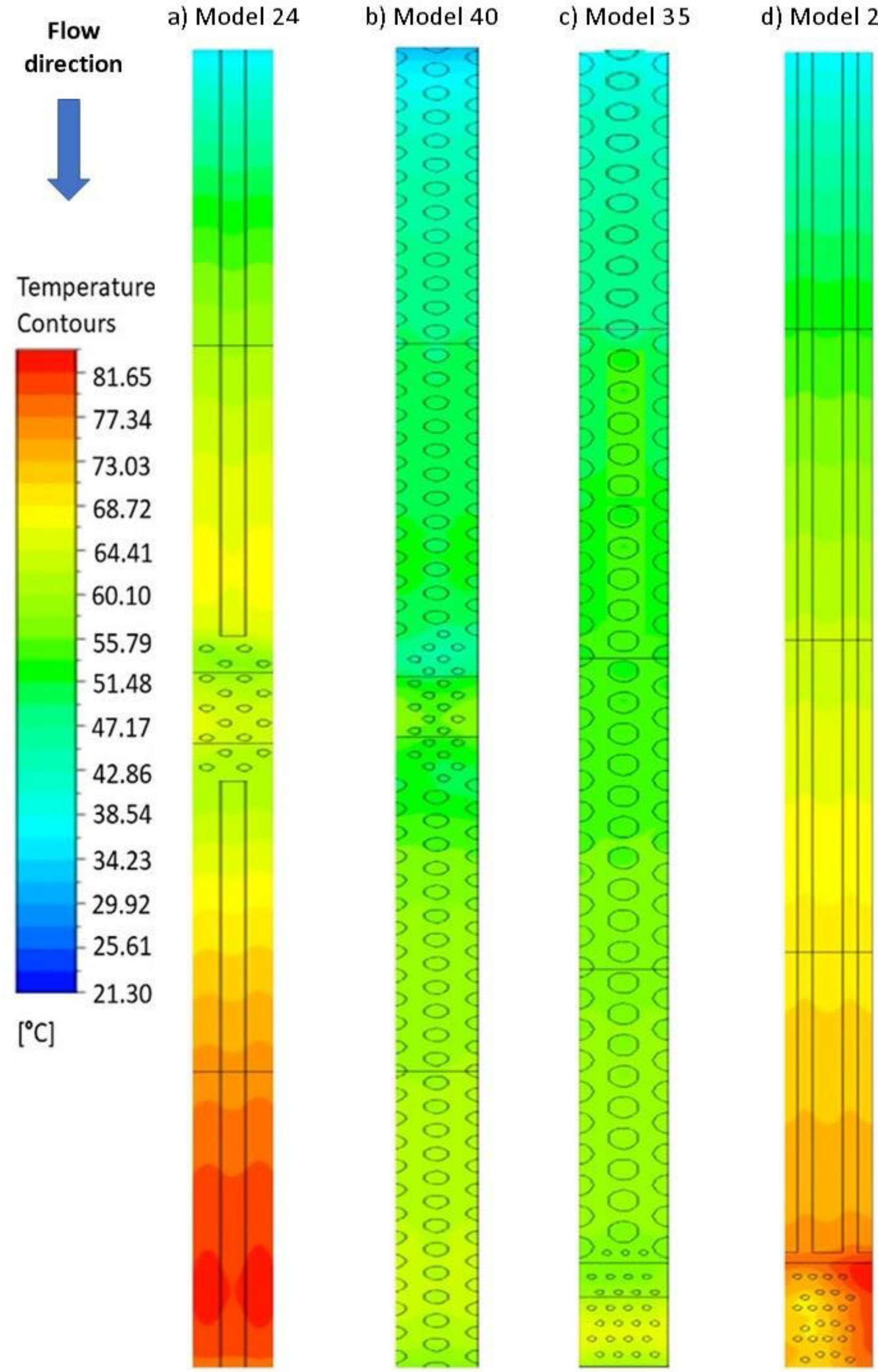

Figure 4.3 Illustration of temperature contours in selected microfluidic cooling systems.

4.3 Statistical interpretation of the obtained results

The simulation results collected in Table 4.1 were statistically processed using the data analysis software Minitab, which has the capability to obtain a statistical database with variances, covariances, and summations, useful for statistical hypothesis [97]. With the generated database, Minitab tools give a graphical visualization of the results for statistical purposes.

Figure 4.4a is a graphical illustration of the parametric effects on the pressure drop. The pressure drop is strongly impacted by the spacing between extended surfaces, extended surface diameter, and the interaction among them. Namely, when both parameters vary, there is a significant impact on the pressure drop, as expected. The relation between pressure drop and the varying parameters with their interaction is highly nonlinear, with small changes on these parameters a significant impact on the pressure drop is generated. Parameters that have lower influence over the pressure drop include the extended surface shape, extended surface height, and some combinations of interactions among parameters shown in Figure 4.4a. On the other hand, the increase in pin-fin density and the hotspot position have a non-significant effect, so any combination of these parameters within the proposed ranges will not result in a significant pressure drop variation.

Figure 4.4b shows no significant effects on the average surface temperature. Thus, it is possible to assume with 95% confidence that the relation among six input parameters and their interactions with the average temperature is almost linear for the ranges studied here.

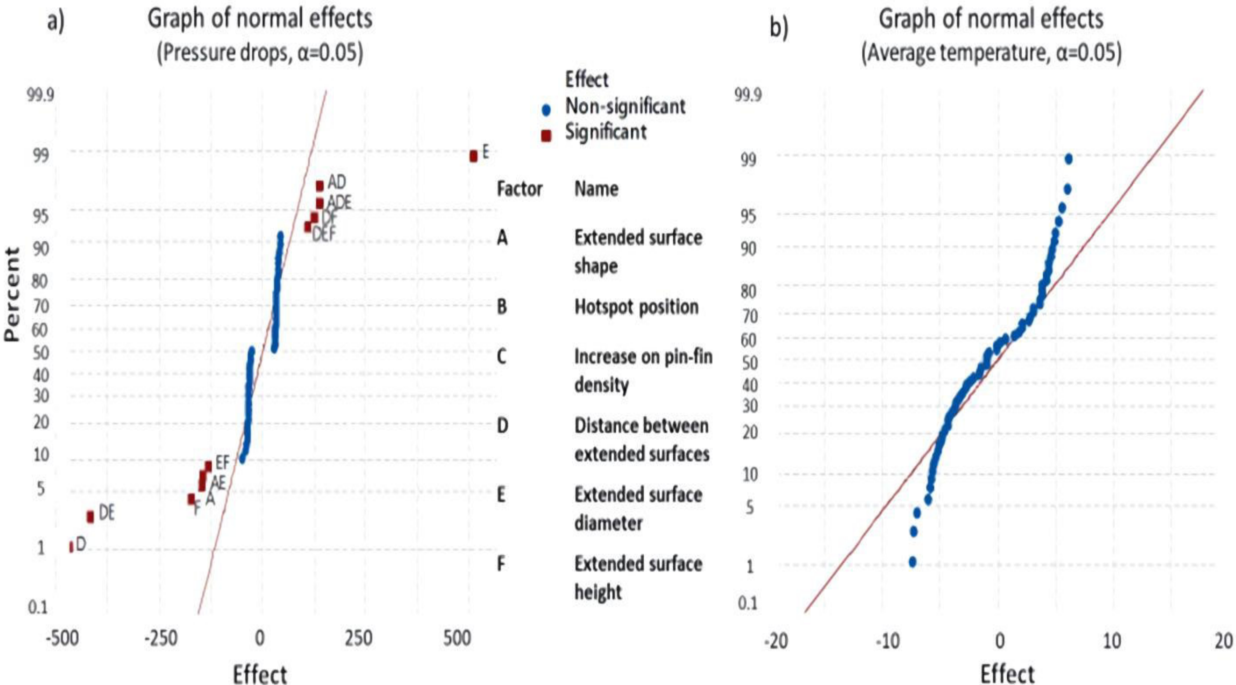

Figure 4.4. Normal effects graphs for pressure drop and the average temperature in proposed microfluidic systems.

Figures 4.5 and 4.6 are Pareto diagrams generated by Minitab, and they provide a better illustration of the post-processed results implementing the design of experiments theory. In these kinds of diagrams, the factors above the dotted line represent 80% of the problems in a specific process. For the particular case, these factors are the parameters which have a higher impact over the output responses. Whereas, the parameters below the line represent the remaining 20% that do not have a considerable effect over the output response.

Figure 4.5 shows the Pareto diagram for the pressure drop; it can be denoted the strong influence of two parameters as they are the distance between centers of extended surfaces, the pin fin diameter, and the interaction among them. Thus, these parameters are in major part the cause of the pressure drop in the proposed microfluidic cooling systems. While, the pin fin height and the channel form have a lower effect in the pressure drop, but it is significant.

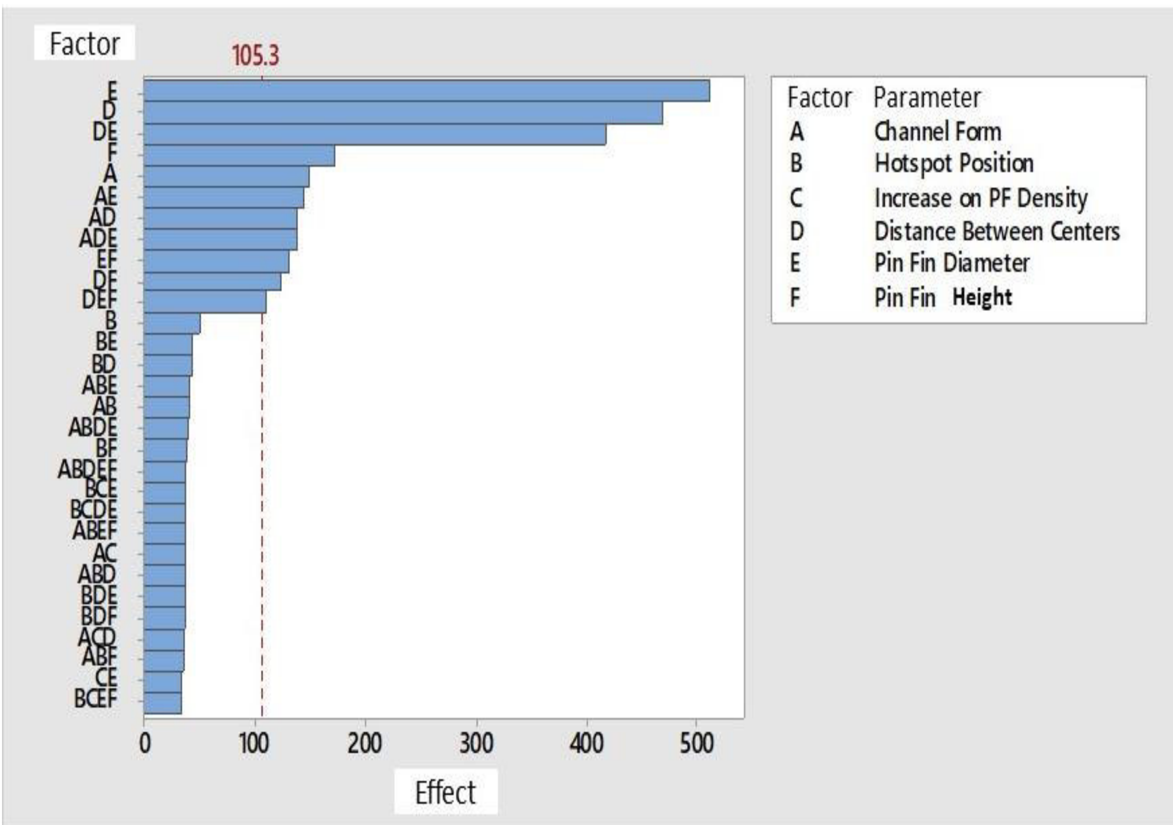

Figure 4.5 Pareto diagram for the pressure drop.

In contrast with the figure 4.5, the Pareto diagram showed in Figure 4.6 does not denote a predominant effect of any parameter in the average temperature of the proposed models. The most significant effect over this response is the interaction among pin fin density increase and pin fin height, adding credibility to the statistical method. Due to, from an engineering point of view, both parameters contribute considerably to increase or decrease

the available heat exchange area, allowing to dissipate higher of lower energy rates. It will have straight repercussion in the temperature fields. Thus, the post-processed information using the presented statistical approach results to be very useful.

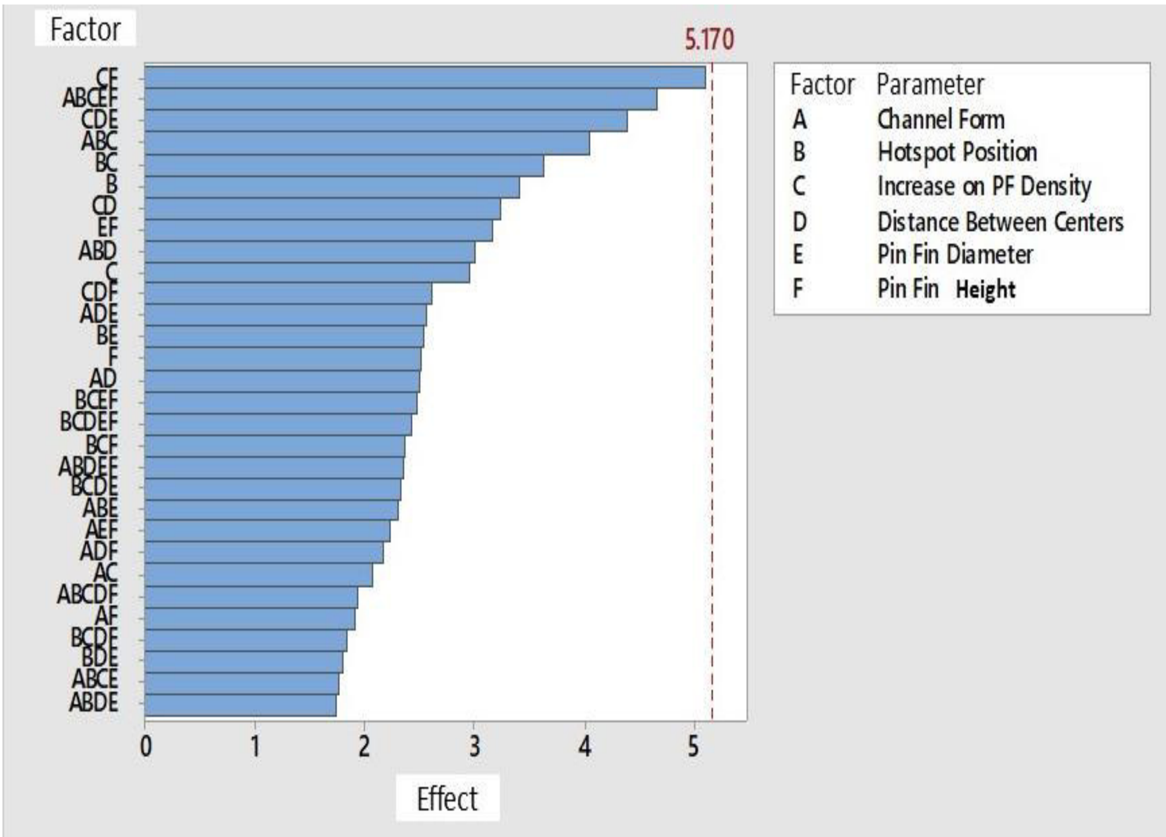

Figure 4.6 Pareto diagram for bottom average temperature.

Based on this statistical interpretation, seeking a balance between the extended surface spacing and extended surface diameter is sought, targeting pressure drop reductions without compromising the thermal performance.

4.4 Optimization of models using statistical tools

The results presented in the previous section allow the identification of the geometrical configurations to be considered parametric central points. Central point designs are models whose dimensions have an intermediate value considered as intermediate level (0), between low level (-1) and high level (+1) for selected parameters in the DoE methodology. These intermediate models can provide more information about a specific process when information obtained from two-parameter levels is not enough in the DoE study [97].

The results from Table 4.1 were divided into eight groups, keeping constant three input geometrical parameters which have lower influence over the global parameters reported, in accordance with the statistical interpretation. The regrouped data are shown in Table 4.2, allowing the selection of new central models by identifying the best data group.

Table 4.2 Regrouped data for the selection of central models.

Group	Fixed parameter			Models with this configuration	Average pressure drop (kPa)	Average heat sink temperature (°C)
	Extended shape area	Hotspot position	Increased pin fin density			
1	**Pin fin**	**Edge**	**2**	**1,25,37,45,49,55,57,60**	250.15	51.3
2	**Wall**	**Edge**	**4**	**2,4,15,16,23,36,48,54**	363.07	57.43
3	**Pin fin**	**Edge**	**4**	**3,8,12,31,33,35,52,63**	258.77	50.23
4	**Pin fin**	**Center**	**4**	**5,9,11,14,21,38,51,59**	952.21	40.08
5	**Pin fin**	**Center**	**2**	**6,18,20,40,43,46,58,61**	257.99	51.53
6	**Wall**	**Edge**	**2**	**7,13,22,29,32,42,47,50**	359.37	56.91
7	**Wall**	**Center**	**2**	**10,24,26,28,30,39,41,44**	518.56	57.25
8	**Wall**	**Center**	**4**	**17,19,27,34,53,56,62,64**	386.56	55.88

It can be noted in Table 4.2 that Groups 1 and 5 have the lowest average pressure drop with acceptable average temperatures. Thus, new geometric configurations were generated for these groups taking middle levels in the remaining parameters whose changes lead to significant variations in exit parameters. The selection of these groups is due to the pressure drop have a high sensitivity when variations are made in input parameters. In addition, Table 4.2 denotes again that micro-pin fin systems have a better performance in comparison to systems that use microchannels to dissipate heat for the proposed heat flux ranges.

Once the central point configurations were generated and simulated, the results obtained from data Groups 1 and 5 with their corresponding intermediate designs were analyzed using the statistical software tool JMP. The JMP tool allows visualizing the responses of a model, using the provided information to generate a predictive pattern which approximates the pressure drop and the average temperature at the bottom of the model with a confidence interval showed graphically.

When a variation is made in one of three independent input parameters between the proposed ranges for each, JMP approximates the possible result on the outlet parameters. Figure 4.7 represents an example of the predicted pressure drop (105.87 kPa) and the average surface temperature (50.91 °C) using the JMP prediction tools. Here the normalized parameters have a fixed value: the distance between centers of 0.9326 (equivalent to 198.31μm), pin fin diameter of 0.446 (136.15 μm), and pin fin height of (200 μm).

As illustrates in Figure 4.7, when the distance between centers is reduced, the average temperature will decrease, but the pressure drop will have a considerable increase. In the opposite case, when the pin fin diameter or pin fin height is reduced, it implies an increase in the average temperature in the silicon surface but a reduction in the pressure drop, due

to the decrease in the available heat exchange area. Thus, a balance between these parameters to get the best thermal management, without investing a high pumping power in microfluidic cooling systems is needed.

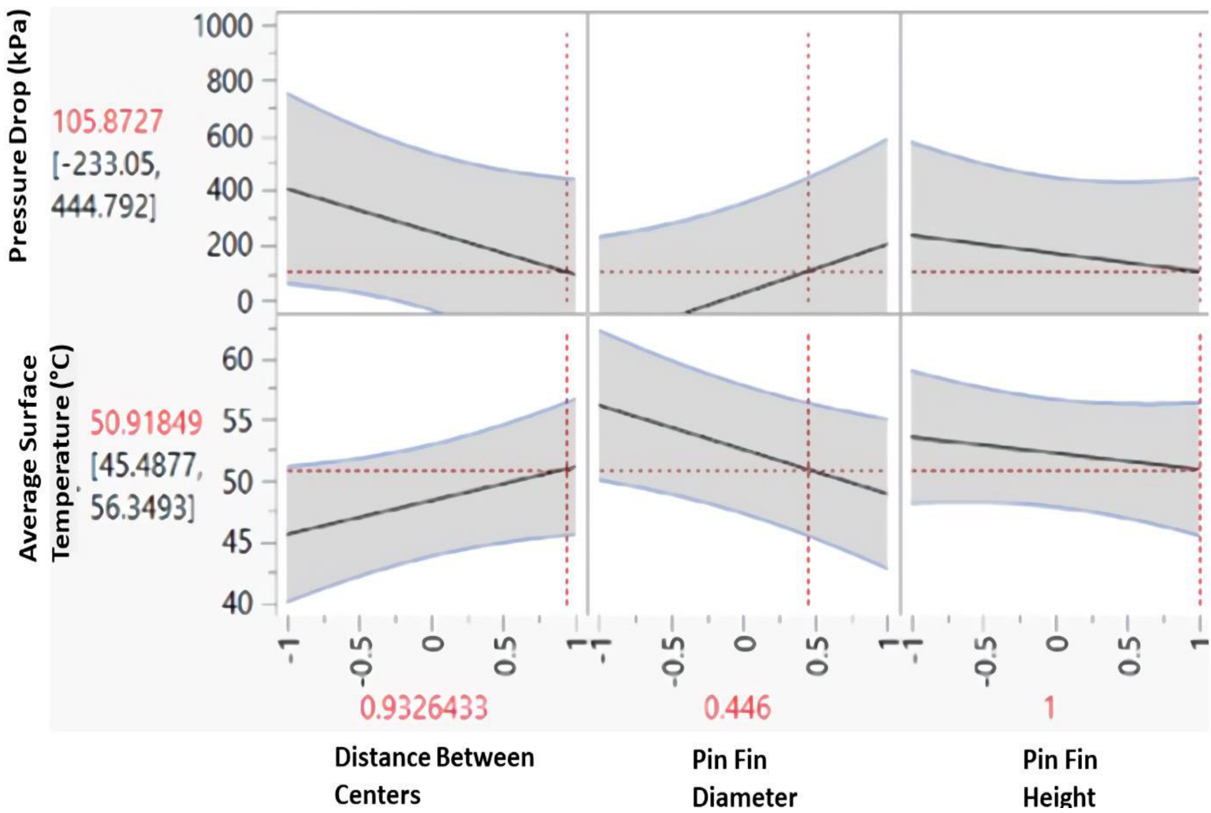

Figure 4.7 Illustration of the predictive graphic model given by JMP.

With the predicted model generated by JMP and its optimization tools, four geometrical configurations are suggested in Table 4.3, which were identified to improve the global performance considerably. The four optimized models keep a balance between thermal and hydraulic behaviors. Two types of improvements are reported: models Opt1G1 and Opt1G5 have a lower pressure drop along with acceptable average temperature in the silicon devices, whereas models Opt2G1 and Opt2G5 significantly reduce average temperature, with a moderate pressure drop. In addition, Table 4.3 shows the middle point models along with optimized model dimensions and their corresponding results, including validation model results as a baseline reference. The generated midpoint models, along with the optimized models, were built, meshed, and run following the numerical methodology established in Chapter 3.

Table 4.3 Dimensions and results for optimized models and middle points.

Model	**Extended shape surface**	**Hotspot position on HS**	**Pin-fin density increase**	**Distance between centers (µm)**	**Pin-fin diameter (µm)**	**Pin-fin height (µm)**	**Pressure drop (kPa)**	**Surface temp. (°C)**
Midpoint Group 1	Pin fin	Center	2	202.5	125	175	102.9	49.6
Midpoint Group 5	Pin fin	Edge	2	202.5	125	175	103.8	50.2
Validation	Pin fin	Center	4	225	150	200	125.7	52.5
Opt1G1	Pin fin	Edge	2	202.5	125	200	96	49.5
Opt2G1	Pin fin	Edge	2	205	150	200	196.8	44.8
Opt1G5	Pin fin	Center	2	196.55	125	200	79.3	50.1
Opt2G5	Pin fin	Center	2	202.5	150	200	185.8	48.2

Figure 4.8 shows the improvements in thermal performance for models Opt1G5 and Opt2G5 concerning to the validation model, considering a central hotspot zone. Using as a baseline of comparison the validation model, Opt1G5 decreases the average temperature in each zone in the heat sink, except for the hotspot zone, because the validation model has a higher pin-fin density. However, the average temperature of the Model Opt1G5 is lower than the validation model, while simultaneously decreasing the pressure drop (from 125.69 kPa for the validation model to 79.26 kPa). On the other hand, the model Opt2G5 reduces the average temperature on each zone by 5 °C or more, while increasing the pressure drop by 71.06 kPa.

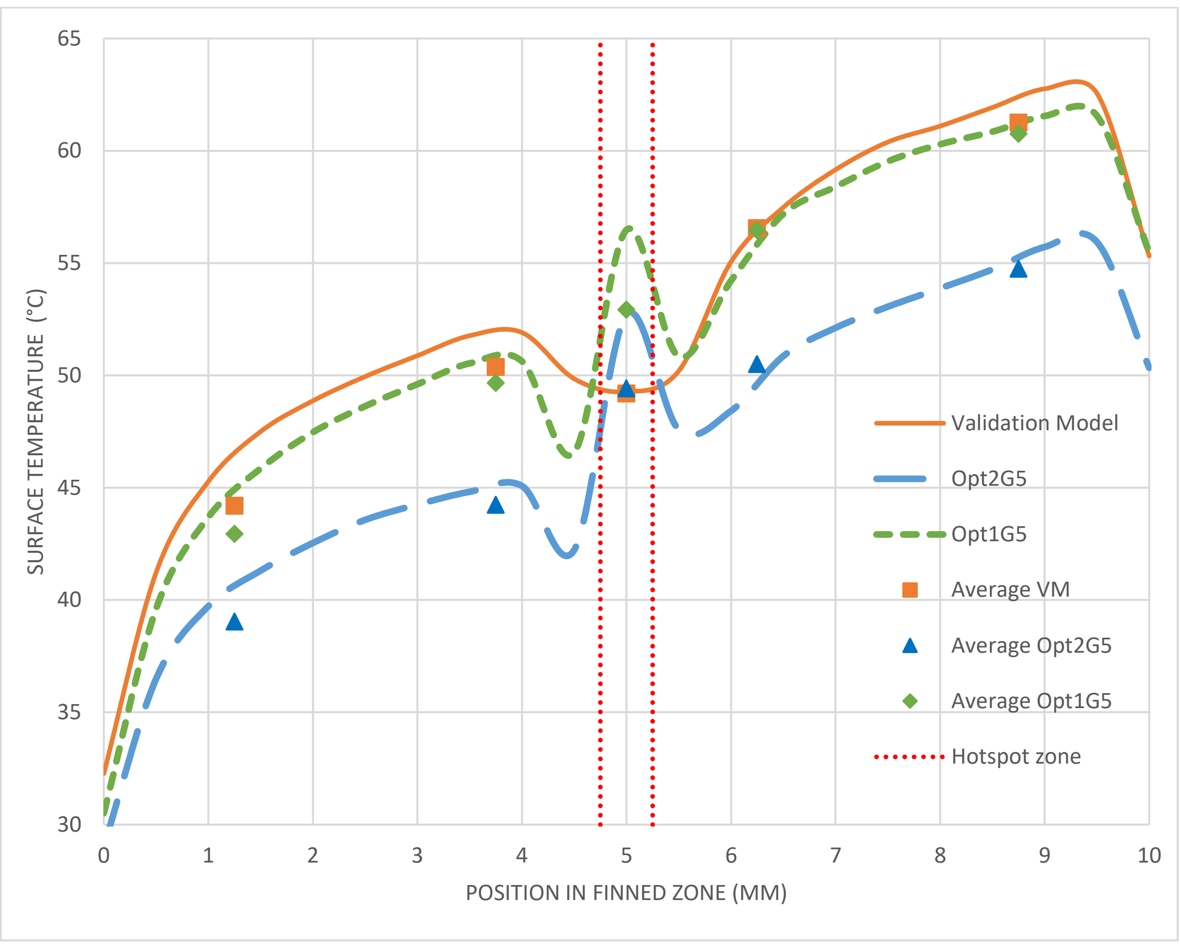

Figure 4.8 Thermal behavior on optimized models against the validation model.

4.5 Thermal evaluation of optimized models

The model Opt1G1 was tested according to the requirements of a U.S company. The geometry and dimensions of the model are illustrated in Figure 4.9. In comparison with the validation model, the model Opt1G1 has a lower distance between pin fin centers, a smaller pin fin diameter, and fewer pin fin density increase for the hotspot zone. By modifying this parameter, the thermal performance in the microfluidic cooling system was improved, reducing the average temperature in the bottom of the model 3 °C, and also decreasing the pressure drop 29.3 kPa, equivalent to 20% of the pumping power in the experimental model.

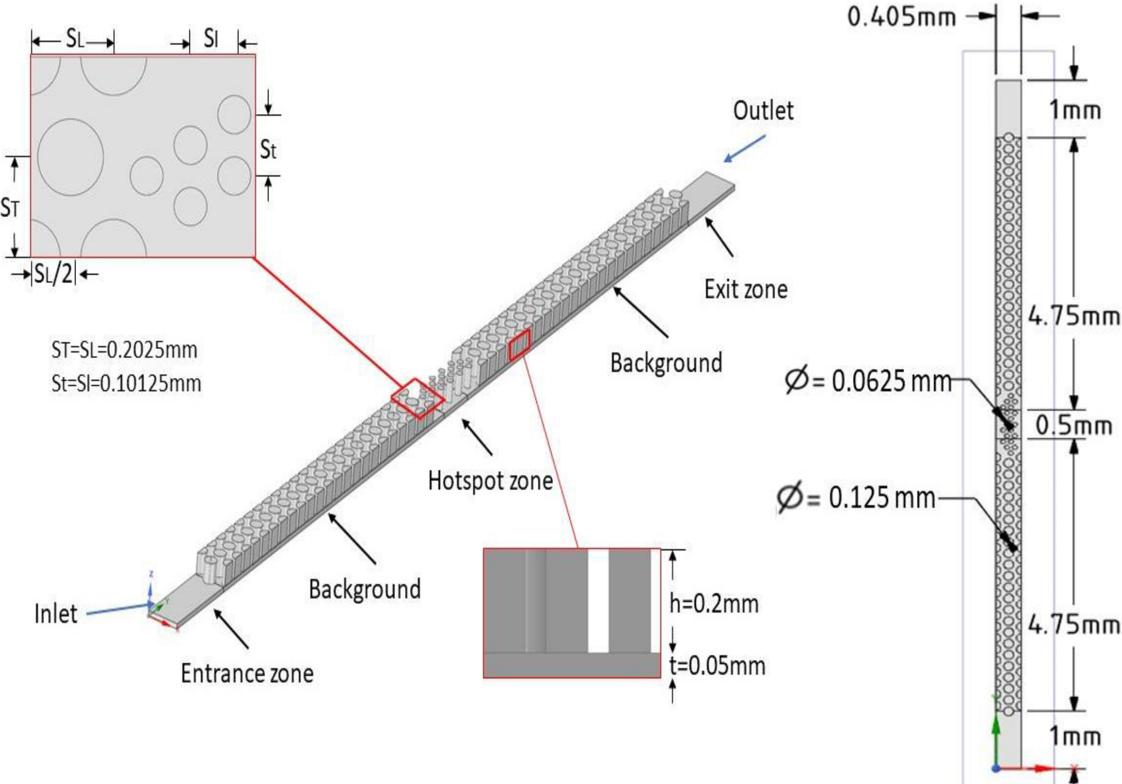

Figure 4.9 Schematic illustration of the model Opt1G1.

The showed model was tested with higher heat fluxes than in the parametric analysis. The background zones were evaluated with a heat flux of 1000 W/cm^2, four times the previous heat flux fixed. Whereas, the hotspot zone managed an energy flux of 1500 W/cm^2, three times the heat flux used in previous simulations, and twice the experimental heat flux reported [78]. The requested heat fluxes have coincidence with the predicted heat fluxes in the near future for tridimensional integrated circuits (3D ICs) [32,33]. Thus, the analysis carried out could be taken as a precedent in future studies on the topic.

The objective of proposing these significant heat fluxes is to evaluate the thermal performance of the optimized model, looking for adequate thermal management without having phase-change in the working fluid. Also, the obtained results were reported to a company that had a particular interest on this study. Figure 4.10 shows the boundary conditions for the analysis made. As is illustrated, the reduced cooling system was evaluated, proposing three different inlet pressures to find an adequate flow rate that do not surpass the limit temperature established for the fluid domain. At the outlet face, a gauge pressure of 0 is fixed, like in all the other cases. The stratum and pin fins material is silicon and the working fluid is DI-water, getting into the model with an inlet temperature of 21.3 °C. The material properties are shown in Table 3.1.

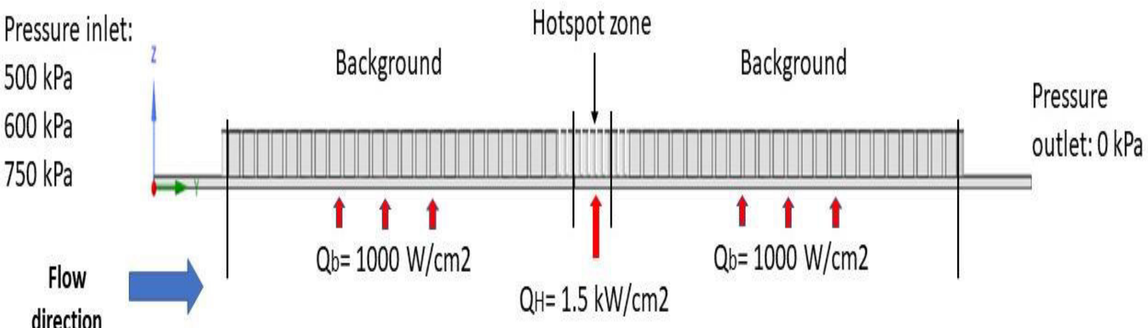

Figure 4.10 Illustration of the boundary conditions in the evaluated model.

Figure 4.11 shows the predicted thermal behavior at the bottom surface for each proposed pressure drop (PD). Also, Figure 4.11 includes the fluid flow rate (FR) associated with each proposed PD. As is shown, the temperature at the average bottom surface will not surpass 100 °C when the pressure drop is up to 500 kPa. This is possible providing a flow rate between 413.17 and 453.86 ml/min, representing a little more than double of the implemented flow rate in the experimental analysis reported [78-80]. In contradiction, the pressure drops will increase more than four times to manage the predicted heat fluxes on 3D ICs. When the flow rate continues increasing, the average temperature decreases considerably, obtaining maximum temperatures close to 90 °C for a flow rate of 497 ml/min. Besides, considering the Section 3.5.1, which talks about the flow distribution in an extended domain. There is a vast possibility of counting with lower temperatures in the physical models. So, for a fluid flow rate close to 413 ml/min in the model Opt1G1 is possible to avoid the working fluid phase-change.

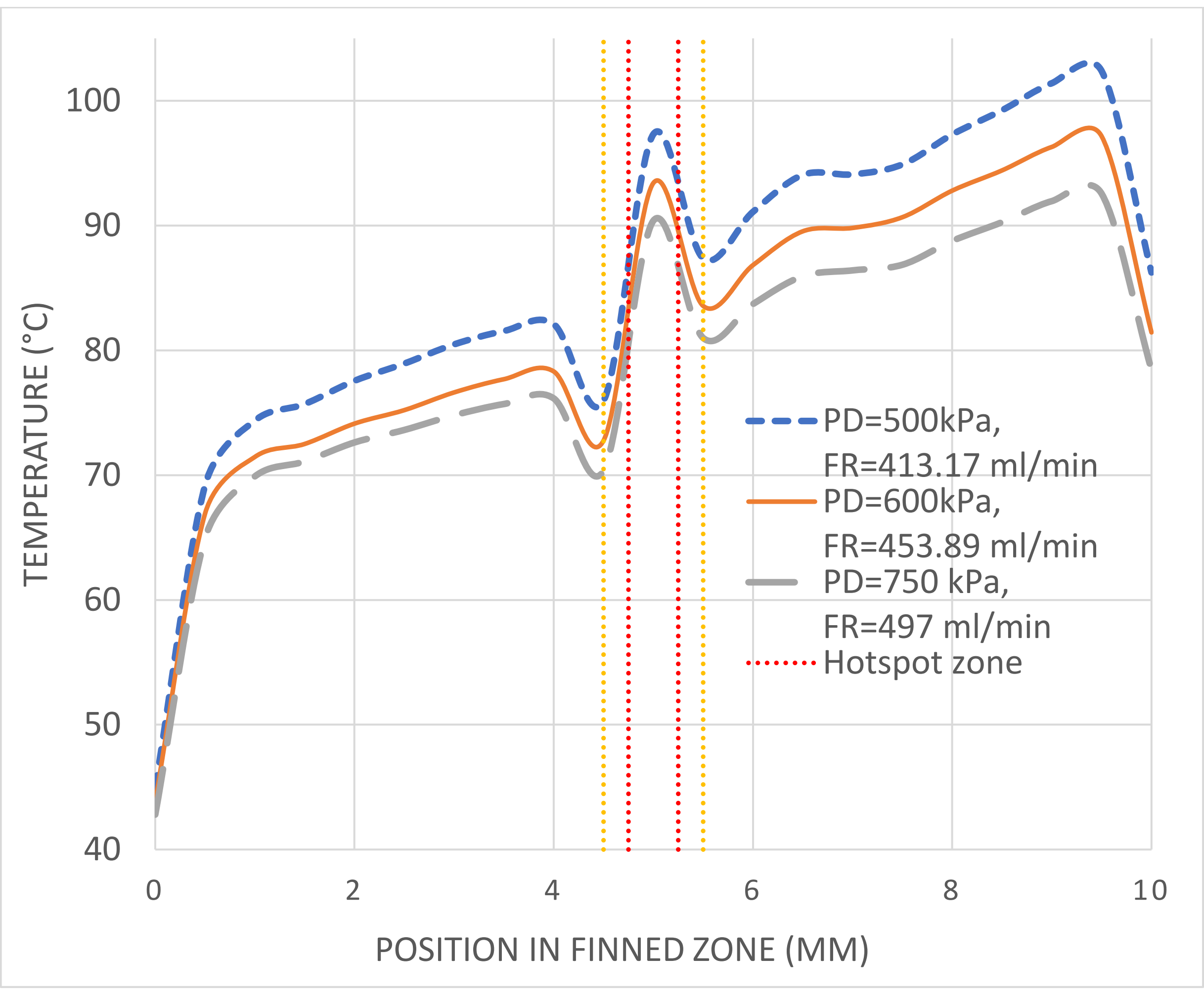

Figure 4.11 Predicted thermal behavior in model Opt1G1 for different pressure drop (PD).

Figure 4.12 shows the temperature contours for an inlet pressure of 600 kPa. In this one, the maximum temperatures are in the bottom zone (the nearest zone to the chip), surpassing the 100 °C by a little. A midplane in the simplified model generates the top view, showing that the pin fins have the maximum temperatures for the said plane. In general, the fluid domain keeps the temperature from 22 to 85 °C, being impossible a phase change in the working fluid. Whereas a significant part of the solid zone possesses adequate temperatures for the operation of a microchip, excepting in the hotspot zone and the exit zone (Zone 4). Thereby, it would be necessary an increase in the heat exchange area, a reduction in the water inlet temperature, or increase the flow rate, just for mentioning some options to improve the thermal management.

Chapter 5 will show the general conclusions of this thesis work, highlighting the contributions in microfluidic cooling systems for computational systems with tri-dimensional integrated circuits.

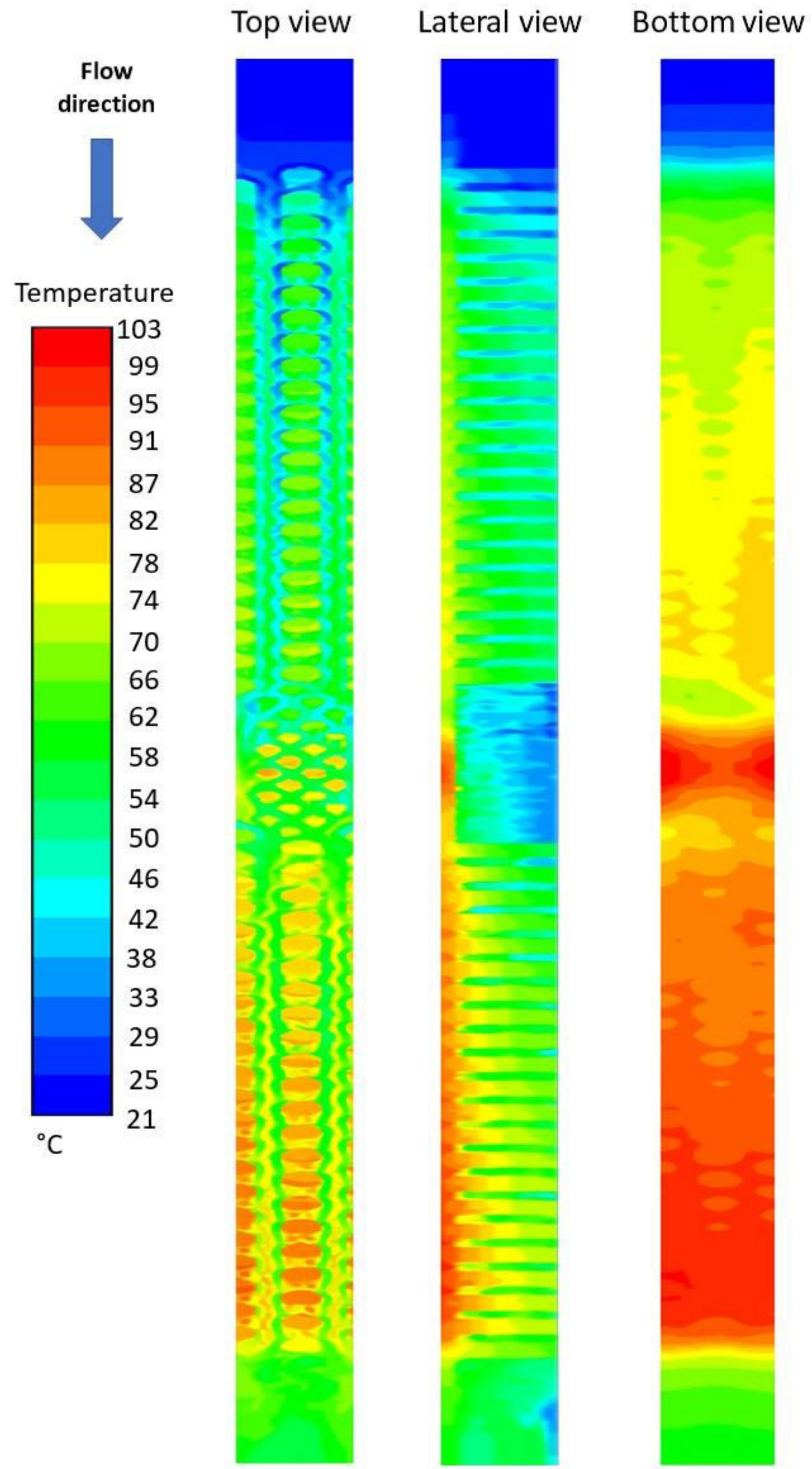

Figure 4.12 Temperature contours for a pressure inlet of 600 kPa in the model Opt1G1.

Chapter 5

Conclusion and future works

5.1 Conclusions

A methodology to get a numerical model of a microfluidic cooling system for 3D ICs was developed and validated against experimental studies performed at the Georgia Tech laboratories. The simplified model has good approximation in comparison with the experimental results, excepting at the outlet zone. An extended model was created and modeled to clarify previous discrepancies, finding that the flow distribution in the model is not uniform, as was supposed in the simple model.

Once clarified the differences between the numerical and experimental model, a parametric study was performed using the design of experiments (DoE) theory. Six geometric parameters were varied between 2 values or levels. The results from the present DoE study point out that input parameters with the most significant influence on the pressure drop and the average surface temperature are spacing between extended surfaces, extended surface diameter, and the interaction between both parameters. The pressure drop is an output parameter with a high sensitivity to parametric variation. While, the average surface temperature of the silicon device has a quasi-linear relation with the investigated parameters.

Based on the result from the initial DoE assessment, new intermediate configurations were developed to understand better the behavior on exit parameters and their relation with entrance parameters. The results of these models were studied along with previous simulation results, and new geometric dimensions were proposed to improve previous results. The optimized configurations considerably enhance the numerical and experimental baseline results, therefore indicating the value of such approach for optimization purposes in such kind of conjugate heat transfer applications.

One of the optimized models was tested using higher heat fluxes, similar to the predicted heat fluxes for 3D ICs technologies. The numerical study shows that the optimized models may provide adequate thermal management by increasing not much the fluid flow rates, but increasing the pressure drops considerably.

Finally, the pin-fin density increase at hotspot zones is an interesting concept to be analyzed in future studies due to its influence over the flow distribution on these microfluidic cooling systems. Results from this study indicate that the use of pin fins as the extended surfaces provides an enhanced thermo-hydraulic performance when compared to the use of

microchannels on embedded microfluidic cooling systems, as proven for the range of parameters covered in this study.

5.2 Future works

As a part of this thesis work, the author proposes the following activities to apport contributions and knowledge in the analyzed topic:

1. The creation of extended models of interest looking for better validation results, taking as base the numerical methodology developed in this document. It is not mandatory to simulate the complete physic model of an optimized geometry, due to this action will involve several spending of computational time.

2. The analysis of the pin fin density increase in the hotspot zone, and the pin fin arrays, looking for an adequate configuration which allows better thermal management.

3. Implement an optimization algorithm or similar in the analyzed cooling systems, seeking the optimal relation of the spacing between extended surfaces and the pin fin diameter. The implementation of said relation may enhance the global performance in the microfluidic cooling systems with embedded pin fins.

References

[1] Mary Bellis, The History of Vacuum Tubes and Their Uses. ThoughtCo, February 4, 2019. https://www.thoughtco.com/the-history-of-vacuum-tubes-1992595

[2] Wikipedia contributors, Vacuum tube. Wikipedia, The Free Encyclopedia, February 2, 2020. https://en.wikipedia.org/wiki/Vacuum_tube

[3] Massimo Guarnieri, The age of Vacuum Tubes: Merging with Digital Computing. IEEE Industrial Electronics Magazine 6 (3) (2012) 52-55. DOI: 10.1109/MIE.2012.2207830

[4] Jack Copeland, Colossus: The First Large Scale Electronic Computer. Wayback Machine, March 23, 2012. http://www.colossus-computer.com/colossus1.html#section02

[5] Joseph Kizza, History of Computing. Ethical and Social Issues in the Information Age, Springer, Cham, December 9, 2017. DOI: https://doi.org/10.1007/978-3-319-70712-9_1

[6] Gerard O' Regan, ENVAC, and ENIAC Computers. The Innovation in Computing Companion, Springer, Cham, December 9, 2018. DOI: https://doi.org/10.1007/978-3-030-02619-6_23

[7] Gerard O' Regan, Transistor. The Innovation in Computing Companion, Springer, Cham, December 9, 2018. DOI: https://doi.org/10.1007/978-3-030-02619-6_52

[8] Gerard O' Regan, Integrated Circuit. The Innovation in Computing Companion, Springer, Cham, December 9, 2018. DOI: https://doi.org/10.1007/978-3-030-02619-6_32

[9] Gerard O’ Regan, Von Neumann Architecture, Springer, Cham, December 9, 2018. DOI: https://doi.org/10.1007/978-3-030-02619-6_54

[10] Migga Kizza Joseph, The first Microprocessor, Springer London, 2010. http://www.maxmon.com/timeline.html

[11] M.M. Waldrop, The chips are down for Moore´s law, Nature 530 (2016) 144-147. DOI: https://www.nature.com/news/the-chips-are-down-for-moore-s-law-1.19338

[12] Gerard O’ Regan, Smartphones and Social Media. The Innovation in Computing Companion, Springer, Cham, December 9, 2018. https://doi.org/10.1007/978-3-030-02619-6_48

[13] Techopedia contributors, Embedded processor. Techopedia, February 11, 2020. https://www.techopedia.com/definition/17105/embedded-processor

[14] Marylin Wolf, Embedded Computing. Computers as Components: Principles of Embedded Computing System Design, Morgan Kaufmann, 2012. DOI: book on google scholar

[15] Michael Barr, Anthony Massa, Introduction. Programming embedded systems: with C and GNU development tools, O'Reilly, 2006. DOI: book on Google Scholar

[16] Michael Barr, Real men program in C. Embedded Systems Design, TechInsights (United Business Media), August 1, 2009.

[17] Wikipedia contributors, Embedded systems. Wikipedia, The Free Encyclopedia, February 11, 2020. https://en.wikipedia.org/wiki/Embedded_system

[18] G.E. Moore, Electronics 38, 1965, pp 114-117.

[19] Wikipedia contributors, Shannon- Hartley theorem. Wikipedia, The Free Encyclopedia, February 11, 2020. https://en.wikipedia.org/wiki/Shannon–Hartley_theorem

[20] Sun Kyu Lim, Regular versus irregular TSV placement for 3D IC. Design for High Performance, Low Power, and Reliable 3D Integrated Circuits, Springer, 2013.

[21] D.H. Kim, S. Mukhopadhyay, S.K. Lim, Through-silicon-via aware interconnect prediction and optimization for 3D stacked ICs. Proceedings of ACM/IEEE International Workshop on System Level Interconnected Prediction, 2009, pp 85-92. DOI: https://doi.org/10.1145/1572471.1572486

[22] Xuchen Zhang, 3D and 2.5 D heterogeneous integration platforms with interconnect stitching and microfluidic cooling, Ph.D. thesis dissertation,2017, pp. 1-18. DOI: http://hdl.handle.net/1853/58647

[23] H. Kristiansen, Thermal Management in Electronics. Chalmers University of Technology, 2001. DOI: http://www.ppd.chalmers.se/edu/mpr235/mpr235_thermgmnt.pdf

[24] R.R. Tummala, Fundamentals of device and systems packaging: technologies and applications, Mc Graw Hill 2th ed., 2019, Chapter 3.

[25] L. Sauciuc, G. Chrysler, R. Mahajan, and M. Szleper, Air-cooling Extension-Performance Limits for Processor Cooling Applications. Semiconductor Thermal Measurement and Management Symposium, 2003, pp. 74–81. DOI: https://ieeexplore.ieee.org/document/1194342

[26] H.E. Ahmed, B.H. Salman, A. Sh. Kherbeet, M.I. Ahmed, Optimization of thermal design of heat sinks: A review. International Journal of Heat and Mass Transfer, 2018, pp. 129-153. DOI: https://doi.org/10.1016/j.ijheatmasstransfer.2017.10.099

[27] A. E. Bergles, The evolution of cooling technology for electrical, electronic, and microelectronic equipment. ASME HTD, vol. 57, pp. 1–9, 1986.

[28] R.C. Chu, R. E. Simons, M. J. Ellsworth, Review of Cooling Technologies for Computer Products. IEEE Transactions on Device and Material Reliability, vol 4., 2004, pp. 568-586.

[29] The Uptime Institute, Heat Density Trends in Data Processing. Computer Systems and Telecommunication Equipment, March 2020. DOI: www.uptimeinsitute.org.

[30] C.J. Lasance, The Need for a Change in Thermal Design Philosophy. Electronics Cooling, vol. 1, 1995, pp. 24-26.

[31] P. Ramm, A. Klumpp, J. Weber, M. M. V. Taklo, 3D System-on-chip technologies for more than Moore systems. Microsystem Technologies 16, 2010, pp. 1051-1055. DOI: https://doi.org/10.1007/s00542-009-0976-1

[32] T. G. Karayiannis, M. M. Mahmoud, Flow boiling in micro-channels: Fundamentals and applications. Appl. Therm. Eng. 115, 2017, pp. 1372–1397. DOI: https://doi.org/10.1016/j.applthermaleng.2016.08.063

[33] J. Wei, Challenges in cooling design on CPU packages for high-performance services. Heat Transfer Engineering 29, 2010, pp. 178-187. DOI: https://doi.org/10.1080/01457630701686727

[34] S.C. Lin, K. Banerjee, Thermal Challenges of 3D ICs. Wafer Level 3D ICs Process Technology, 2008, pp. 1-26. DOI: https://doi.org/10.1007/978-0-387-76534-1_14

[35] R.C. Chu, A Review of IBM Sponsored Research and Development Projects for Computer Cooling. 15th IEEE Semi-Thermal Symposium, 1999.

[36] J. U. Knickerbocker, An advanced multichip module (MCM) for high performance UNIX servers. IBM Journal Researches and Developments, vol. 46, no. 6, 2002, pp. 779–804.

[37] S.M. Sohel Murshed, C.A. Nieto da Castro, A critical review of traditional and emerging techniques and fluids for electronics cooling. Renewable and Sustainable Energy Reviews 78, 2017, pp. 821-833. DOI

[38] T. Kordyban, Hot Air Rises and Heat Sinks: Everything you know about cooling electronic is wrong. ASME Press, 1998.

[39] Arrow electronics contributors, Understanding Heat Sinks: Functions, Types & More. Arrow, March 2020. DOI: https://www.arrow.com/en/research-and-events/articles/understanding-heat-sinks-functions-types-and-more

[40] C.H. Huang, Y.H. Chen, H.Y. Li, An impingement heat sink module design problem in determining optimal non-uniform fin widths. International Journal of Heat and Mass Transfer, Volume 67, 2013, pp. 992-1006. DOI: https://doi.org/10.1016/j.ijheatmasstransfer.2013.08.103

[41] C.H. Huang, Y.H. Chen, An impingement heat sink module design problem in determining simultaneously the optimal non-uniform fin widths and heights. International Journal of Heat and Mass Transfer, Volume 73, 2014, pp. 627-633. DOI: https://doi.org/10.1016/j.ijheatmasstransfer.2014.02.026

[42] C.H. Huang, Y.H. Chen, An optimal design problem in determining non-uniform fin heights and widths for an impingement heat sink module. Applied Thermal Engineering, Volume 63, 2014, pp. 481-494. DOI: https://doi.org/10.1016/j.applthermaleng.2013.11.008

[43] W. Al-Sallami, A. Al-Damook, H.M. Thompson, A numerical investigation of thermal airflows over strip fin heat sinks. International Communications in Heat and Mass Transfer, Volume 75, 2016, pp. 183-191. DOI: https://doi.org/10.1016/j.icheatmasstransfer.2016.03.014

[44] A. Al-Damook, N. Kapur, J.L. Summers, H.M. Thompson, Computational design and optimization of pin fin heat sinks with rectangular perforations. Applied Thermal Engineering, Volume 105, 2016, pp. 691-703. DOI: https://doi.org/10.1016/j.applthermaleng.2016.03.070

[45] Y.T. Yang, S.C. Lin, Y.H. Wang, J.C. Hsu, Numerical simulation and optimization of impingement cooling for rotating and stationary pin-fin heat sink. International Journal of Heat and Fluid Flow, Volume 44, 2013, pp. 383-393. DOI: https://doi.org/10.1016/j.ijheatfluidflow.2013.07.008

[46] C.F. Ma and A.E. Bergles, "Boiling Jet Impingement of Simulated Microelectronic Chips," ASME HTD, volume 28, 1983, pp. 5-12.

[47] L. Jiji and Z. Dagan, Experimental Investigation of Single Phase Multi Jet Impingement Cooling of an Array of Microelectronic Heat Sources Modern. Developments in Cooling Technology for Electronic Equipment, Hemisphere Publishing Corporation, 1988, pp. 265-283.

[48] P. Naphon, S. Wongwises, Investigation on the jet liquid impingement heat transfer for the central processing unit of personal computers. International Communications in Heat and Mass Transfer, volume 37, 2010, pp. 822–826. DOI: https://doi.org/10.1016/j.icheatmasstransfer.2010.05.004

[49] F. P. Incropera, Liquid immersion cooling of electronic components. Heat Transfer in Electronic and Microelectronic Equipment, 1990.

[50] A. E. Bergles, A. Bar-Cohen, Direct liquid cooling of microelectronic components". Advances in Thermal Modeling of Electronic Components and Systems, 1990, volume 2, pp. 233–342.

[51] D. K. Kim, Thermal optimization of branched-fin heat sinks subject to a parallel flow. International Journal of Heat and Mass Transfer, Volume 77, 2014, pp. 278-287. DOI: https://doi.org/10.1016/j.ijheatmasstransfer.2014.05.010

[52] T. Turkakar, T. Okutucu-Ozyurt, Dimensional optimization of heat sink with multiple heat sources. International Journal of Thermal Sciences, Volume 62, 2012, pp. 85-92. DOI: https://doi.org/10.1016/j.ijthermalsci.2011.12.015

[53] V.L. Vidnodhan, K.S. Rajan, Computational analysis of new microchannel heat sink configuration. Energy Conversion and Management, Volume 86, 2014, pp. 595-604. DOI: https://doi.org/10.1016/j.enconman.2014.06.038

[54] G.D. Xia, J. Jiang, J. Wang, Y.L. Zhai, D.D. Ma, Effects of different geometric structures on fluid flow and heat transfer performance in microchannel heat sinks. International Journal of Heat and Mass Transfer, Volume 80, 2015, pp. 439-447. DOI: https://doi.org/10.1016/j.ijheatmasstransfer.2014.08.095

[55] D. Lelea, The tangential micro-heat sink with multiple fluid inlets. International Communications in Heat and Mass Transfer, Volume 39, 2012, pp. 190-195. DOI: https://doi.org/10.1016/j.icheatmasstransfer.2011.12.005

[56] R. Chein, J. Chen, Numerical study of the inlet/outlet arrangement effect on microchannel heat sink performance. International Journal of Thermal Sciences, Volume 48, 20009, pp. 1627-1638. DOI: https://doi.org/10.1016/j.ijthermalsci.2008.12.019

[57] A.J. Shkarah, M.Y. Sulaiman, M.R. Ayob, A 3D numerical study of heat transfer in a single-phase microchannel heat sink using graphene, aluminum and silicon as substrates. International Communications in Heat and Mass Transfer, Volume 48, 2013, pp. 108-115. DOI: https://doi.org/10.1016/j.icheatmasstransfer.2013.08.006

[58] H.A. Mohammed, P. Gunnasergaran, N.H. Shuaib, Influence of various base nanofluids and substrate materials on heat transfer in trapezoidal microchannel heat sinks. International Communications in Heat and Mass Transfer, Volume 38, 2011, 194-201. DOI: https://doi.org/10.1016/j.icheatmasstransfer.2010.12.010

[59] Y. Chen, B. Peng, X. Hao, G. Xie, Fast approach of Pareto-optimal solution recommendation to multi-objective optimal design of serpentine-channel heat sink. Applied Thermal Engineering, Volume 70, 2014, pp. 263-273. DOI: https://doi.org/10.1016/j.applthermaleng.2014.05.004

[60] P. Naphon, S. Klanchart, Effects of outlet port positions on the jet impingement heat transfer characteristics in the mini-fin heat sink. International Communications in Heat and

Mass Transfer, Volume 38, 2011, pp. 1400-1405. DOI: https://doi.org/10.1016/j.icheatmasstransfer.2011.08.017

[61] J. Wang, H. Kong, Y. Xu, J. Wu, Experimental investigation of heat transfer and flow characteristics in finned copper foam heat sink subjected to jet impingement cooling. Applied Energy, Volume 241, 2019, pp. 433-443. DOI: https://doi.org/10.1016/j.apenergy.2019.03.040

[62] R. E. Simons, The evolution of IBM high performance cooling technology. IEEE Transactions CPMT-Part A, volume 18, 1995, pp. 805–811.

[63] S. Sander, B. Zajaczkowski, Z. Krolicki, Review on flow boiling of refrigerants R236fa and R245fa in mini and microchannels. International Journal of Heat and Mass Transfer, Volume 126 Part A, 2018, pp. 591-617. DOI: https://doi.org/10.1016/j.ijheatmasstransfer.2018.05.048

[64] S. Mori, Y. Utaka, Critical heat flux enhancement by surface modification in saturated pool boiling: A review. International Journal of Heat and Mass Transfer, volume 108 Part B, 2017, pp. 2534-2557. DOI: https://doi.org/10.1016/j.ijheatmasstransfer.2017.01.090

[65] W.A. Scott, Cooling of electronic equipment. John Wiley and Sons, 1974.

[66] A. A. El-Nasr, S. El-Haggar, Effective thermal conductivity of heat pipes. *Heat and Mass Transfer, volume* 32, 1996, 97–101. DOI: https://doi.org/10.1007/s002310050097

[67] M. Mochizuki, T. Nguyen, K. Mashiko, Y. Saito, T. Nguyen, V. Wuttijumnong. A review of heat pipe application including new opportunities. Frontiers in Heat Pipe, 2011. DOI: https://doi.org/10.5098/fhp.v2.1.3001

[68] Amir Faghri, Heat pipe science and technology. Taylor & Francis Group, 1995. DOI: https://books.google.com.mx/books?hl=es&lr=&id=9QpQAQAAQBAJ&oi=fnd&pg=PR15&ots=MRHHQWCULg&sig=5sFia6l3wuCII_7lt56elNXQrtU&redir_esc=y#v=onepage&q&f=false

[69] Amir Faghri, Review and Advances in Heat Pipe Science and Technology. ASME Journal of Heat Transfer, Volume 134, 2012. DOI: https://doi.org/10.1115/1.4007407

[70] Y. W. Chang, C.H. Cheng, J.G. Wang, S.L. Chen, Heat pipe for cooling of electronic equipment. Energy Conversion and Management, Volume 49, 2008, pp 3398-3404. DOI: https://doi.org/10.1016/j.enconman.2008.05.002

[71] S.C. Yao, S. Deb, N. Hammouda, Impacting spray boiling for thermal control of electronic systems. ASME-HTD Heat Transfer and Electronics, 1989.

[72] G. Pautsch, A. Bar-Cohen, Thermal management to multichip modules with evaporative spray cooling. Advanced Electronic Package, 1999, pp. 1453–1461.

[73] L. Lin, R. Ponnappan, Heat transfer characteristics of spray cooling in a close loop. International Journal of Heat and Mass Transfer, volume 46, 2003, pp. 3737-3746. DOI: https://doi.org/10.1016/S0017-9310(03)00217-5

[74] W. Deng, A. Gomez, Electrospray cooling for microelectronics. International Journal of Heat and Mass Transfer, volume 54, 2011, pp. 2270-2275. DOI: https://doi.org/10.1016/j.ijheatmasstransfer.2011.02.038

[75] Z.M. Wang, G.Q. Guo, K.L. Su, W.K. Tu, W. Liu, Experimental analysis of flow and heat transfer in miniature porous heat sink for high heat flux application. International Journal of Heat and Mass Transfer, Volume 55, July 2012, pp. 4437-4431. DOI: https://doi.org/10.1016/j.ijheatmasstransfer.2012.04.013

[76] S.S. Feng, J.J. Kuang, T. Wen, T.J. Lu, K. Ichimiya, An experimental and numerical study of finned metal foam heat sinks under impinging air jet cooling. International Journal of Heat and Mass Transfer, Volume 77, 2014, pp. 1063-1074. DOI: https://doi.org/10.1016/j.ijheatmasstransfer.2014.05.053

[77] Y. Li, L. Gong, M. Xu, Y. Joshi, Enhancing the performance of aluminum foam heat sinks through integrated pin fins. International Journal of Heat and Mass Transfer, Volume 151, 2020. DOI: https://doi.org/10.1016/j.ijheatmasstransfer.2020.119376

[78] D. Lorenzini, C. Green, T .E. Sarvey, X. Zhang, Y. Hu, A. G. Fedorov, M. S. Bakir, Y. Joshi, Embedded single-phase microfluidic thermal management for non-uniform heating and hotspots using micro gaps with variable pin fin clustering, International Journal of Heat Mass Transfer, Volume 103, 2016, pp. 1359–1370. DOI: https://doi.org/10.1016/j.ijheatmasstransfer.2016.08.040

[79] T. E. Sarvey, Y. Hu, C. E. Green, P. A. Kottke, D. C. Woodrum, Y. Joshi, A. G. Fedorov, S. K. Sitaraman, M. S. Bakir, Integrated Circuit Cooling Using Heterogeneous Micro pin-Fin Arrays for Non-uniform Power Maps, IEEE Transactions on Components, Packaging and Manufacturing Technology Volume 7, 2017, pp. 1465-1475. DOI: https://doi.org/ 10.1109/TCPMT.2017.2704525

[80] D. Lorenzini, Y. Joshi, Numerical Modeling and Experimental Validation of Two-Phase Microfluidic Cooling in Silicon Devices for Vertical Integration of microelectronics. International Journal of Heat and Mass Transfer, Volume 138, 2019, pp. 194-207. DOI: https://doi.org/10.1016/j.ijheatmasstransfer.2019.04.036

[81] S. Feng, Y. Yan, H. Li, Z. Yang, L. Li, L. Zhang, Theoretical and numerical investigation of embedded microfluidic thermal management using gradient distribution micro pin fin arrays. Applied Thermal Engineering, Volume 153, 2019, pp. 748-760. DOI: https://doi.org/10.1016/j.applthermaleng.2019.03.017

[82] D.B. Tuckerman, R. Pease, High-performance heat sinking for VLSI. IEEE Electron Device Letters, Volume 2, 1981, pp. 126-129. DOI: https://doi.org/ 10.1109/EDL.1981.25367

[83] S. K. Samal, M. K. Moharana, Thermo-hydraulic performance evaluation of a novel design recharging microchannel, International Journal of Thermal Sciences, Volume 135, 2019, pp. 459-470. DOI: https://doi.org/10.1016/j.ijthermalsci.2018.09.006

[84] R. Wu, X. Zhang, Y. Fan, R. Hu, X. Luo, A Bi-Layer compact thermal model for uniform chip temperature control with non-uniform heat sources by genetic-algorithm optimized microchannel cooling. International Journal of Thermal Sciences, Volume 136, 2019, pp. 337-346. DOI: https://doi.org/10.1016/j.ijthermalsci.2018.10.047

[85] K. P. Drummond, D. Back, M. D. Sinanis, D. B. Janes, D. Peroulis, Justin A. Weibel, S. V. Garimella. Characterization of hierarchical manifold microchannel heat sinks arrays under simultaneous background and hotspot heating conditions, International Journal of Heat and Mass Transfer, Volume 128, 2018, pp. 1289-1301. DOI: https://doi.org/10.1016/j.ijheatmasstransfer.2018.05.127

[86] Y. Wang, JH. Shin, C. Woodcock, X. Yu, Y. Peles, Experimental and numerical study about local heat transfer in a microchannel with a pin fin, International Journal of Heat and Mass Transfer, Volume 121, 2018, pp. 534-546. DOI: https://doi.org/10.1016/j.ijheatmasstransfer.2018.01.034

[87] D. Ansari, KY. Kim, Hotspot management using a hybrid heat sink with stepped pin-fins, International Journal of Thermal Sciences, Volume 134, 2018, pp. 27-39. DOI: https://doi.org/10.1080/10407782.2019.1599272

[88] A. Mohammadi, A. Kosar, Review on heat a fluid flow in micro pin fin heat sinks under single-phase and two-phase flow conditions, Nanoscale and Microscale Thermophysical Engineering, Volume 22, 2018, pp. 153-197. DOI: https://doi.org/10.1080/15567265.2018.1475525

[89] S. Wang, Y. Yin, C. Hu, P. Rezai, 3D Integrated circuit cooling with microfluidics. Micromachines, Volume 9, 2018. DOI: https://doi.org/10.3390/mi9060287

[90] K. Yuki, T. Hara, S. Ikezawa, K. Anju, K. Suzuki, T. Ogushi, T. Ide, M. Murakami, Immersion cooling of electronics utilizing lotus-type porous copper, Transactions of The Japan Institute of Electronics Packaging, Volume 9, 2016, pp. E16-013-1 – E16-013-1. DOI: https://doi.org/10.5104/jiepeng.9.E16-013-1

[91] G. Kunti, J. Dhar, A. Bhattacharya, S. Chakraborty, Alternating Current Electro-Thermal Flow for Energy Efficient Thermal Management of Microprocessor Hot Spots. 25th International Workshop on Thermal Investigation of ICs and Systems (THERMINIC), 2019. DOI: https://doi.org/ 10.1109/THERMINIC.2019.8923474

[92] G. S. Bindiganavale, M. Amaya, H. Moon, Demonstration of hotspot cooling using digital microfluidic device, Journal of Micromechanics and Microengineering, Volume 28, 2018, 125015 (10 pp). DOI: https://iopscience.iop.org/article/10.1088/1361-6439/aae883/meta

[93] D. Ansari and K.-Y. Kim, Performance analysis of double-layer microchannel heat sinks under non-uniform heating conditions with random hotspots, Micromachines, Volume 8, 2017, 54. DOI: https://doi.org/10.3390/mi8020054

[94] D. Lorenzini, S. G. Kandlikar, Variable Fin Density Flow Channels for Effective Cooling and Mitigation of Temperature Nonuniformity in Three-Dimensional Integrated Circuits. Journal of Electronic Packaging, Volume 136, 2014, 021007 (11 pp). DOI: https://doi.org/10.1115/1.4027091

[95] S. Xu, W. Wang, K. Fang, and C.-N. Wong, Heat transfer performance of a fractal silicon microchannel heat sink subjected to pulsation flow, International Journal of Heat and Mass Transfer, Volume 81, 2015, pp. 33-40. DOI: https://doi.org/10.1016/j.ijheatmasstransfer.2014.10.002

[96] ANSYS contributors, ANSYS Meshing User’s Guide. ANSYS Inc, version 16.0, 2015.

[97] D.C. Montgomery, Analysis and design of experiments. Limusa Wiley 2th edition, 2004, pp. 170-350.